



저작자표시-비영리-변경금지 2.0 대한민국

이용자는 아래의 조건을 따르는 경우에 한하여 자유롭게

- 이 저작물을 복제, 배포, 전송, 전시, 공연 및 방송할 수 있습니다.

다음과 같은 조건을 따라야 합니다:



저작자표시. 귀하는 원저작자를 표시하여야 합니다.



비영리. 귀하는 이 저작물을 영리 목적으로 이용할 수 없습니다.



변경금지. 귀하는 이 저작물을 개작, 변형 또는 가공할 수 없습니다.

- 귀하는, 이 저작물의 재이용이나 배포의 경우, 이 저작물에 적용된 이용허락조건을 명확하게 나타내어야 합니다.
- 저작권자로부터 별도의 허가를 받으면 이러한 조건들은 적용되지 않습니다.

저작권법에 따른 이용자의 권리는 위의 내용에 의하여 영향을 받지 않습니다.

이것은 [이용허락규약\(Legal Code\)](#)을 이해하기 쉽게 요약한 것입니다.

[Disclaimer](#)

공학박사학위논문

대심도 터널에서 운행되는
고속열차의 공력특성 및
철도차량 안전기준을 적용한 분석

Aerodynamic analysis considering
the railway safety criteria and
aerodynamics of the high-speed train travelling
in underground tunnels

2014년 8월

서울대학교 대학원

기계항공공학부

최 중 근

대심도 터널에서 운행되는 고속열차의 공력특성 및 철도차량 안전기준을 적용한 분석

Aerodynamic analysis considering
the railway safety criteria and aerodynamics
of the high-speed train travelling in underground tunnels

지도교수 김 규 홍

이 논문을 공학박사학위논문으로 제출함

2014년 6월

서울대학교 대학원

기계항공공학부

최 중 근

최중근의 공학박사 학위논문을 인준함

2014년 7월

위 원 장 : _____

부위원장 : _____

위 원 : _____

위 원 : _____

위 원 : _____

Abstract

South Korea is proposing to construct a new public transportation system. The Great Train eXpress (GTX) will be built underground as the present subway system. However, the cruise speed will be 200 km/h which is about two times faster than the present subway. When the train speed increases in a tunnel, the problems related to the aerodynamics are the important issues: aerodynamic drag, wind load on the platform screen door and aural discomfort for passengers.

Therefore, we performed the analysis of aerodynamic phenomena in a subway tunnel and conceptual design of GTX. First, the effect of the speed increase on the aerodynamic parameters was investigated as the train speed increases by the speed of GTX (200 km/h) based on the speed of present subway (100 km/h). And the trend of the aerodynamic parameters (aerodynamic drag, pressure wave and pressure change inside the train) is analyzed by changing the design parameters (nose shape, tunnel cross-sectional area and shaft). After that, GTX is designed conceptually from the tendency analysis. The conceptual design is evaluated by the design criteria of the high-speed train and subway.

An analysis to estimate the aerodynamic characteristics of the train in the tunnel is performed using Computational Fluid Dynamics (CFD). Numerical simulations were also performed by the axisymmetric method.

Through the analysis of the simulation results, it is found that the design of GTX should be carried out carefully. The nose shape of GTX should be a streamlined shape like KTX-Sancheon to reduce the aerodynamic drag. The tunnel cross-sectional area should be larger than the present subway tunnel. Tighter criteria about the design of the platform screen door is needed for the high-speed subway like GTX. a

sealed train is needed to prevent the internal pressure change from the rapid external pressure change for passenger safety and comfort.

These results are applicable for the basic design of the proposed GTX and tunnel system.

keywords : Great Train eXpress, Aerodynamic drag, Train nose shape,
Tunnel cross-sectional area, Wind load, Aural discomfort

Student Number : 2007 - 30821

Table of Contents

Abstract	I
Table of Contents	III
List of Tables	V
List of Figures	VI
1. Introduction	1
2. Research objectives	7
3. Method and Validation	9
3.1. Simulation methods	9
3.1.1 Modeling of the train travelling in tunnels	9
3.1.2 Flow solver and turbulence modeling	11
3.1.3 Modeling of the train running	12
3.1.4 Boundary conditions	16
3.2. Validation cases	19
3.2.1 Compression wave generated by the entry of a high-speed train into a tunnel	19
3.2.2 Pressure wave propagation in tunnels-I: 1/164th scale model ..	25
3.2.3 Pressure wave propagation in tunnels-II: Emmequerung tunnel ..	30
4. Simulation results and analysis	35
4.1. Effects of design parameters in regard to aerodynamic parameters ..	35
4.1.1 Aerodynamic drag	35
4.1.1.1 Effect of speed increase	38

4.1.1.2	Effect of nose shape	45
4.1.1.3	Effect of tunnel cross-sectional area	50
4.1.2	Wind pressure on platform screen door	55
4.1.2.1	Effect of speed increase	59
4.1.2.2	Effect of nose shape	61
4.1.2.3	Effect of tunnel cross-sectional area	64
4.1.2.4	Effect of train interference	68
4.1.2.5	Effect of shaft	71
4.1.3	Pressure change inside train	72
4.1.3.1	Effect of speed increase	74
4.1.3.2	Effect of nose shape	78
4.1.3.3	Effect of tunnel cross-sectional area	81
4.1.3.4	Effect of train interference	84
4.1.3.5	Effect of shaft	88
4.2.	Conceptual design of GTX considering aerodynamic drag and evaluation	92
4.2.1	Conceptual design	92
4.2.2	Evaluation of wind pressure on platform screen door	97
4.2.2.1	Single train	97
4.2.2.2	Two trains	98
4.2.3	Evaluation of Pressure change inside train	101
4.2.3.1	Single train	101
4.2.3.2	Two trains	105
5.	Conclusions	112
	References	115
	국문초록	122

List of Tables

Table 1 Pressure maxima and relative error	24
Table 2 Maxima of pressure gradient and relative error	24
Table 3 Configuration of 1/164th Scale model	26
Table 4 Simulation cases for aerodynamic drag analysis	37
Table 5 Wall shear stress according to the train speed	45
Table 6 Wall shear stress according to the nose length	49
Table 7 Wall shear stress according to the blockage ratio	54
Table 8 Design criteria of platform screen door (allowable horizontal load) [51]	56
Table 9 Simulation cases for wind pressure analysis	57
Table 10 The safety criteria of the railway train related to the pressure change inside the train [51]	73
Table 11 Configuration data of KTX-Sancheon	92

List of Figures

Fig. 1 Aerodynamic problems of the tunnel train travelling in a tunnel	6
Fig. 2 Two Etr 500 passing in tunnel at 280 km/h: Pressures on middle car; c3(right position), c5(top position) and c6(left position) [18]	10
Fig. 3 Axisymmetric grid system for a train passing through a tunnel [49]	10
Fig. 4 Full axisymmetric domain for the numerical simulation of the train travelling in the tunnel	14
Fig. 5 Divided domains for the modeling of the train running	14
Fig. 6 Layering method for the modeling of the train running	15
Fig. 7 Dynamic Layering	15
Fig. 8 Boundary conditions of the train-tunnel domain	17
Fig. 9 Boundary conditions of the train-tunnel domain with shafts	18
Fig. 10 Geometry data and nose shapes	20
Fig. 11 Domains and boundary conditions for the validation	21
Fig. 12 Mesh independence study: (a) Mesh independence results with experimental data [13], (b) Resolution of (540x50) mesh	22
Fig. 13 Comparison of jumps (left) and gradients (right) of pressure for the three shapes of the nose; (a):circular cone, (b):paraboloid of rev., (c):ellipsoid of rev., —:numerical results, ···: experimental results [13]	23
Fig. 14 Experimental setup of Train Tunnel Test Facility (T3F) in NLR	25
Fig. 15 Schematic domain for the validation of 1/164th scale model	27
Fig. 16 Comparison of pressure history on the tunnel between the experiment and numerical results (— : present simulation	

results, \cdots : experimental results [23]): (a) 1.87 m, (b) 4.55 m, (c) 6.24 m	29
Fig. 17 Emmequerung Tunnel and Vent Shaft Configurations [27]	31
Fig. 18 Schematic domain for the validation of Emmequerung Tunnel with Vent Shaft	32
Fig. 19 Comparison of pressure history at the monitoring point for 204 km/h	34
Fig. 20 Train blunt nose shape of Seoul Subway Line 8	36
Fig. 21 Schedules of train run in accordance with cruise speed: 100 km/h (—), 200 km/h (---)	36
Fig. 22 Comparison of the drag histories according to an increase in speed: (a) 100 km/h, (b) 200 km/h	39
Fig. 23 Comparison of the drags according to an increase in speed ..	39
Fig. 24 Comparison of the surface pressures at the center of the constant speed section: (a) 100 km/h, (b) 200 km/h	41
Fig. 25 Comparison of the pressure contours around the head and tail: (a) 100 km/h, (b) 200 km/h	41
Fig. 26 Pressure coefficient on the train surface with respect to the speed increase	42
Fig. 27 Velocity profile between the train and tunnel walls	43
Fig. 28 Comparison of the normalized velocity profiles by the same train speed ($U_{\text{train}} = 200$ km/h) between 100 km/h and 200 km/h	44
Fig. 29 Comparison of the normalized velocity profile by the respective speeds (100 km/h and 200 km/h)	45
Fig. 30 Comparison of the drags according to the nose length	46
Fig. 31 Comparison of the surface pressures according to the nose length at the center of the constant speed section: (a) 0.5 m, (b) 1 m, (c) 2 m, (d) 5 m, (e) 10 m	47

Fig. 32 Comparison of the pressure contours around the head and tail according to the nose length: (a) 0.5 m, (b) 1 m, (c) 2 m, (d) 5 m, (d) 10 m	48
Fig. 33 Comparison of the normalized velocity profiles according to the nose length	49
Fig. 34 Comparison of the drags according to the tunnel cross-sectional area	51
Fig. 35 Comparison of the surface pressures according to the blockage ratio (β) at the center of the constant speed section: (a) $\beta = 0.281$, (b) $\beta = 0.25$, (c) $\beta = 0.2$, (d) $\beta = 0.15$, (e) $\beta = 0.1$	52
Fig. 36 Comparison of the pressure contours around the head and tail according to the blockage ratio : (a) $\beta = 0.281$, (b) $\beta = 0.25$, (c) $\beta = 0.2$, (d) $\beta = 0.15$, (e) $\beta = 0.1$	53
Fig. 37 Comparison of the normalized velocity profiles according to the blockage ratio	54
Fig. 38 Measurement points based on a simulation case: (a) Only tunnel case, (b) Tunnel with shafts, (c) Tunnel with two trains	58
Fig. 39 Comparison of wind load on the platform screen door according to the train speed: (a) 100 km/h, (b) 200 km/h	60
Fig. 40 Comparison of wind load on the platform screen door according to the nose length at Station 1 and 2: (a) Wind load at the Station 1, (b) Wind load at the Station 2	62
Fig. 41 Comparison of wind load on the platform screen door according to the nose length at Middle	63
Fig. 42 Strength of compression wave in accordance with nose shape and blockage ratio	64
Fig. 43 Comparison of wind load on the platform screen door according to the blockage ratio at Station 1 and 2: (a) Wind load at the Station 1, (b) Wind load at the Station 2	66

Fig. 44 Comparison of wind load on the platform screen door according to the blockage ratio at Middle	67
Fig. 45 Comparison of the pressure histories measured at Station 1, 2 and 3 to identify the train interference	70
Fig. 46 Comparison of the pressure histories measured at the middle of the stations to identify the train interference	70
Fig. 47 Pressure history measured in the tunnel with shafts	71
Fig. 48 Two measurement points (A and B) to analyse the pressure change inside the train	73
Fig. 49 External pressure history according to the train speed	74
Fig. 50 Comparison of pressure change per second according to the train speed	76
Fig. 51 Comparison of pressure change for 3 seconds according to the train speed	76
Fig. 52 Comparison of pressure change for 10 seconds according to the train speed	77
Fig. 53 Comparison of pressure change for 60 seconds according to the train speed	77
Fig. 54 External pressure history according to the nose length	78
Fig. 55 Comparison of pressure change per second according to the nose length	79
Fig. 56 Comparison of pressure change for 3 seconds according to the nose length	79
Fig. 57 Comparison of pressure change for 10 seconds according to the nose length	80
Fig. 58 Comparison of pressure change for 60 seconds according to the nose length	80
Fig. 59 External pressure history according to the blockage ratio	81
Fig. 60 Comparison of pressure change per second according to the	

blockage ratio	82
Fig. 61 Comparison of pressure change for 3 seconds according to the blockage ratio	82
Fig. 62 Comparison of pressure change for 10 seconds according to the blockage ratio	83
Fig. 63 Comparison of pressure change for 60 seconds according to the blockage ratio	83
Fig. 64 External pressure history of the lead and trailing train	85
Fig. 65 Comparison of pressure change per second between the lead and trailing train	86
Fig. 66 Comparison of pressure change for 3 seconds between the lead and trailing train	86
Fig. 67 Comparison of pressure change for 10 seconds between the lead and trailing train	87
Fig. 68 Comparison of pressure change for 60 seconds between the lead and trailing train	87
Fig. 69 External pressure history of the train in the tunnel with shaft ..	89
Fig. 70 Pressure change per second of the train in the tunnel with shaft	90
Fig. 71 Pressure change for 3 seconds of the train in the tunnel with shaft	90
Fig. 72 Pressure change for 10 seconds of the train in the tunnel with shaft	91
Fig. 73 Pressure change for 60 seconds of the train in the tunnel with shaft	91
Fig. 74 Selection of tunnel cross-sectional area based on the drag; comparison of the drags between in tunnel and in open field ..	94
Fig. 75 Comparison of the drag in the tunnel and an open field in accordance with the train speed from 100 km/h to 200 km/h ..	96

Fig. 76 Comparison of the drag coefficient in the tunnel and an open field in accordance with the train speed from 100 km/h to 200 km/h	96
Fig. 77 Wind load measured at Station 1, 2 and Middle from the conceptual design	98
Fig. 78 Wind load measured at Station 1, 2 and 3 from the conceptual design to identify the train interference	99
Fig. 79 Wind load measured at the middle between the stations from the conceptual design to identify the train interference	101
Fig. 80 External pressure history measured from the conceptual design ..	102
Fig. 81 Pressure change per second from the conceptual design	103
Fig. 82 Pressure change for 3 seconds from the conceptual design ..	103
Fig. 83 Pressure change for 10 seconds from the conceptual design ..	104
Fig. 84 Pressure change for 60 seconds from the conceptual design ..	104
Fig. 85 Comparison of external pressure from the conceptual design to identify the train interference: (a) Lead train, (b) Trailing train ..	106
Fig. 86 Comparison of pressure change per second from the conceptual design to identify the train interference: (a) Lead train, (b) Trailing train	108
Fig. 87 Comparison of pressure change for 3 seconds from the conceptual design to identify the train interference: (a) Lead train, (b) Trailing train	109
Fig. 88 Comparison of pressure change for 10 seconds from the conceptual design to identify the train interference: (a) Lead train, (b) Trailing train	110
Fig. 89 Comparison of pressure change for 60 seconds from the conceptual design to identify the train interference: (a) Lead train, (b) Trailing train	111

1. Introduction

High-speed trains are operated and developed worldwide. For example, Eurostar is a high-speed railway service that connects London to Paris and Brussels. The Eurostar train set a new British speed record of 334.7 km/h on the first section of High Speed 1 on July 30, 2003 [41]. The Train à Grande Vitesse (TGV) operates as a high-speed rail service in France. A TGV test train set the fastest wheeled train record at 574.8 km/h on April 3, 2007. TGV technology has been adopted in South Korea [45]. The InterCity Express (ICE) is a system of high-speed trains that operate in Germany and the surrounding countries. The maximum speed of the ICE 3 is 330 km/h [46]. In Japan, the Shinkansen is a network of high-speed railway lines with a maximum operating speed of 320 km/h. South Korea is developing the High-speed Electric Multiple Unit-430 km/h eXperiment (HEMU-430X) with a maximum speed of 430 km/h [44]. South Korea is planning to construct the Great Train eXpress (GTX) as a new public transportation system. Since 2012, the maximum commercial speed for most high-speed rail lines is about 300 km/h [48].

Straighter tracks are needed for high-speed rail lines because of the increase of the operating speed. The lines require longer and more numerous tunnel sections to avoid obstacles and to reduce environmental impact [14]. For example, tunnels are planned for development through the Alps (The Lyon-Torino connection with a 54 km long tunnel [4] or the Swiss AlpTransit [19] project with about 120 km of tunnels) [2]. All Eurostar trains traverse the Channel Tunnel between the United Kingdom and France. The Channel Tunnel holds the record for the longest undersea section worldwide (37.9 km under

the sea) [43]. The Seikan Tunnel in Japan is a 53.85 km railway tunnel with a 23.3 km long portion under the seabed [47]. The high-speed rail line connecting Seoul to Pusan in South Korea has 83 tunnels that cover 46% of the 412 km total line [8]. All GTX lines will use tunnels that will be built underground.

As mentioned before, there is a plan to construct a new public transportation system in South Korea [42]. The GTX is a new subway system which is faster than the present subway and expected to facilitate easier connections between Seoul and Gyeonggi Province. Therefore, traffic jams during rush hour is expected to be reduced. Three lines of about 145.5 km were proposed to connect Seoul to Gyeonggi Province. The GTX subway system will be different than the present subway system. All subway lines will be built underground. The tunnels will be located at a depth of 40 ~ 50 m below the surface which is deeper than the current subway system. The maximum cruise speed in tunnels of the GTX will be 200 km/h which is two times faster than the present subway [45]. Since the GTX is a new subway system that has not yet been constructed in South Korea, a technical analysis and technology development plan about the design of the tunnel and train travelling at high-speed in tunnels must be performed prior to construction.

A train that operates in tunnels has different aerodynamic problems than a train that operates in an open field (Fig. 1). Compression and expansion waves are generated when the train enters the tunnel. The pressure waves cause relevant aerodynamic loads on vehicle and tunnel structures. Aerodynamic noise, forces and moments, and especially aerodynamic drag acting on the train increase due to the confinement of the surrounding space [14, 31]. The aerodynamic drag is important because the portion of the aerodynamic drag on a high-speed train

traveling in a tunnel can exceed 90% of the total drag [2]. The entity of the aerodynamic drag depends on several parameters such as the blockage ratio (ratio of a vehicle to free tunnel cross-sectional area, $\beta = S_{\text{train}}/S_{\text{tunnel}}$), tunnel network geometry and surface, number of pressure relief ducts, train type and train speed, and the presence of other trains [21, 22]. The required operating speed of the train cannot be attained if the aerodynamic drag is underestimated during the design phase [29]. When high-speed train enters the tunnel, the compression wave of which the propagation speed is the speed of sound is generated and reflected at the portals [34]. Therefore, pressure in tunnels is changed by the interaction of pressure waves. It affects the pressure inside the train [32, 33]. If the pressure change is intense, passengers feel the aural discomfort. The train is sealed to prevent the aural discomfort. There is a criteria about the sealing of the high-speed train [30]. Besides the criteria about the train, there is a criteria related with a station structure. There is a structure at which the wind load by the train is acting [35, 36, 37]. That is a platform screen door. When the platform screen door is designed and installed, there was a lot of researches to evaluate the strength of wind load because the platform screen door must stand the wind load. The platform screen door installed at the present subway stands the wind load and satisfies the design criteria as the train speed is not fast. However, GTX is about two times faster than the present subway. Thus, the wind load according to the speed increase should be evaluated whether the wind load satisfies the design criteria or not.

A subway that uses underground tunnels also has different issues for passenger safety. The ventilation and smoke control systems in a subway is one of the important issues [9, 10, 38, 39]. In addition, the effects of the vent shaft location and platform screen door are

important for the performance of the ventilation system and passenger safety in the case of a subway train fire accident [17, 7, 40].

Studies to solve the aerodynamic problems related to the train travelling in tunnels were performed. The Transient Aerodynamics for Railway System Optimisation (TRANSAERO-Project) is the first project within the Community research framework of the European Union. TRANSAERO provides a major step in progress for the physical understanding and the technical development of the time-dependent effects of side-wind forces, trains passing, and pressure waves in tunnels [18]. Bellenoue and Kageyama.[3] tested the generation of pressure waves by the entry of a high-speed train into a tunnel using the reduced-scale experimental method. He compared the results of 3-dimensional model to a simpler axially symmetrical model. A 1/77 model representing the first vehicle of ETR500/2 train was used for 3-dimensional configurations as well as an equivalent axially-symmetrical train. The results show that the planar compression waves in the tunnel can be well reproduced by a simpler axially symmetrical model. The cross section of the train nose and nose profile seem to constitute critical parameters. The hybrid numerical method was developed to enhance the time efficiency of computational simulation. It takes a lot of time to solve the long-tunnel problems with a 3-dimensional calculation. The hybrid model is based on the physics related to the propagation of the pressure wave in tunnels. Pressure wave propagating in the tunnel is a 1-dimensional phenomenon. Thus, the tunnel except the train and stations is described in 1-dimensional model. And the train and stations are described in 2-dimensional model. The result of the hybrid method is the same as the 2-dimensional model. And the simulation time is considerably reduced [23].

A compression wave that is caused by the entrance of a train in a

tunnel propagates along the tunnel to the opposite portal. A part of the wave radiates in the environment due to the reflection process at the portal. So-called micro-pressure waves can cause structural responses of structures close to the tunnel exit. Micro-pressure waves can also annoy the public. Yoon and Lee[54, 55] proposed new methods for the prediction of sonic-boom noise. The first method combines acoustic monopole analysis and the method of characteristics with the Kirchhoff method. The second method couples the Kirchhoff formulation with the Euler equation. They suggested that the combined acoustic monopole/method of characteristics-Kirchhoff method is very efficient in that less computation time is involved from the engineering viewpoint. Hwang[53] developed a three-dimensional inviscid method based on three types of domain decomposition techniques. And train/tunnel interaction problems for double track railway system are investigated and aerodynamics loads histories during the crossing events -train/train interaction problem- are presented and discussed. Ku[49] performed multi-step design optimization using the Broyden-Fletcher-Goldfarb-Shanno (BFGS) algorithm with a response surface model to improve the shape of the train nose. As a result, the intensity of the micro-pressure wave was reduced by 18-27 % compared to a parabolic nose through the nose shape optimization. Another research related to micro-pressure waves were carried out by Ehrendorfer et al.[5], who compared the numerical results of a 2-dimensional axisymmetric model and the results of reduced scale model and full scale experiments. A 2-dimensional finite volume Euler solver was programmed. Two micro-pressure wave measurements of the North-portal of Terranuova-Tunnel were investigated. The first measurement consisted of a ETR500 with 221 km/h to Florence. The second experiment consisted of a measurement with two parallel ETR500 with 230 km/h to

Florence. A comparison of the results shows that the numerical tools of the 2-dimensional axisymmetric model are adequate for the numerical investigation of the micro pressure wave problem.

In 2002, the aerodynamic field generated by a high-speed train travelling under partial vacuum through the Basle-Zurich Swissmetro tunnel was analyzed by quasi 1-dimensional numerical simulations of the induced air flow and the computational domain [14]. The effect of different tunnel configurations on the aerodynamic drag of very high-speed trains was studied. The quasi 1-dimensional model can predict the large-scale behavior of air flow in a train-tunnel system. However, the quasi 1-dimensional model needs suitable corrective models to capture the local 3-dimensional features of air flow in some peculiar regions of the flow field (such as the close vicinity of a train and tunnel wall). Kim et al. [11] studied the aerodynamic drag of a maglev train travelling at 500~2000 km/h. An axisymmetric 2-dimensional model was used to simulate the trend of aerodynamic drag for each blockage ratio, internal tube pressure and operating speed. The study provided guidelines for the construction of a tube train system.

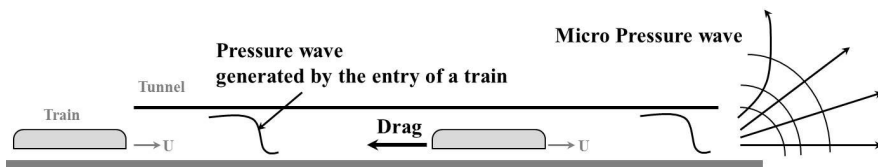


Fig. 1 Aerodynamic problems of the tunnel train travelling in a tunnel

2. Research objectives

GTX is basically similar with a present subway but the speed is faster than the subway. The aerodynamic drag in GTX is one of the important issues because GTX is a high-speed train travelling in the tunnel. In addition, the pressure wave which is a significant research topic about the high-speed train entering into the tunnel is also a important issue of GTX. However, it is expected that the phenomena in GTX are different with the high-speed train entering in the tunnel because GTX does not enter at high-speed in the tunnel but starts gradually in the tunnel. Because GTX is a high-speed train system that will be operated in a different situation unlike the present high-speed train, GTX needs to analyze the aerodynamic phenomena which fit the GTX system before constructing GTX.

This study is concerned with the analysis of aerodynamic phenomena in a subway tunnel and conceptual design of GTX. There are several aerodynamic and design parameters related with the aerodynamic phenomena in the tunnel. Aerodynamic parameters considering significant are aerodynamic drag, pressure wave and pressure change inside the train. Design parameters are the nose shape, tunnel cross-sectional area and shaft.

First, we investigate the speed effect on the aerodynamic parameters as the train speed increases by the speed of GTX (200 km/h) based on the speed of present subway (100 km/h). And the trend of the aerodynamic parameters is analyzed by changing the design parameters. The nose shape is changed from a blunt shape like the present subway to a streamlined shape like the high-speed train. The numerical simulation is performed changing the tunnel cross-sectional area because the tunnel cross-sectional area of present subway is

smaller than that of high-speed train. The shaft effect with regard to pressure wave is investigated because the pressure is disturbed at the shafts located in tunnels. The interference effect by two trains is also investigated.

After that, GTX is designed conceptually from the tendency analysis. The conceptual design according to the drag is carried out because the aerodynamic drag is the main parameter to achieve the desired speed. The conceptual design is evaluated by the design criteria of the high-speed train and subway. This work will provide a guideline for the construction of the GTX and related research.

3. Method and Validation

3.1. Simulation methods

3.1.1 Modeling of the train travelling in tunnels

The pressure wave propagation and pressure distribution around the train except the nose and tail are one-dimensional phenomena [18]. These phenomena was verified by the previous papers. The pressures measured at the top, right and left in tunnels are almost the same (Fig. 2). There was a train model experiment. Pressure wave by three-dimensional model was compared with pressure wave by axisymmetric model. The results of the axisymmetric model is in good agreement with those of the three-dimensional model. An equivalent axially symmetrical model can favorably replace a three-dimensional mode.

Numerical simulations were also performed by the axisymmetric method (Fig. 3). The method was used to study the micro pressure wave by the pressure wave radiation at the portal of the tunnel and to optimize the nose shape causing the micro pressure wave [49]. Therefore, in this paper, the axisymmetric simulation is performed to understand the train travelling in tunnels.

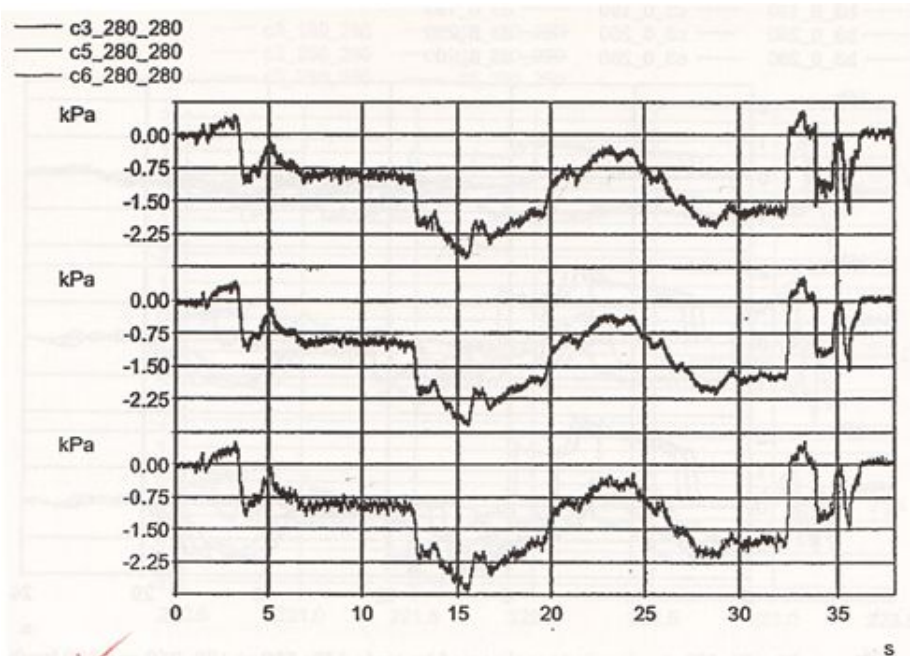


Fig. 2 Two Etr 500 passing in tunnel at 280 km/h: Pressures on middle car; c3(right position), c5(top position) and c6(left position) [18]

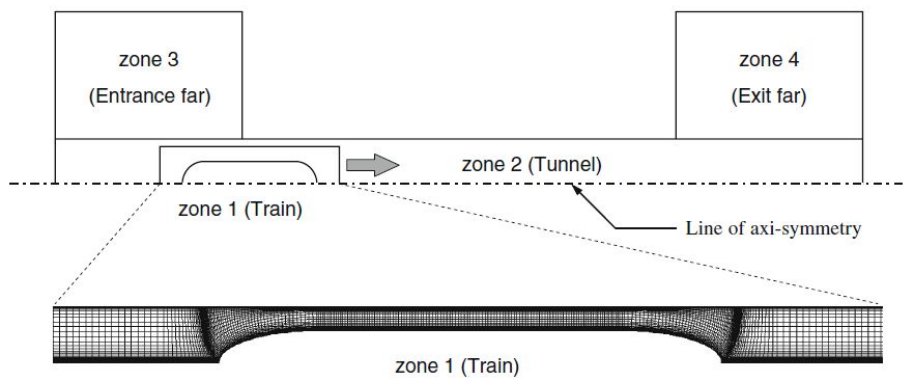


Fig. 3 Axisymmetric grid system for a train passing through a tunnel [49]

3.1.2 Flow solver and turbulence modeling

The unsteady flow generated by the trains travelling inside the tunnels is a compressible and turbulent flow [2]. The flow by GTX whose maximum speed is 200 km/h in tunnels is also a unsteady compressible and turbulent flow. The two-dimensional axisymmetric model can reproduce the global pattern of the three-dimensional model.

Therefore, the axisymmetric unsteady compressible Navier-Stokes equations are used to simulate the unsteady flow in the tunnels. The Roe's Flux Difference Scheme is used for spatial discretization and the dual-time stepping is employed for time integration. The standard κ - ε turbulence model is also applied because the geometry is simple and the flow is not complex. The standard κ - ε turbulence model is the simplest complete turbulence mode. The standard κ - ε turbulence model also has the broadest range of applicability, and is simple and usually accurate for simple flows [16]. The enhanced wall function is applied to the near wall modeling.

The system of governing equations for a single-component fluid, written to describe the mean flow properties, is cast in integral Cartesian form for an arbitrary control volume V with differential surface area dA as follows [50]:

$$\frac{\partial}{\partial t} \int_V W dV + \oint [F - G] dA = \int_V H dV$$

where the vectors W , F and G are defined as

$$W = \begin{Bmatrix} \rho \\ \rho u \\ \rho v \\ \rho E \end{Bmatrix}, \quad F = \begin{Bmatrix} \rho v \\ \rho v u + p \hat{i} \\ \rho v v + p \hat{j} \\ \rho v E + p v \end{Bmatrix}, \quad G = \begin{Bmatrix} 0 \\ \tau_{xi} \\ \tau_{yi} \\ \tau_{ij} v_j + q \end{Bmatrix}$$

and the vector H contains source terms such as body forces and energy sources.

Here ρ , v , E , and p are the density, velocity, total energy per unit mass, and pressure of the fluid, respectively. τ is the viscous stress tensor, and q is the heat flux.

Total energy E is related to the total enthalpy H by

$$E = H - p/\rho$$

where

$$H = h + |v|^2/2$$

3.1.3 Modeling of the train running

We assumed that the cross-sectional area of the station and the tunnel are the same in the simulation because the platform screen door is installed for passenger safety at the subway stations (Fig. 4). The basic domain is the shape that the train is located in the long tunnel. The basic domain is divided into three domains to describe the motion of the train (Fig. 5): one center domain and two tunnel domains. The tunnels except the center domain are set as two domains located ahead of the center domain and behind the center domain. When the train runs as scheduled, the center domain also moves with the train.

The center domain is moved by UDF (User Defined Function) of ANSYS FLUENT. When the center domain moves, dynamic layering method is applied to two tunnel domains (Fig. 6). Dynamic layering method is to add or remove layers of cells adjacent to a moving boundary, based on the height of the layer adjacent to the moving surface [6]. The dynamic mesh model in ANSYS FLUENT allows users to specify an ideal layer height on each moving boundary (Fig. 7). The layer of cells adjacent to the moving boundary (layer j) is split or merged with the layer of cells next to it (layer i) based on the height (h) of the cells in layer j .

There are some cases with shafts among the test cases to identify the effect of the shaft. The shaft is also described as an axisymmetric model. The actual area of the shaft is maintained the same area in the axisymmetric model.

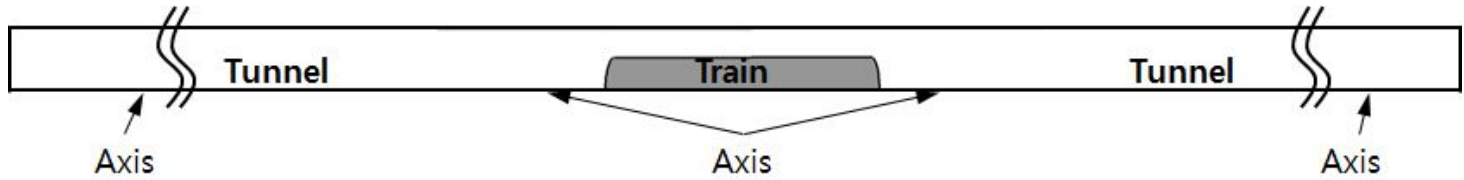


Fig. 4 Full axisymmetric domain for the numerical simulation of the train travelling in the tunnel

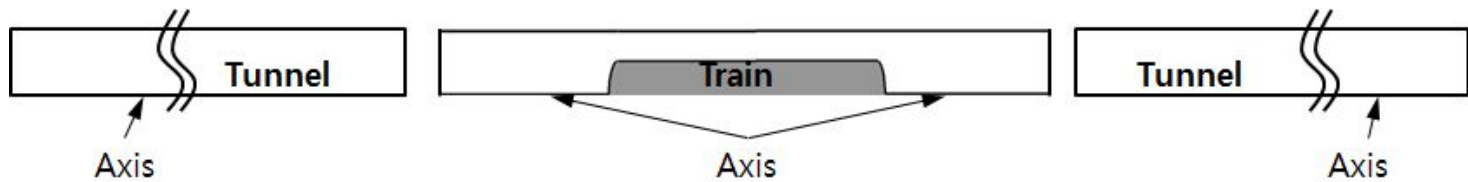


Fig. 5 Divided domains for the modeling of the train running

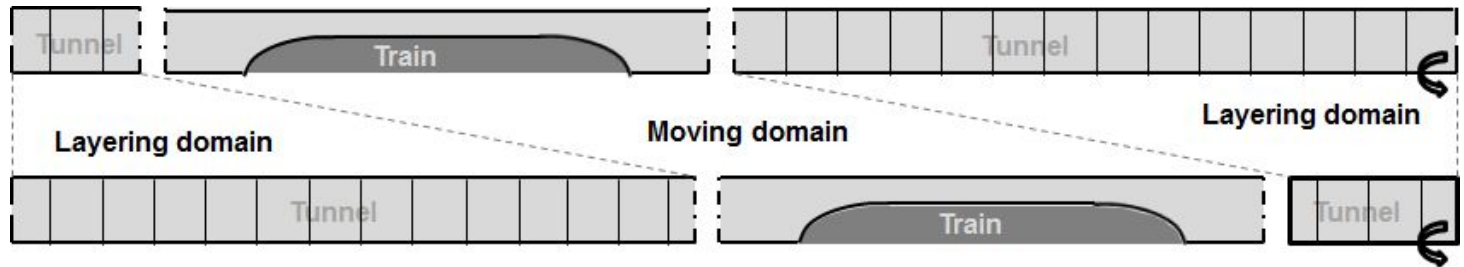


Fig. 6 Layering method for the modeling of the train running

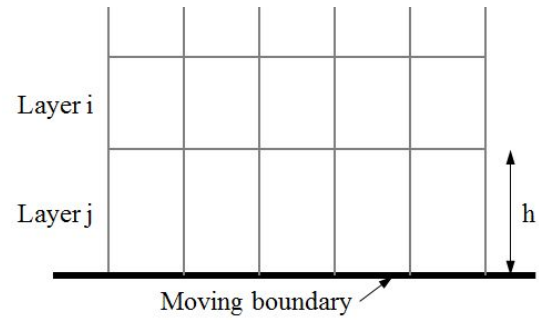


Fig. 7 Dynamic Layering

3.1.4 Boundary conditions

Boundary conditions are applied at the domain based on the physical phenomenon (Fig. 8). When the train runs as scheduled, the center domain also moves with the train. The velocity in accordance with the schedule was applied to the train wall. No-slip condition is applied at the tunnel wall. The axisymmetric condition is applied to the bottom line which is the axis of the domain. The pressure wave is generated and propagated when the train is moving. However, the pressure wave should not reflect at the end of the domain. A non-reflecting boundary condition is applied to the right and left side of the domain to prevent the reflection of the pressure wave.

In the shaft cases, the no-slip condition at the tunnel wall is changed to the interface condition (Fig. 9). The interface condition is also applied at the bottom line of the shaft meeting with the tunnel wall. The pressure far-field boundary condition is applied at the upper line of the shaft because the shaft is connected to the atmosphere.

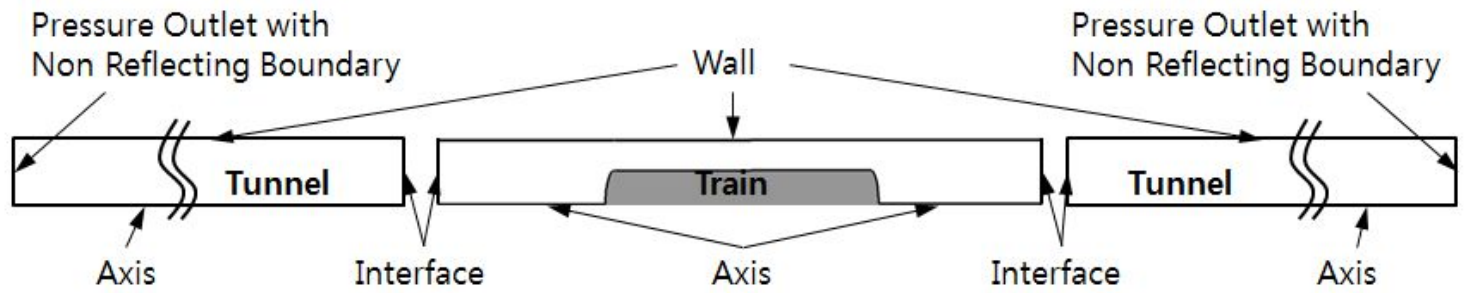


Fig. 8 Boundary conditions of the train-tunnel domain

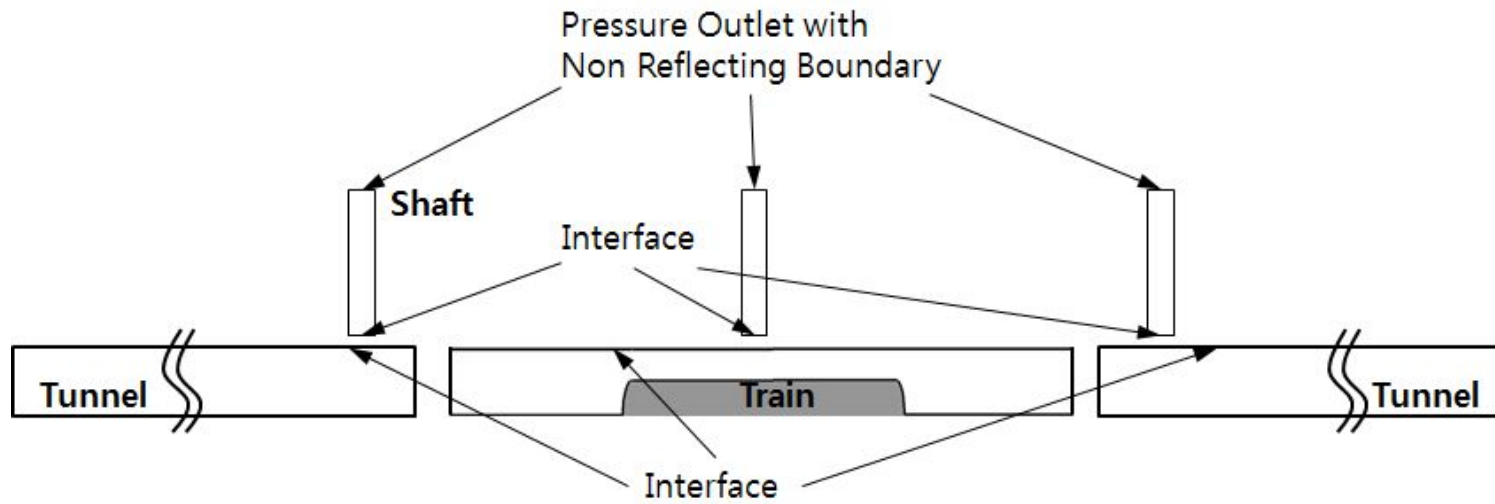


Fig. 9 Boundary conditions of the train-tunnel domain with shafts

3.2. Validation cases

3.2.1 Compression wave generated by the entry of a high-speed train into a tunnel

Experiment result of Maeda et al. [13, 25, 28] is used for the validation of axisymmetric method. Maeda et al. carried out pressure measurements on a reduced scale model to study the influence of the nose shape of the train on the initial compression wave. The prediction of the initial compression wave is important because it is related to the magnitude of the micro pressure wave at the tunnel portal.

The influence of three nose shapes (conical, parabolic and elliptic) on the initial compression wave generated by the entry of the train into a tunnel is studied with a reduced scale model in the experiment (Fig. 10). The body of the reduced scale model is cylindrical. A pressure sensor is located 1 m from the entrance of the cylindrical tunnel. The blockage ratio is 0.116 and the train is launched at 232 km/h (Mach number of 0.188) where the speed is similar to the cruise speed of the proposed GTX.

Numerical domains consist of two-dimensional axisymmetric domains due to the symmetry of the configuration. Because the train starts in an open field, the far field domain is added to the domain in the only tunnel domain (Fig. 11). The mesh independence test is performed with the parabolic profile before comparing the numerical results with the experiment results (Fig. 12). The grid points are resized to one fourth and four times points based on a (540x50) mesh for the mesh independence test. The jump of the pressure is compared to each other (Fig. 12(a)). The result of (540x50) mesh is similar to the (1080x100) mesh. However, the result of the (270x25) mesh is different

from the others. Therefore, the (540x50) mesh is chosen for this study (Fig. 12(b)).

The jumps and gradients of pressure measured at the pressure sensor is compared with the experimental result (Fig. 13). The graph and maxima presented in Tables (Table 1 and 2) show a good agreement between the computational results and the experimental data. The errors on the compression wave do not exceed 7%. The errors of this study are similar with the numerical results of Uystepuyst et al. [20]. The geometrical discontinuity of the conical nose between the nose and body implies this important error.

The pressure gradients are changed in accordance with the nose shape. The pressure rise by the blunt shape (ellipse shape) is faster than the pressure rise by the relatively sharp shape (circular cone and parabola shape) because the high pressure at the nose acts on the wider area of the ellipse shape than the others when the train enters in the tunnel. Thus, the ellipse shape reaches the pressure maxima first.

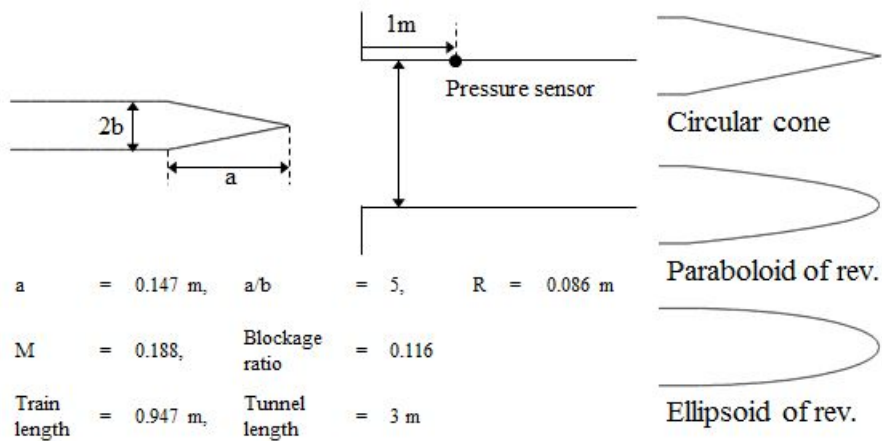


Fig. 10 Geometry data and nose shapes

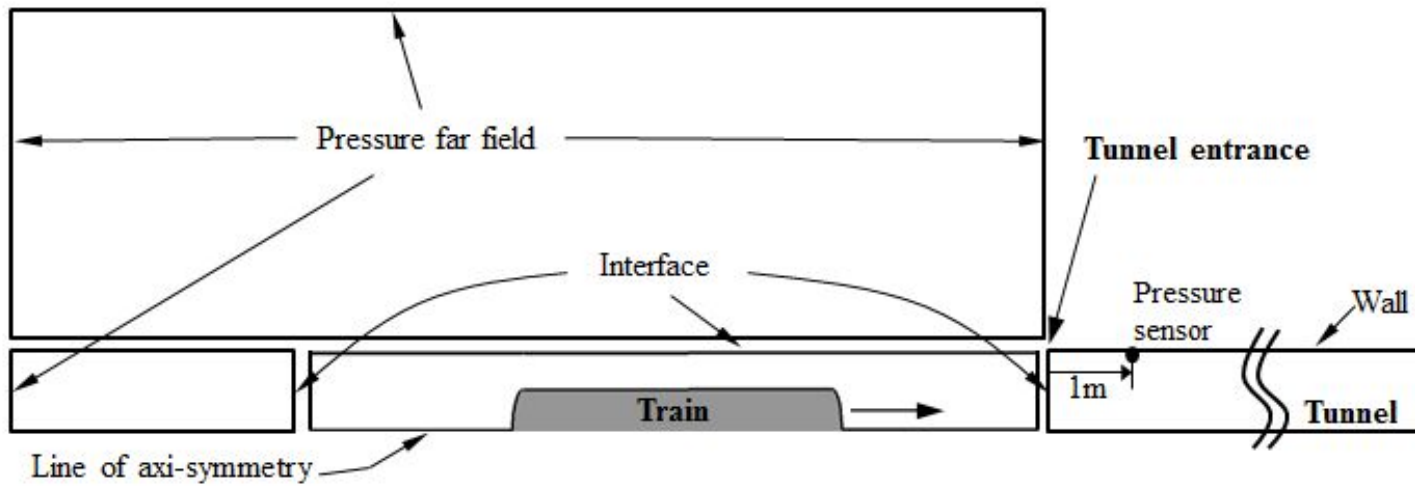


Fig. 11 Domains and boundary conditions for the validation

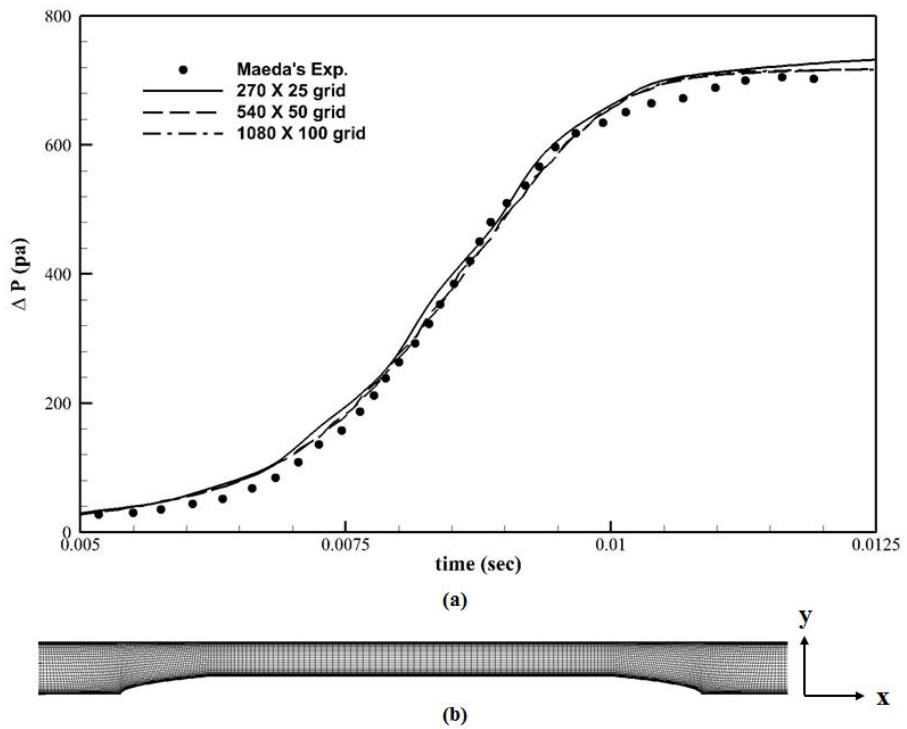


Fig. 12 Mesh independence study:

(a) Mesh independence results with experimental data [13],

(b) Resolution of (540x50) mesh

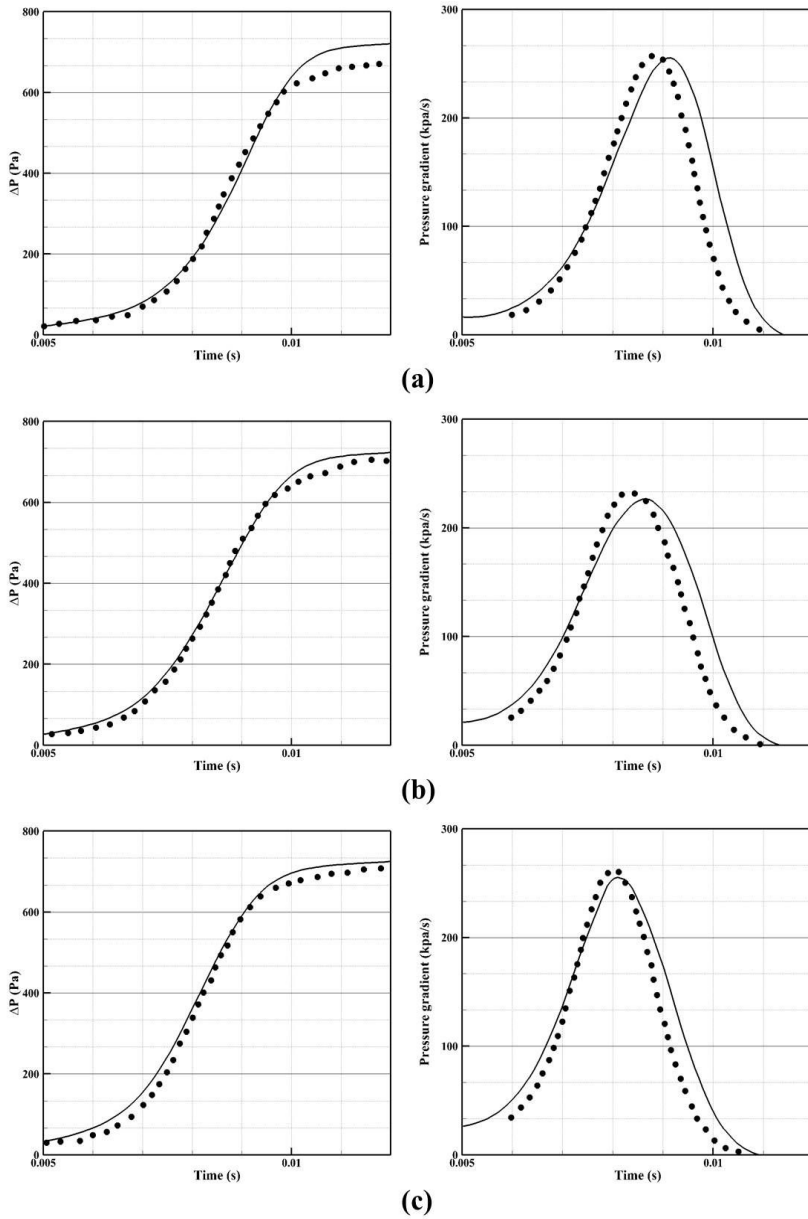


Fig. 13 Comparison of jumps (left) and gradients (right) of pressure for the three shapes of the nose;
 (a):circular cone, (b):paraboloid of rev., (c):ellipsoid of rev.,
 —:numerical results, ···: experimental results [13]

Table 1 Pressure maxima and relative error

Shape	ΔP_{\max}	
	Value (Pa)	(Num.-Exp.)/Exp. (%)
<i>Circular cone</i>		
Maeda, 1993 (Exp.)	660	
Uystepuyst et al., 2011 (Num.)	702	+6
Present study (Num.)	710	+7
<i>Paraboloid of rev.</i>		
Maeda, 1993 (Exp.)	684	
Uystepuyst et al., 2011 (Num.)	712	+4
Present study (Num.)	710	+3
<i>Ellipsoid of rev.</i>		
Maeda, 1993 (Exp.)	689	
Uystepuyst et al., 2011 (Num.)	717	+4
Present study (Num.)	715	+3

Table 2 Maxima of pressure gradient and relative error

Shape	$(\partial P/\partial t)_{\max}$	
	Value (kPa/s)	(Num.-Exp.)/Exp. (%)
<i>Circular cone</i>		
Maeda, 1993 (Exp.)	255	
Uystepuyst et al., 2011 (Num.)	265	+4
Present study (Num.)	255	0
<i>Paraboloid of rev.</i>		
Maeda, 1993 (Exp.)	232	
Uystepuyst et al., 2011 (Num.)	229	-1
Present study (Num.)	227	-2
<i>Ellipsoid of rev.</i>		
Maeda, 1993 (Exp.)	262	
Uystepuyst et al., 2011 (Num.)	259	-1
Present study (Num.)	256	-2

3.2.2 Pressure wave propagation in tunnels-I: 1/164th scale model

The validation of pressure wave propagation is performed with 1/164th scale model experiment (Fig. 14). The experiment for train-tunnel interaction was conducted at the moving model test rig (T3F, Train Tunnel Test Facility) of NLR (National Aerospace Laboratory, Netherlands) to measure the pressure transient and the micro pressure wave for various parameters such as the train speed, the train-tunnel blockage ratio and the nose shape [23, 26]. An experiment result among them is used to validate the axisymmetric method. Table 3 shows the configuration data for the validation case. Pressure is measured at three points in the tunnel: 1.87 m, 4.55 m and 6.24 m.

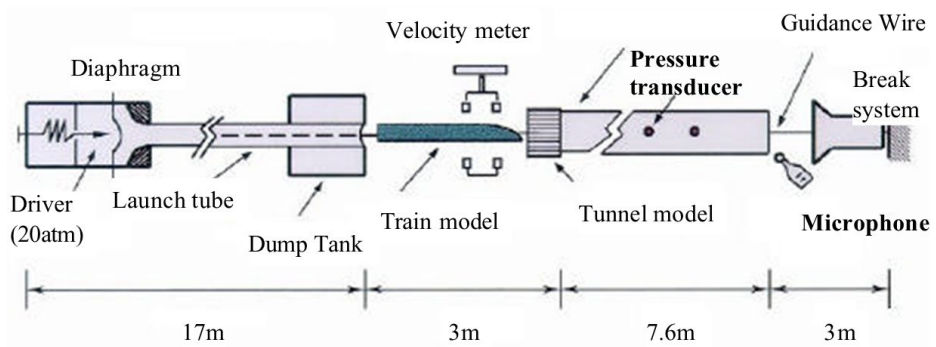


Fig. 14 Experimental setup of Train Tunnel Test Facility (T3F) in NLR

Table 3 Configuration of 1/164th Scale model

1/164th scale model configuration	
Train length	2.34 m
Tunnel length	7.64 m
Blockage ratio	0.081
Train speed	350 km/h
Diameter of train	20 mm
Nose slenderness	11.25

The simulation domain is composed with the configuration data of experiment. Far field domains are added to the left and right of the train-tunnel domain (Fig. 15). Pressure is measured to compare with the experiment data at the same three points.

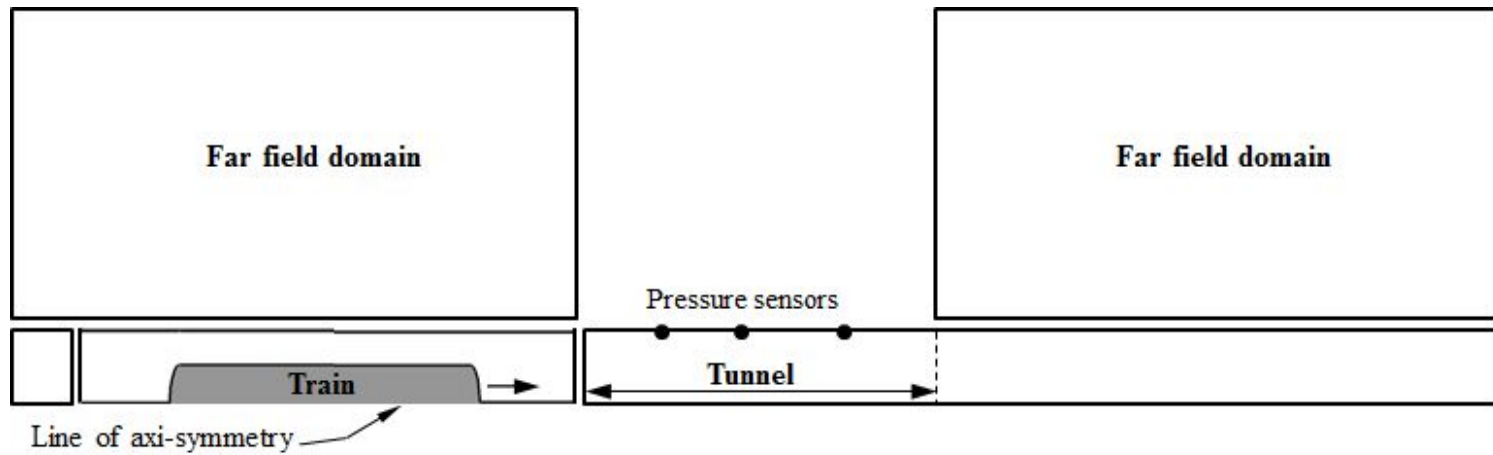


Fig. 15 Schematic domain for the validation of 1/164th scale model

The numerical results at three points are compared with the experiment data (Fig. 16). When the train enters in the tunnel, pressure rapidly jumps and gradually increases. After entering the train, pressure generated by the train propagates to the portal and the pressure whose phase is changed reflects at the portal. Thus, the values of pressure history measured in the tunnel show the positive and negative values. The graph shows a good agreement between the computational results and the experiment data.

There is a small pressure difference between 0.08 s and 0.1 s in Fig. 16(c). The similar phenomena exists in the reference paper. In the paper, the reason was explained that the train speed in the experiment seems to be underestimated to yield these discrepancies. A very small difference of the train speed can cause the difference in propagation time of pressure wave generated by the train. The pressure generated by the train having a small difference in speed affects the interference among the pressure waves existing in the tunnel. Thus, the pressure difference in the period seems to be caused in this condition.

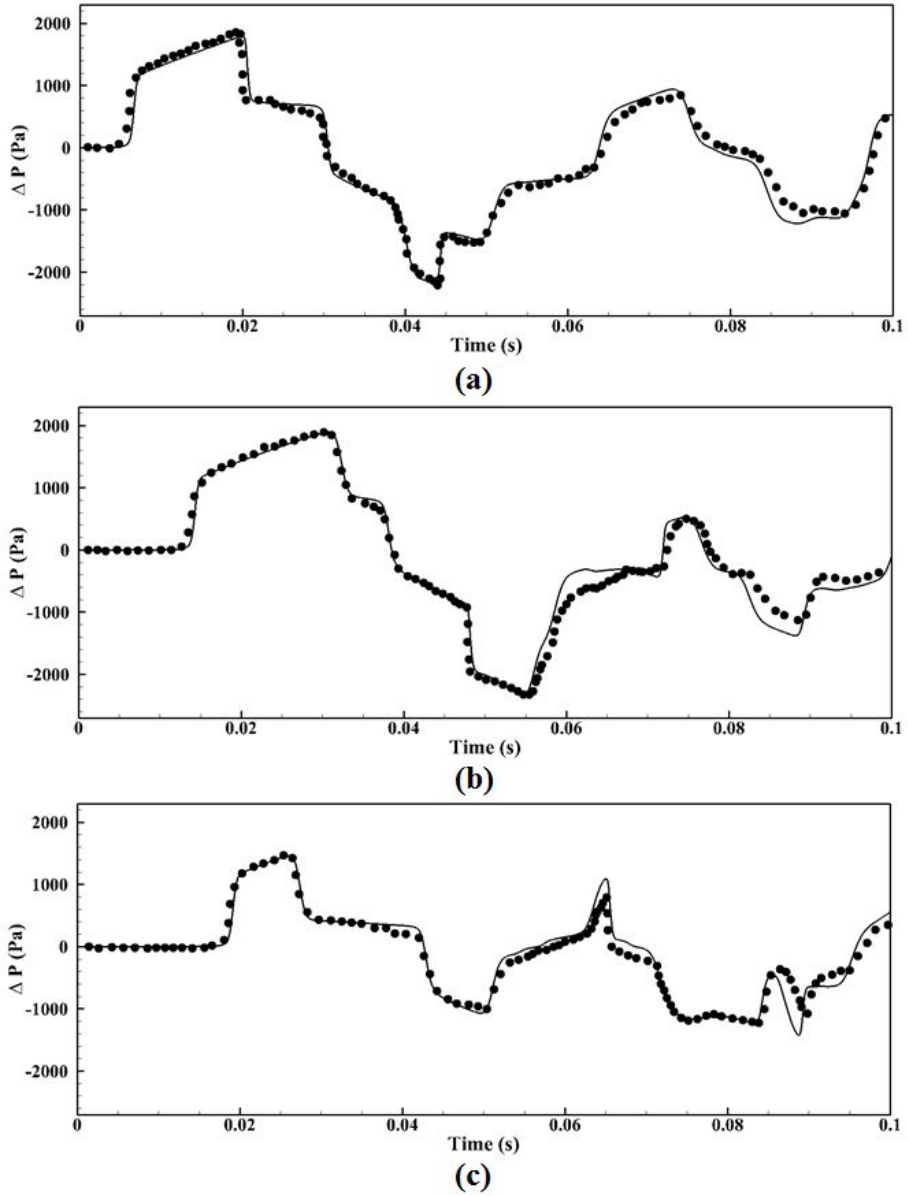


Fig. 16 Comparison of pressure history on the tunnel between the experiment and numerical results (— : present simulation results, ··· : experimental results [23]):
 (a) 1.87 m, (b) 4.55 m, (c) 6.24 m

3.2.3 Pressure wave propagation in tunnels-II: Emmequerung tunnel

The pressure data measured in the tunnel which is in Switzerland is compared with the numerical results for the validation [24, 27]. The tunnel is on a railway line SBB 2000. The measurements were undertaken in October 2004 during commissioning trials for the railway. SBB 2000 is a railway in Switzerland enabling trains to travel at 200 km/h. The tunnels have airshafts to provide pressure relief. SBB decided to assess the effectiveness of the shafts by measuring pressures on board trains during some of the commissioning trials. The usefulness of the axisymmetric method with the shafts is tested through comparing the actual measurement results with the numerical results.

Emmequerung tunnel is in Switzerland, about 20 km north-east of Berne. It is approximately 1.6 km long and has two airshafts (Fig. 17 and 18). The airflow measurements were made at the top of the south airshaft, which is approximately 542 m from the south portal. In addition, pressure measurements were made at a location about 462 m from the south portal (i.e. 80 m before the shaft). The tunnel cross-section is uniform in the region under consideration. Its perimeter and cross sectional area are approximately 33.7 m and 75.9 m² respectively. The wall surface is smooth concrete. The cross sectional area of the south shaft is 12.25 m². However, there was no information regarding the geometrical configurations, i.e. location and cross-sectional area, of the North Vent Shaft. The test train was an ETR 470 Pendolino (Cisalpino) manufactured by Astom. It had 9 units including the power cars at each end and its total length was 236.5 m. Its cross sectional area is 10 m². One test among the tests in regard to several speeds was selected for the validation. The result at 204 km/h is

selected because its speed is similar with GTX.

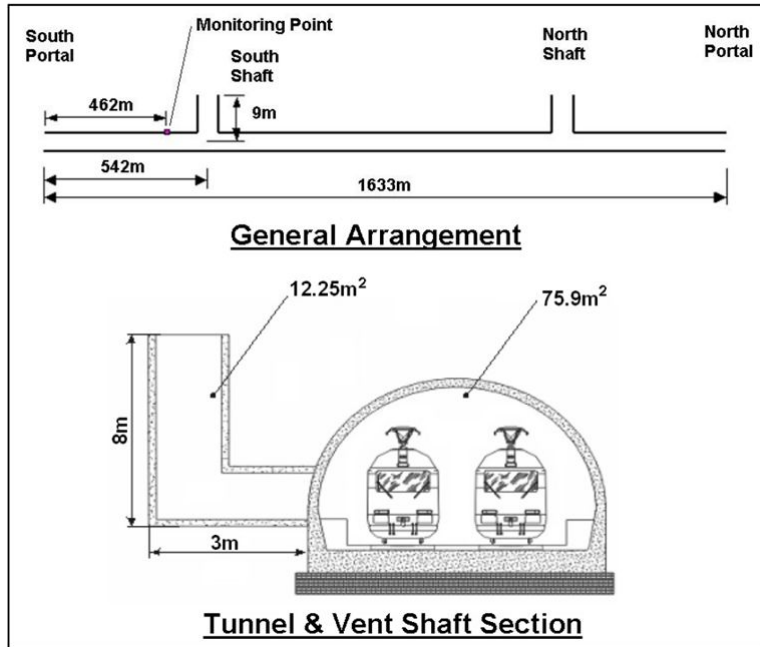


Fig. 17 Emmequerung Tunnel and Vent Shaft Configurations [27]

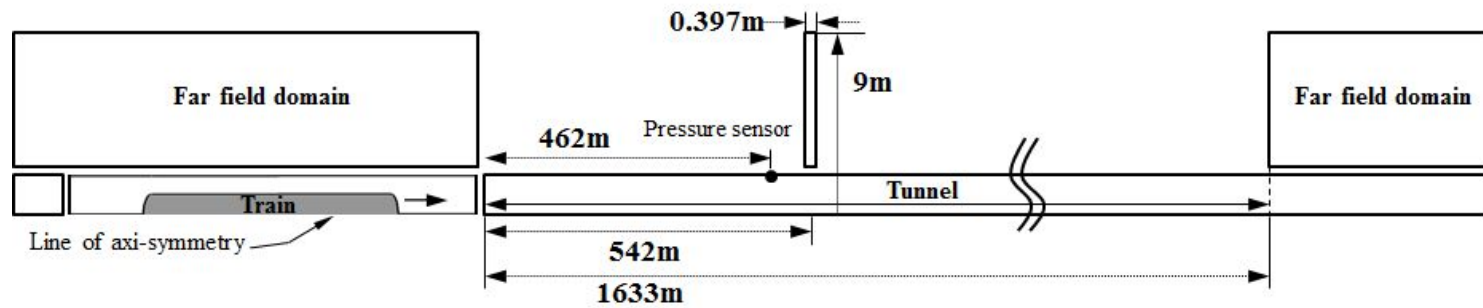


Fig. 18 Schematic domain for the validation of Emmequerung Tunnel with Vent Shaft

The trend of pressure history is similar with each other although the actual condition is converted into the axisymmetric model (Fig. 19). The pressure rises rapidly when the train enters in the tunnel between 0 s and 2 s. After the train enters in the tunnel between 2 s and 4 s, the pressure drops and rises a little. This phenomena is related to the shaft. The pressure wave by the train entry propagates to the shaft. If the pressure wave meets the shaft, the pressure wave whose phase is changed reflects to the entrance. Therefore, the pressure is dropped between 2 s and 4 s.

There is a pressure difference between the experiment result and simulation result from 8 s to 12 s. During the period, the train is passing through the monitoring point. The axi-symmetrical model using this software would not describe the flow field around the train in detail. After 12 s, the axi-symmetrical model could be good enough for predicting the pressure wave in the tunnel. This trend of the pressure is similar to the previous researcher applied the axi-symmetrical model with this software for the same simulation [27].

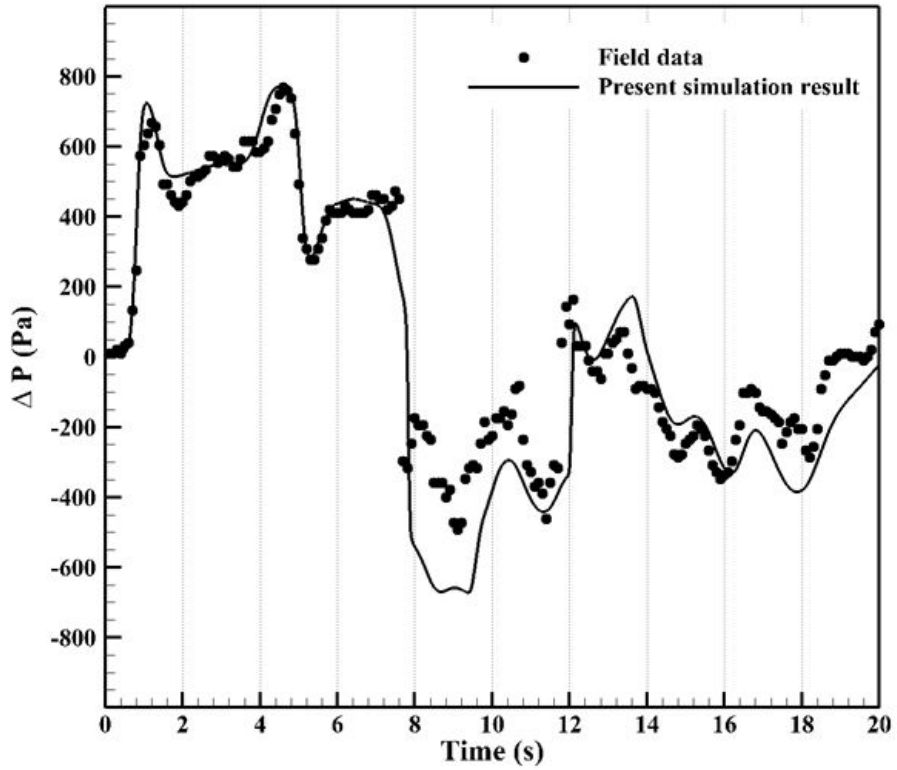


Fig. 19 Comparison of pressure history at the monitoring point for 204 km/h

4. Simulation results and analysis

4.1. Effects of design parameters in regard to aerodynamic parameters

4.1.1 Aerodynamic drag

Computation simulations are performed to identify the effects of design parameters in regard to aerodynamic drag based on Seoul Subway Line 8. The cross-sectional area and the length of the train are 12.8 m^2 and 160 m . The nose shape of the train is a blunt and square box shape as shown in Fig. 20.

The cross-sectional area of the tunnel is 45.58 m^2 [41]. To evaluate the effect of the cross-sectional area of the tunnel, tests are carried out by changing the blockage ratio from 0.281 to 0.1. The blockage ratio of 0.1 is similar to the blockage ratio of the tunnel and the Korea Train eXpress (KTX) operating in South Korea [15]. Test cases are arranged in Table 4. Changes of aerodynamic drag were identified according to the change of train speed, nose shape and tunnel cross-sectional area. Aerodynamic drag is divided into pressure drag and viscous drag and they are evaluated to identify the effect of aerodynamic parameters respectively.

Fig. 21 shows train run schedules according to the train speed. In the base model case, the acceleration is $+1 \text{ m/s}^2$. Thus, it takes 27.78 s to reach a cruise speed of 27.78 m/s (100 km/h). After reaching the cruise speed, the train maintains 27.78 m/s for 30 s , and then decelerates at -1 m/s^2 for 27.78 s until it stops. The total time of the train schedule is 85.56 s . The cruise, acceleration and deceleration times

are applied equally to the other case simulations. However, the cruise speed for the other cases is 55.56 m/s (200 km/h), which is the cruise speed of the proposed GTX. The simulation takes 141.12 s from the beginning to the end for the other cases applying this speed. The tunnel length is 5,960 m, and is similar to the average distance between the stations of the GTX.



Fig. 20 Train blunt nose shape of Seoul Subway Line 8

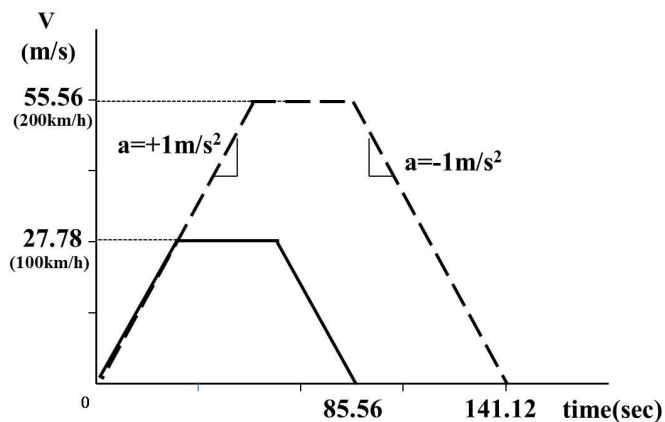
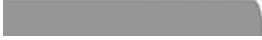








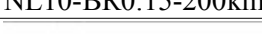


Fig. 21 Schedules of train run in accordance with cruise speed: 100 km/h (—), 200 km/h (---)

Table 4 Simulation cases for aerodynamic drag analysis

Train-tunnel configuration	Nose length (m)	Tunnel diameter (m)	Blockage ratio	Max. velocity (km/h)
 NL0.5-BR0.281-100km/h	0.5	7.62	0.281	100
 NL0.5-BR0.281-200km/h	0.5	7.62	0.281	200
 NL1-BR0.281-200km/h	1.0	7.62	0.281	200
 NL2-BR0.281-200km/h	2.0	7.62	0.281	200
 NL5-BR0.281-200km/h	5.0	7.62	0.281	200
 NL10-BR0.281-200km/h	10.0	7.62	0.281	200
 NL10-BR0.25-200km/h	10.0	8.08	0.25	200
 NL10-BR0.2-200km/h	10.0	9.04	0.2	200
 NL10-BR0.15-200km/h	10.0	10.44	0.15	200
 NL10-BR0.1-200km/h	10.0	12.78	0.1	200

4.1.1.1 Effect of speed increase

The results of 100 km/h and 200 km/h are compared to identify the effect of the speed increase. Fig. 22 shows the drag histories according to the speed increase of the base model. The trend of aerodynamic drag history is similar for the 100 km/h configuration and 200 km/h configuration. In the acceleration region, the total aerodynamic drag increases and the drag history curve is a parabolic shape until the train reaches the constant speed region. In the deceleration region, the total drag decreases and the drag history curve illustrates a parabola as in the acceleration region. The negative drag occurs at the end of the deceleration region. Even though the train decelerates, the flow behind the tail of the train has inertia. Because of the inertia, the flow strikes the tail of the train. Therefore, the pressure of the tail is higher than the nose. This pressure distribution results in the negative drag at the end of the deceleration region.

The drag values at the center of the constant speed section is used to analyse the drag increase because the drag is the maximum drag during the train running (Fig. 23). When the train speed increases from 100 km/h to 200 km/h, total drag increases significantly from 15,910 N to 52,220 N (about 3.3 times). Pressure drag and viscous drag are increased together. Pressure drag increases about 3.1 times and viscous drag increases about 3.7 times.

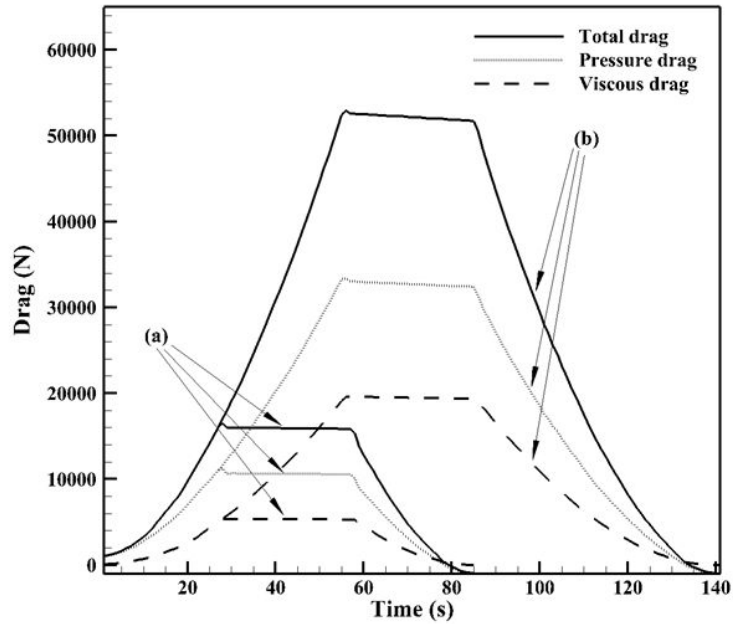


Fig. 22 Comparison of the drag histories according to an increase in speed: (a) 100 km/h, (b) 200 km/h

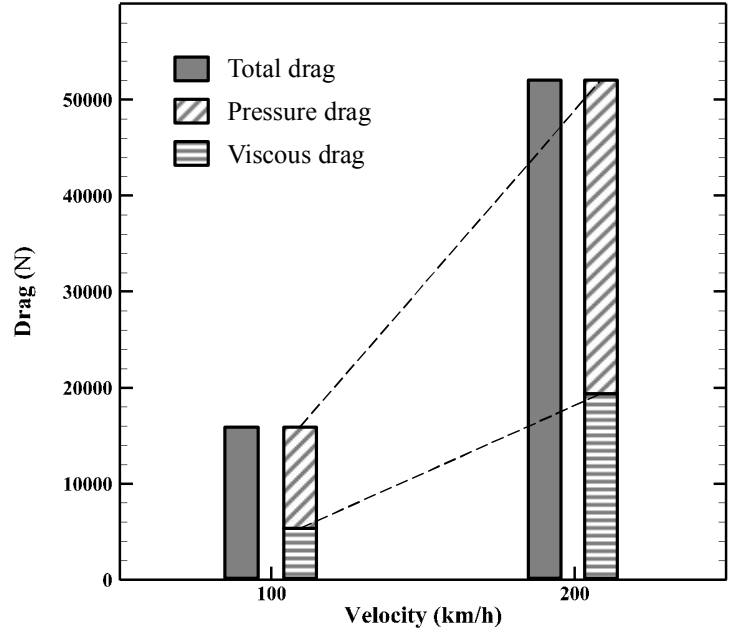


Fig. 23 Comparison of the drags according to an increase in speed

Pressure distribution (Fig. 24) and pressure contour (Fig. 25) are compared to analyze the increase of pressure drag. Pressure drag is related to the pressure difference between the head and tail. The pressure of the head in 200 km/h is higher than The pressure in 100 km/h. And the pressure of the tail in 200 km/h is lower than the pressure in 100 km/h. This pressure differences also can be identified from the pressure contour.

Pressure coefficient (C_p) on the train surface between 100 km/h and 200 km/h is compared to analyze the flow characteristic in accordance with the velocity. Pressure coefficient is calculated by

$$C_p = \frac{p - p_\infty}{\frac{1}{2} \rho_\infty V_{train}^2}$$

where V_{train} represents the maximum cruise speed of the train. Thus, V_{train} according to the train speed is 100 km/h and 200 km/h respectively.

The pressure coefficient distribution on the train surface with regard to the speed increase is almost the same (Fig. 26). There is no big difference of the flow characteristic between 100 km/h and 200 km/h. Because the pressure coefficient is almost the same, the value of surface pressure is lower in proportion to the square of the operating speed. This characteristic is identified in Fig. 24.

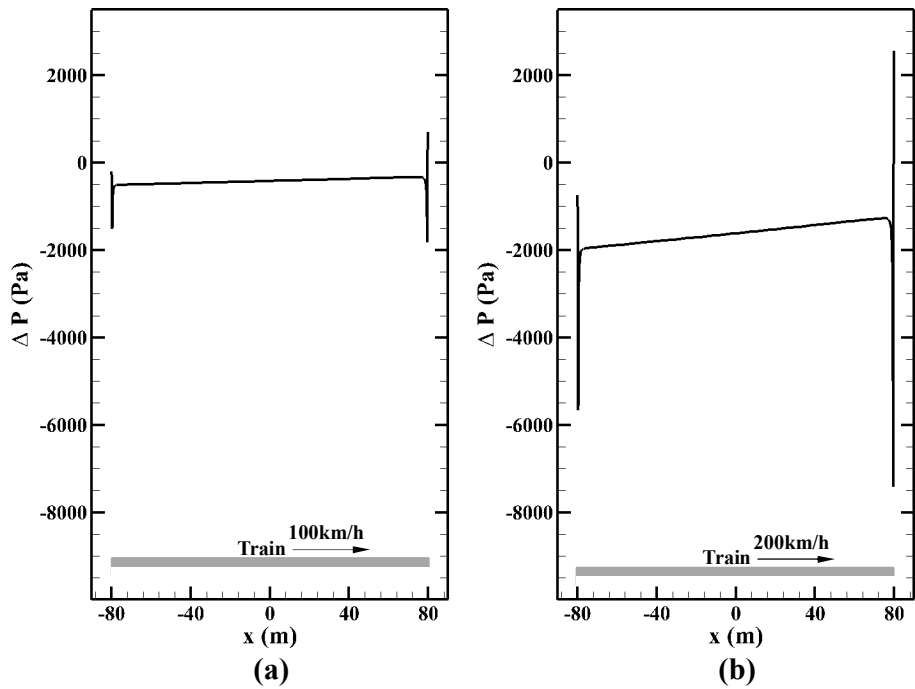


Fig. 24 Comparison of the surface pressures at the center of the constant speed section: (a) 100 km/h, (b) 200 km/h

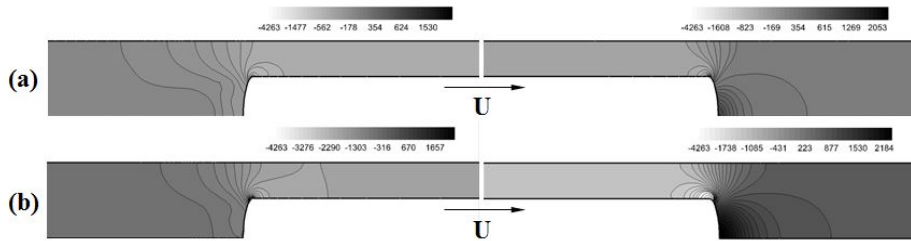


Fig. 25 Comparison of the pressure contours around the head and tail: (a) 100 km/h, (b) 200 km/h

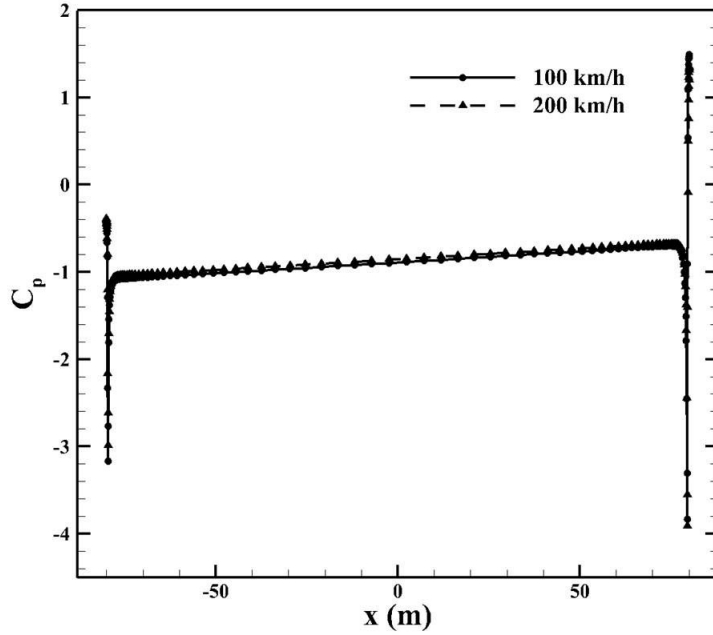


Fig. 26 Pressure coefficient on the train surface with respect to the speed increase

The velocity profile and wall shear stress (τ_w) are compared to analyze the increase of viscous drag. Viscous drag is related to the velocity profile near the train wall [1]. The wall shear stress is proportional to the velocity gradient in the y -direction, $\tau_w \propto (\partial u / \partial y)_{y=0}$. Therefore, the velocity profiles including the boundary layer near the wall, $(\partial u / \partial y)_{y=0}$, are compared to analyze the viscous drag qualitatively. The wall shear stress is used to compare with the increase of viscous drag quantitatively.

Fig. 27 shows the velocity profile between the train wall and the tunnel wall. By the way, the scale difference among the train speed (U_{train}), flow velocity and distance between the train and tunnel (Δy) is large. Therefore, it is difficult to compare with the velocity profiles. To

compare with them easily, the velocity profile and distance are normalized by the train cruise speed (U_{train}) and distance (Δy) from the tunnel to the train.

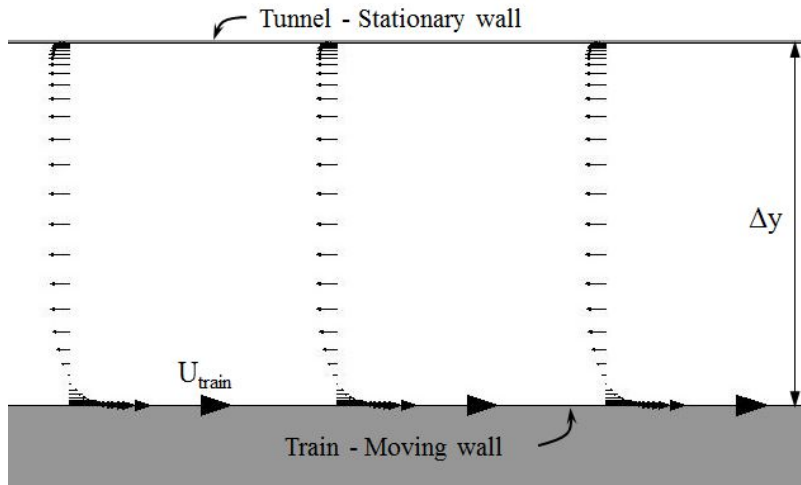


Fig. 27 Velocity profile between the train and tunnel walls

As the velocity profiles of two cases (100 km/h and 200 km/h) are compared with each other, the maximum velocity of 200 km/h is faster than that of 100 km/h (Fig. 28) since the same amount of fluid should move in a short time. It can be assumed that the shear stress of the 200 km/h is bigger than that of 100 km/h because the velocity slope near the train wall is steep. Shear stresses near the train wall are directly compared in accordance with the increase of the train speed (Table 5). Shear stress of 200 km/h are about 3 times larger than that of 100 km/h.

Skin friction coefficient and normalized velocity profile by the respective speeds are compared to analyze the flow characteristic according to the speed increase. The skin friction coefficients are

similar to each other although the wall shear stress of 200 km/h is bigger than that of 100 km/h (Table 5). And the normalized velocity profiles by the respective speeds are also similar to each other (Fig. 29). The flow characteristics are identified that are similar to each other within velocity range from 100 km/h to 200 km/h.

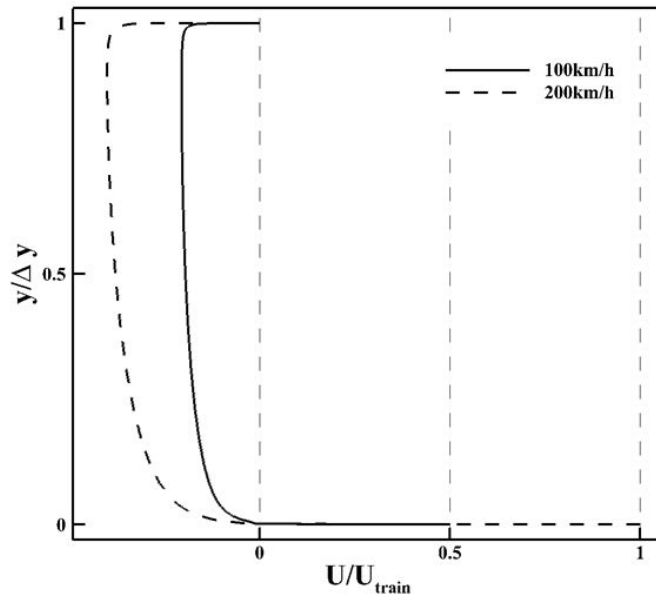


Fig. 28 Comparison of the normalized velocity profiles by the same train speed ($U_{\text{train}} = 200$ km/h) between 100 km/h and 200 km/h

Table 5 Wall shear stress according to the train speed

Train-tunnel configuration	Train speed (km/h)	Wall shear stress (Pa)	Skin friction coefficient (C_f)
NL0.5-BR0.281-100km/h	100	2.576	5.449×10^{-3}
NL0.5-BR0.281-200km/h	200	9.519	5.034×10^{-3}

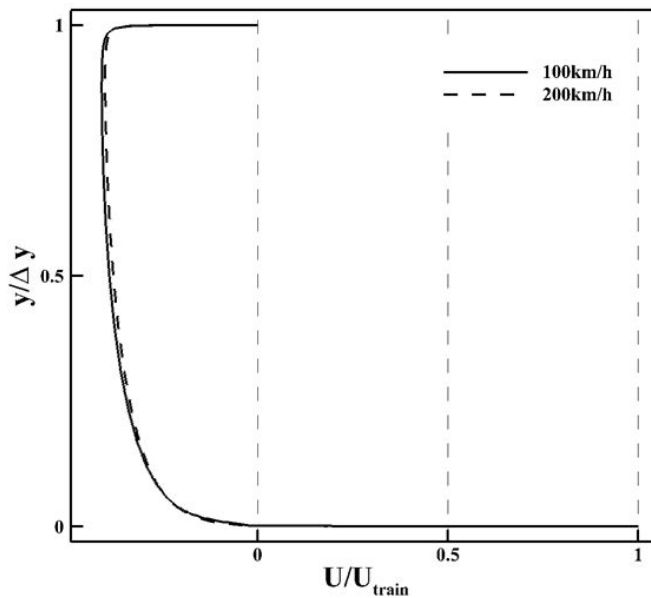


Fig. 29 Comparison of the normalized velocity profile by the respective speeds (100 km/h and 200 km/h)

4.1.1.2 Effect of nose shape

The results that the nose length is from 0.5 m to 10 m are compared to identify the effect of the nose shape (Fig. 30). When the nose length increases, total drag decreases from 52,550 N to 30,165 N

(a decrease of about 43 %). Pressure drag also decreases like total drag. However, the viscous drag of 0.5 m is the same as the others.

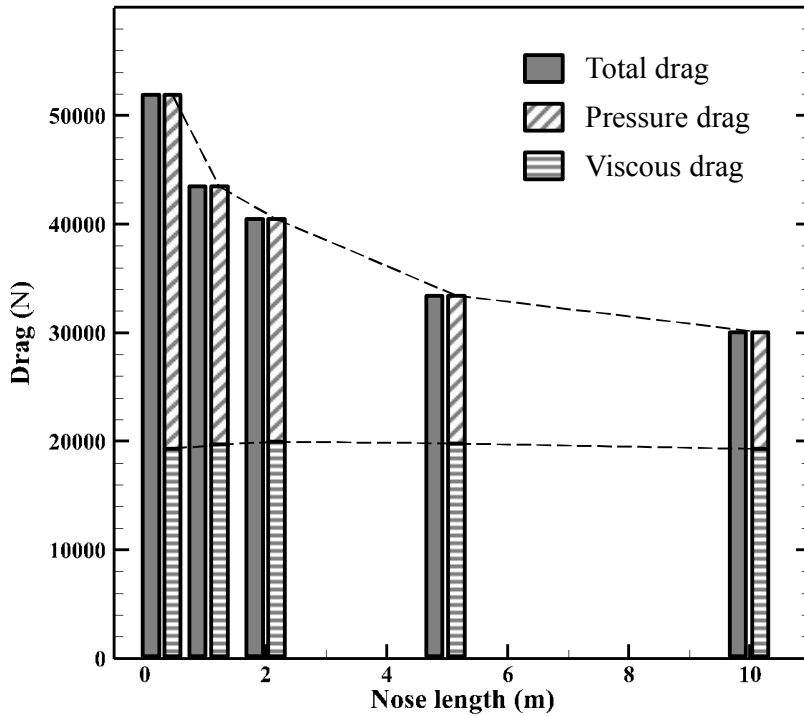


Fig. 30 Comparison of the drags according to the nose length

Pressure distribution and pressure contour are compared to analyze the decrease of pressure drag. Although the blunt shape is changed into the streamlined shape, the maximum pressure at the head is the same as each other (Fig. 31). But the pressure at the tail is recovered after the nose shape is changed to the streamlined shape. Thus, the pressure difference between the head and tail is reduced.

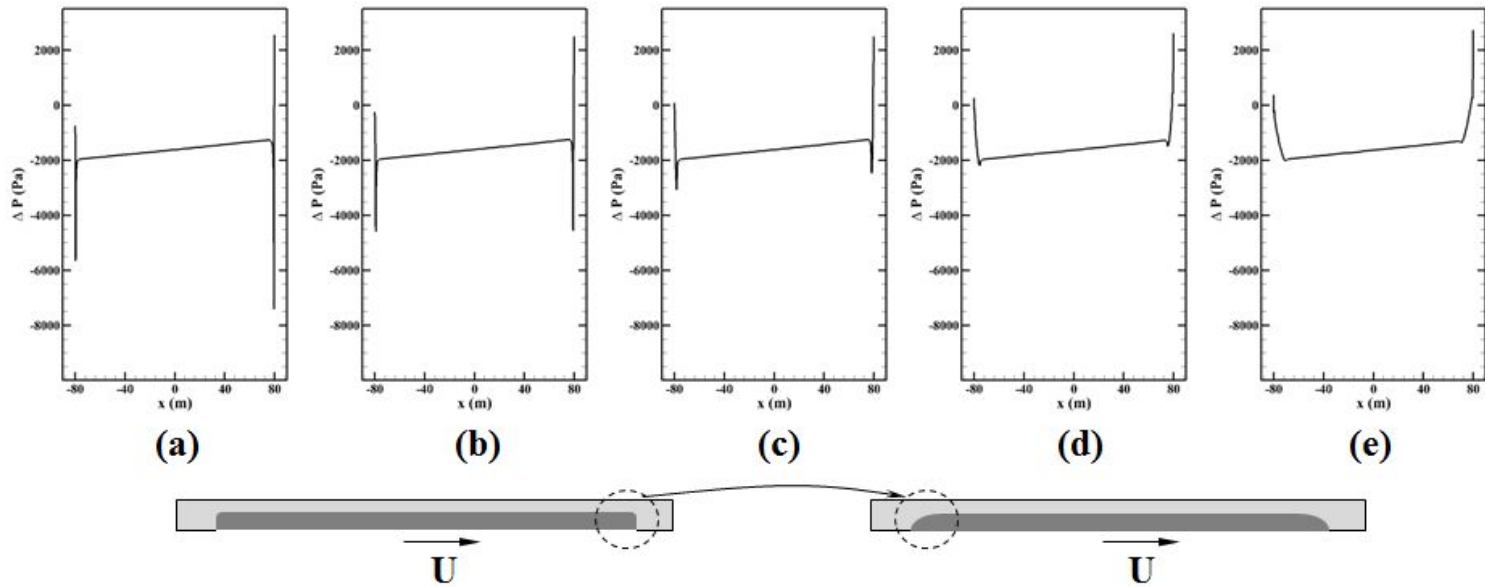


Fig. 31 Comparison of the surface pressures according to the nose length at the center of the constant speed section: (a) 0.5 m, (b) 1 m, (c) 2 m, (d) 5 m, (e) 10 m

High pressure is affecting at the wide region of the head in 0.5 m case (Fig. 32). On the other hand, high pressure is affecting at the small region of the head in 10 m case. Even though the magnitude of high pressure is almost the same as each other, the area at which high pressure is affecting is small. And the pressure at the tail of the streamlined shape is recovered more than that of the blunt shape. Therefore, pressure drag is reduced in accordance with the change of the nose shape.

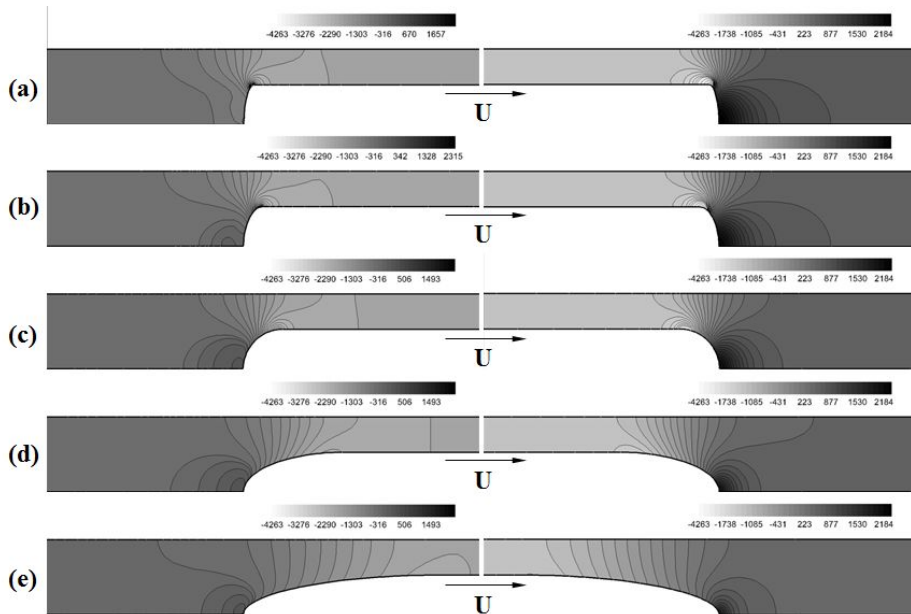


Fig. 32 Comparison of the pressure contours around the head and tail according to the nose length:

(a) 0.5 m, (b) 1 m, (c) 2 m, (d) 5 m, (e) 10 m

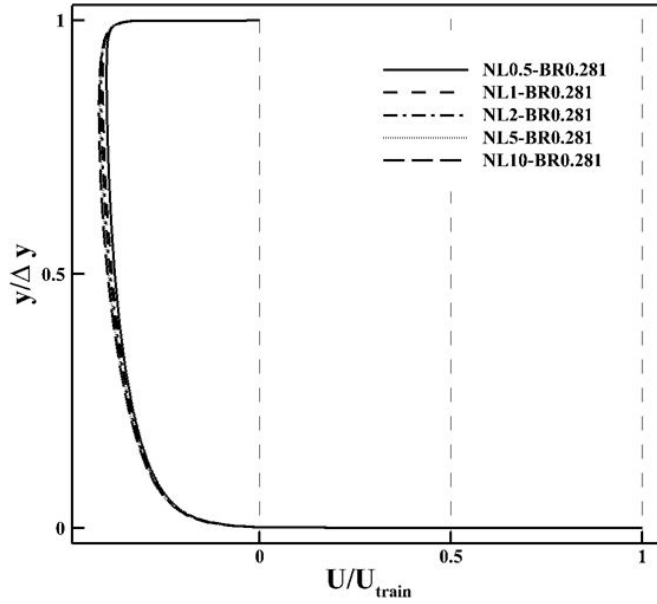


Fig. 33 Comparison of the normalized velocity profiles according to the nose length

Table 6 Wall shear stress according to the nose length

Train-tunnel configuration	Nose length (m)	Wall shear stress (Pa)	Skin friction coefficient (C_f)
NL0.5-BR0.281-200km/h	0.5	9.519	5.034×10^{-3}
NL1 -BR0.281-200km/h	1	9.609	5.082×10^{-3}
NL2 -BR0.281-200km/h	2	9.653	5.105×10^{-3}
NL5 -BR0.281-200km/h	5	9.690	5.124×10^{-3}
NL10-BR0.281-200km/h	10	9.713	5.140×10^{-3}

The velocity profile and shear stress are compared to analyze the trend that is little change in spite of the change of the nose shape (Fig. 33). The maximum velocity and velocity profiles are similar to each other. It can be assumed that the shear stress near the train wall

is also similar to each other. This trend is also shown in Table 6. Although the nose shape is changed into the streamlined shape, the shear stress near the train wall is changed little unlike the case of the speed increase.

4.1.1.3 Effect of tunnel cross-sectional area

The results that the blockage ratio is from 0.281 to 0.1 are compared to identify the effect of the tunnel cross-sectional area (Fig. 34). When the tunnel cross-sectional area increases, total drag decreases from 30,165 N to 15,983 N (a decrease of about 47 %). Pressure and viscous drag decrease together. However, the effect of the cross-sectional area against the drag decrease is rapidly reduced after the blockage is 0.15.

Pressure distribution (Fig. 35) and pressure contour (Fig. 36) are compared to analyze the decrease of pressure drag. The maximum pressure at the head decreases a little and the maximum pressure at the tail is also recovered a little. Although the difference of the maximum pressure between the head and tail is not reduced significantly, the pressure difference acting on the surface of the head and tail is reduced considerably. As the pressure distribution at the middle of the train is compared with each other, there is a definite change at the middle of the train. The pressure around the tail is lower than that around the head along the train body in the case of the blockage ratio, 0.281. But the pressure difference along the train body from the head to the tail is reduced significantly in the case of the blockage ratio, 0.1. This trend can be found in pressure contour.

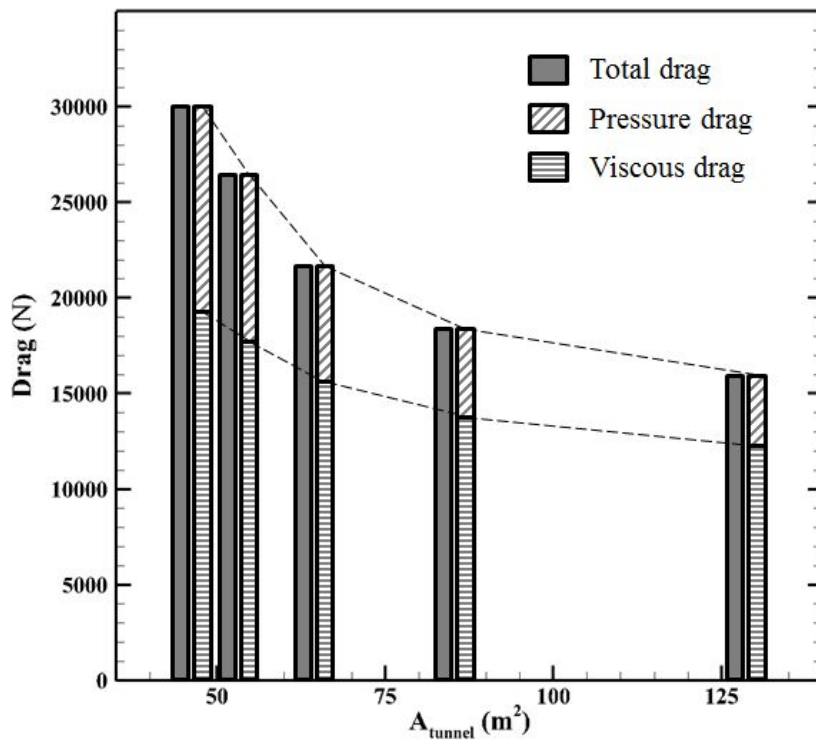


Fig. 34 Comparison of the drags according to the tunnel cross-sectional area

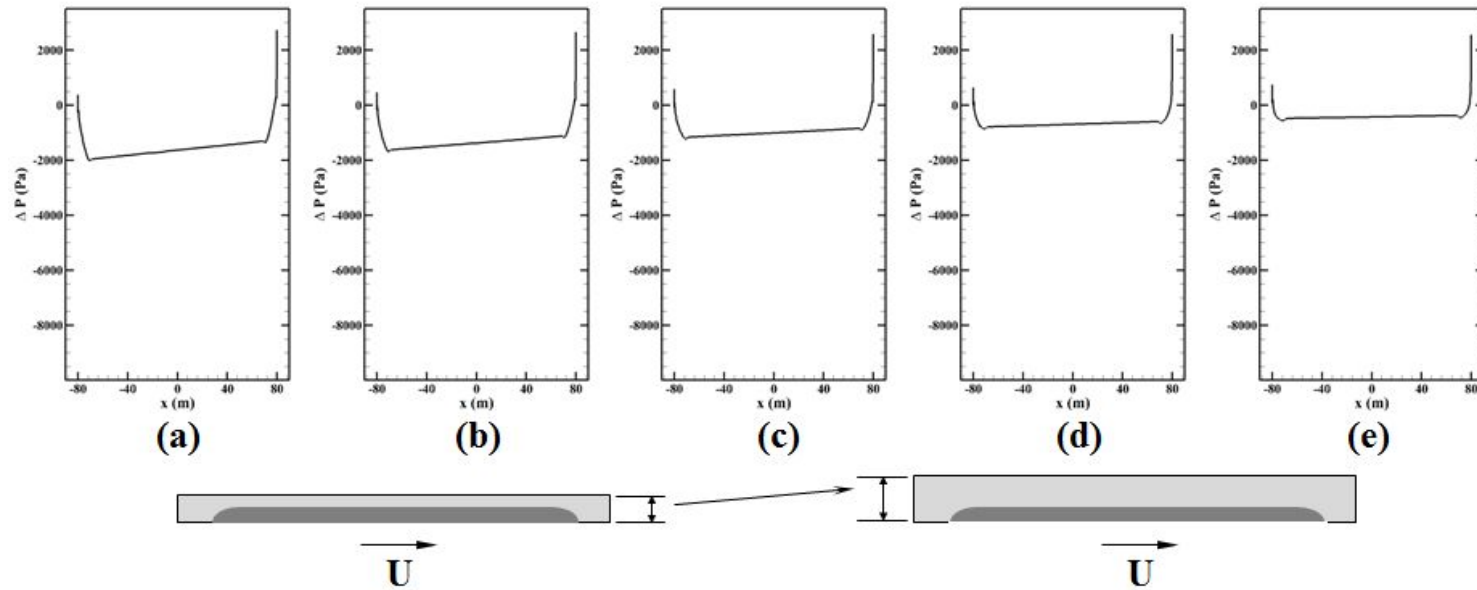


Fig. 35 Comparison of the surface pressures according to the blockage ratio (β) at the center of the constant speed section: (a) $\beta=0.281$, (b) $\beta=0.25$, (c) $\beta=0.2$, (d) $\beta=0.15$, (e) $\beta=0.1$

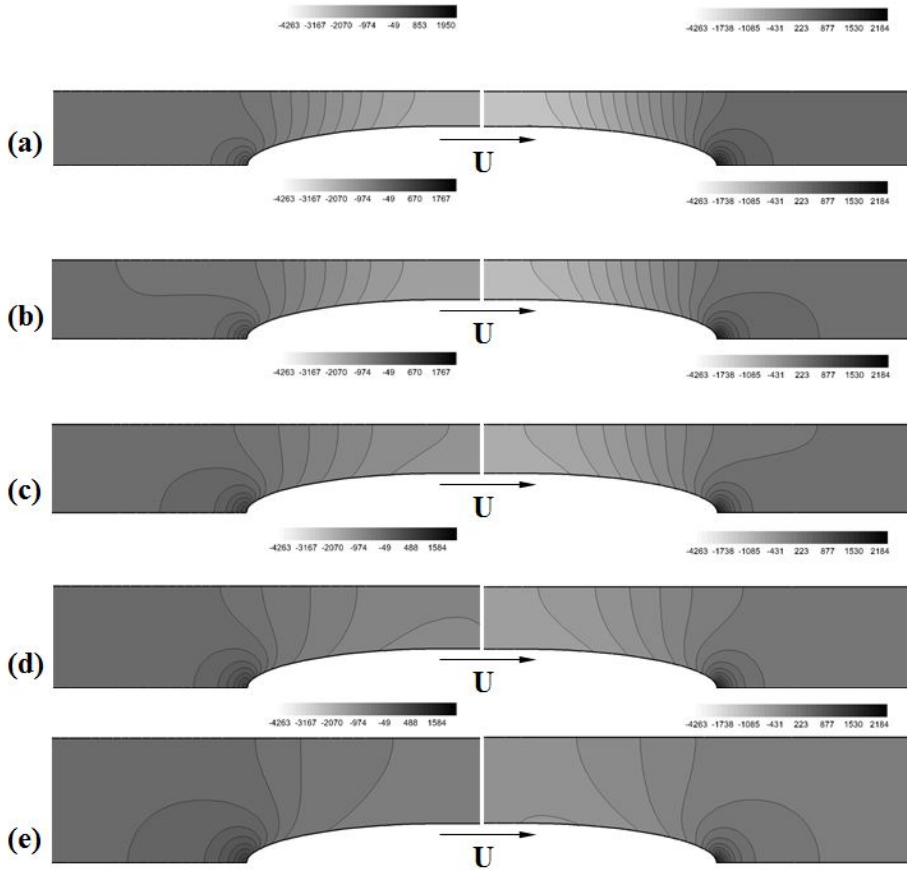


Fig. 36 Comparison of the pressure contours around the head and tail according to the blockage ratio :

(a) $\beta=0.281$, (b) $\beta=0.25$, (c) $\beta=0.2$, (d) $\beta=0.15$, (e) $\beta=0.1$

The velocity profile and shear stress are compared to analyze the decrease trend of the viscous drag (Fig. 37). The maximum velocity becomes slow as the tunnel cross-sectional area increases. It means that the velocity gradient and shear stress near the train wall are reduced together. Table 7 shows the decrease of the shear stress directly. However, the decrease rate of the shear stress is reduced as compared with the increase rate of the tunnel cross-sectional area. Skin friction

coefficient clearly reduces in accordance with the tunnel cross-sectional area unlike the previous aerodynamic parameters (velocity increase and nose length).

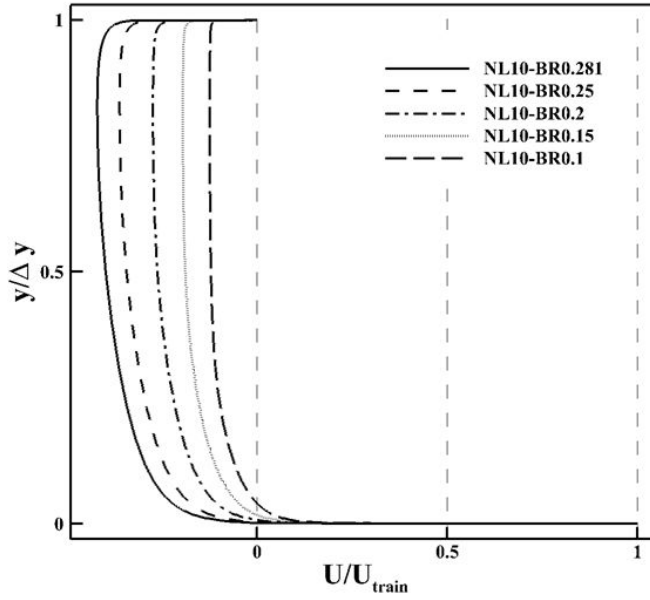


Fig. 37 Comparison of the normalized velocity profiles according to the blockage ratio

Table 7 Wall shear stress according to the blockage ratio

Train-tunnel configuration	Cross-sectional area (m ²)	Wall shear stress (Pa)	Skin friction coefficient (C _f)
NL10-BR0.281-200km/h	45.62	9.713	5.140×10 ⁻³
NL10-BR0.25 -200km/h	51.25	8.911	4.712×10 ⁻³
NL10-BR0.2 -200km/h	64.09	7.781	4.115×10 ⁻³
NL10-BR0.15 -200km/h	85.46	6.820	3.607×10 ⁻³
NL10-BR0.1 -200km/h	128.19	6.090	3.220×10 ⁻³

In addition, the total drag of the train whose nose length is 5 m in the blockage ratio, 0.1, is compared with the total aerodynamic drag measured for the Transrapid 07 whose nose length is about 5 m. The total drag of the train is simulated as 20,986 *N*. A 52 m long Transrapid 07 vehicle requires a power of 3.1 MW at 400 km/h to overcome aerodynamic drag in an open field [2]. Because the total aerodynamic power is calculated by $W_{total} = (D_p + D_v)U_t$, the total drag can be found using an inverse operation. D_p and D_v represent the pressure drag and the viscous drag respectively. Supposing that total drag increases in proportion to the square of the operating speed, that pressure drag is 10% of the total drag and that friction drag is a linear function of train length, the total drag for a 160 m long Transrapid could be estimated to be approximately 20,012 *N*. This result has the same order of magnitude as the value obtained by the total drag (20,986 *N*) of the train with a 0.5 m nose length simulated additionally where aerodynamic drag is maybe overestimated because of the train is surrounded by the tunnel wall.

4.1.2 Wind pressure on platform screen door

Computation simulations were performed to identify the effects of design parameters in regard to wind pressure on platform screen door based on Seoul Subway Line 8. Changes of wind pressure were identified in accordance with the change of the train speed, nose shape and tunnel cross-sectional area in the same with the aerodynamic drag. Because trains run together and there are shafts in the actual system, in addition, two tests are added: two trains travelling in tunnels and a train travelling in tunnels with shafts (Table 9). The results are evaluated by the design criteria of platform screen door. Fig. 38

indicates the measurement points according to the simulation cases.

The wind pressure is evaluated on the quality certification criteria of the platform screen door (Table 8). The platform screen door should stand the fatigue load (500 N/m^2) and maximum pressure load ($2,649 \text{ N/m}^2$). This criteria is related to the present subway whose speed is 100 km/h. Thus, it should be verified that the wind pressure by GTX whose speed is 200 km/h is below the criteria for the passenger safety.

Table 8 Design criteria of platform screen door (allowable horizontal load) [51]

Half height type	Horizontal distributed load of safety wall
	: $3,679 \text{ N}$ (375 kgf) and over
	Horizontal distributed load of PSD
	: 981 N (100 kgf) and over
Full-closed type or Semi-closed type	Horizontal distributed load
	: 981 N (100 kgf) and over
	Fatigue load
	: 500 N/m^2 (51 kgf/m^2) 500,000 times and over
	Maximum wind pressure
	: $2,649 \text{ N/m}^2$ (270 kgf/m^2)
	Maximum instantaneous wind speed
	: 30 m/s (50 m/s on the ground)

Table 9 Simulation cases for wind pressure analysis

Train-tunnel configuration	Nose length (m)	Tunnel diameter (m)	Blockage ratio	Max. velocity (km/h)
NL0.5-BR0.281-100km/h	0.5	7.62	0.281	100
NL0.5-BR0.281-200km/h	0.5	7.62	0.281	200
NL1 -BR0.281-200km/h	1.0	7.62	0.281	200
NL2 -BR0.281-200km/h	2.0	7.62	0.281	200
NL5 -BR0.281-200km/h	5.0	7.62	0.281	200
NL10 -BR0.281-200km/h	10.0	7.62	0.281	200
NL10 -BR0.25 -200km/h	10.0	8.08	0.25	200
NL10 -BR0.2 -200km/h	10.0	9.04	0.2	200
NL10 -BR0.15 -200km/h	10.0	10.44	0.15	200
NL10 -BR0.1 -200km/h	10.0	12.78	0.1	200
NL0.5-BR0.281-200km/h with 2 trains	0.5	7.62	0.281	200
NL0.5-BR0.281-200km/h with 3 shafts	0.5	7.62	0.281	200

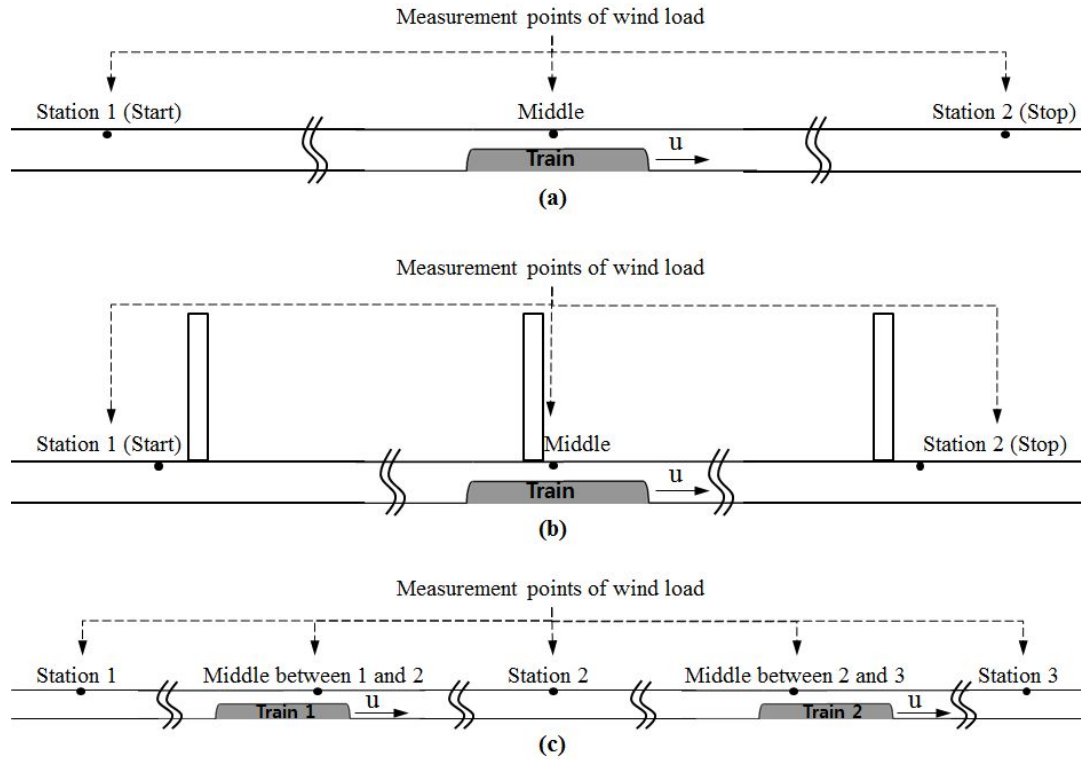


Fig. 38 Measurement points based on a simulation case:
 (a) Only tunnel case, (b) Tunnel with shafts, (c) Tunnel with two trains

4.1.2.1 Effect of speed increase

Pressure is measured at three positions: a starting station(Station 1), an arrival station(Station 2) and a middle of the tunnel(Middle) (Fig. 39). The pressure measuring at Station 1 and 2 means wind pressure acting on platform screen door as the train departs and arrives. The pressure measuring at Middle means wind pressure acting on platform screen door as the train passes by the station like a express train.

The pressure history of Station 1 and 2 has the opposite-signed pressure. Compression wave propagates through the tunnel forward and expansion wave propagates backwards. In case of a express train, the positive pressure is measured before the train is passing by the position. But the negative pressure is measured after the train is passing by the position. And the pressure is suddenly dropped into the negative pressure at the point in time when the train is passing by because the low pressure of the train surface affects the platform screen door.

The maximum of the positive and negative pressure in 100 km/h are +247 Pa and -510 Pa. And the maximum of the positive and negative pressure in 200 km/h are +795 Pa and -1967 Pa. The positive and negative pressure acting on platform screen door increases about 3.2 times and 3.9 times respectively. The pressure acting on platform screen door exceeds the fatigue load (500 Pa), though the pressure did not exceed the maximum wind pressure limit (2,649 Pa).

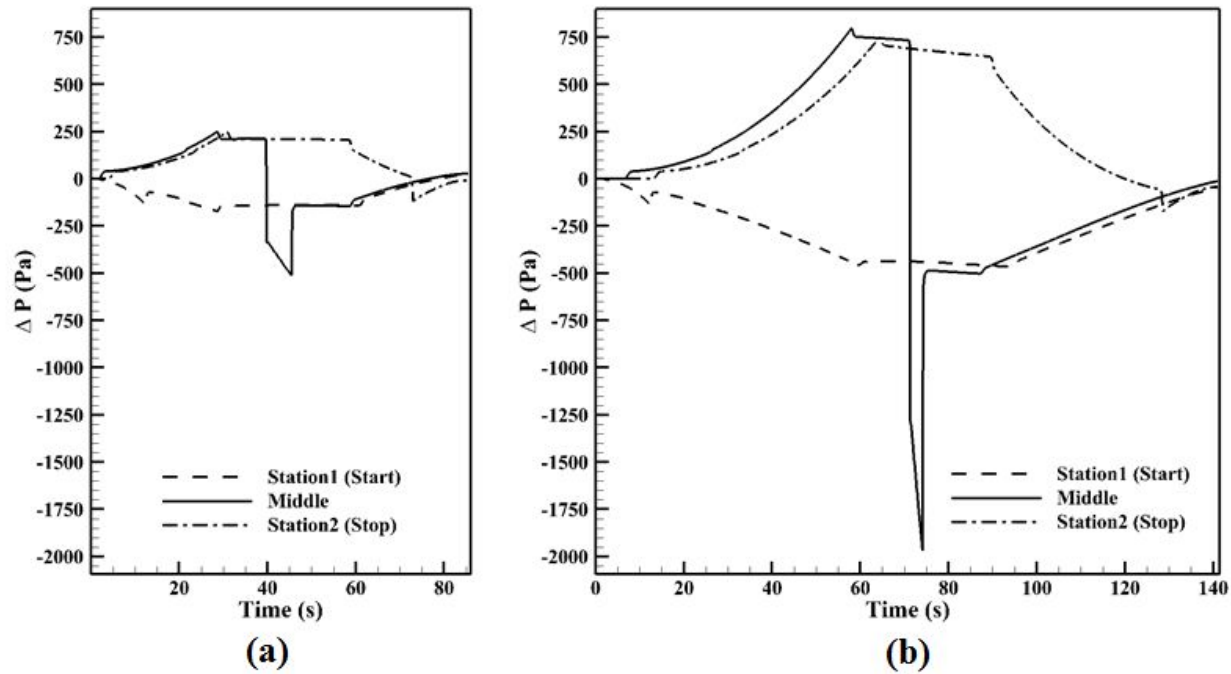
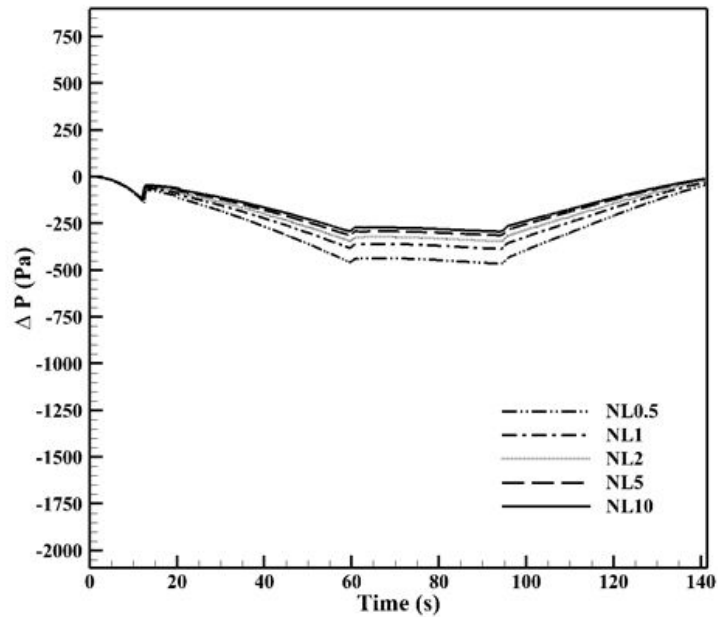


Fig. 39 Comparison of wind load on the platform screen door according to the train speed:
 (a) 100 km/h, (b) 200 km/h

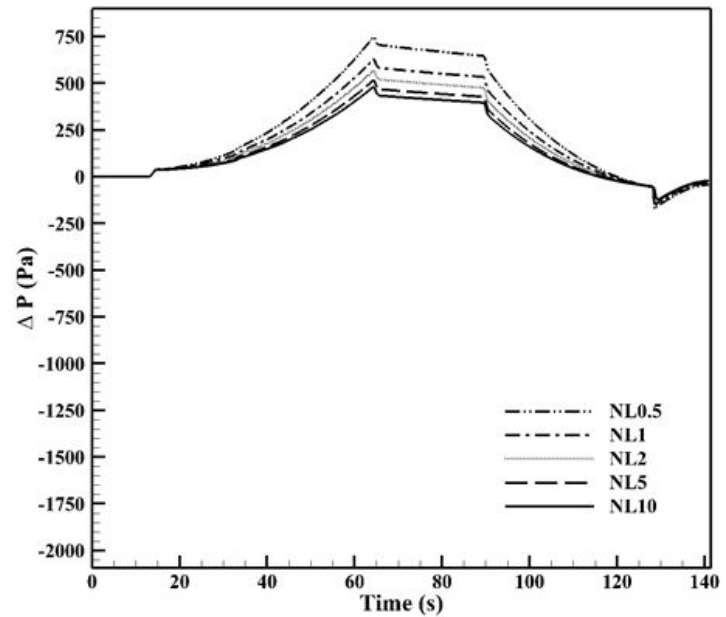
4.1.2.2 Effect of nose shape

The pressure acting on the Station 1 and 2 decreases as the nose shape is changed from the blunt shape to the streamlined shape: the maximum negative pressure (from -457 Pa to -291 Pa) and the maximum positive pressure (from $+746 \text{ Pa}$ to $+479 \text{ Pa}$) (Fig. 40). The energy propagating forward by the pressure acting on the blunt surface (0.5 m long nose) is reduced by changing to the streamlined shape (10 m long nose). The effect of the nose length is less effective between 5 m and 10 m.

A different phenomenon is observed in the case in which the pressure measured in the middle (Fig. 41). The pressure measured at the time that the train is passing by is the lowest pressure ($-1,962 \text{ Pa}$) and invariable without the nose shape. Because the pressure is not depend on the nose shape but the train speed and blockage ratio. Thus, the negative pressure acting on the platform screen door by the express train is constant unless the train speed and blockage ratio is changed.



(a)



(b)

Fig. 40 Comparison of wind load on the platform screen door according to the nose length at Station 1 and 2:
 (a) Wind load at the Station 1, (b) Wind load at the Station 2

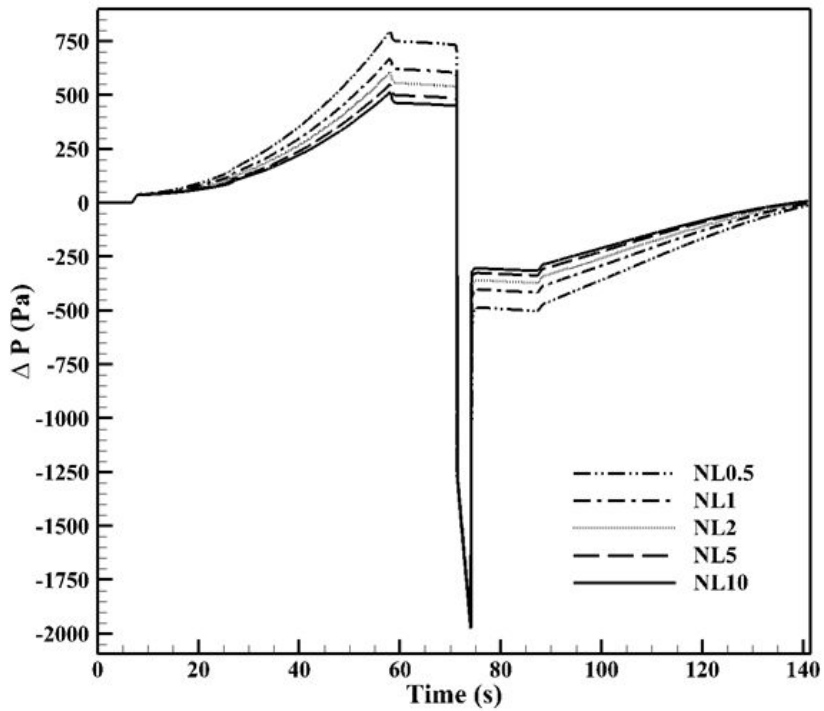


Fig. 41 Comparison of wind load on the platform screen door according to the nose length at Middle

The decreasing trend of compression wave according to the length of the ellipse nose shape in this paper is similar with a previous researcher[52]. The nose shape has a little effect when the blockage ratio is 0.1 and a/b is bigger than 1 (Fig. 42). If the tunnel cross-sectional area is big and the nose is a streamlined shape, the high pressure generated by the train is diffused in the wide area. Therefore, the strength of pressure wave propagating forward becomes weak. However, the nose shape have a great effect when the blockage ratio is 0.281 which is based on the present subway system. If the tunnel cross-sectional area is small, the high pressure generated by the train is

not diffused and is propagated forward. Thus, the strength of the pressure wave is stronger than that of the large cross-sectional area.

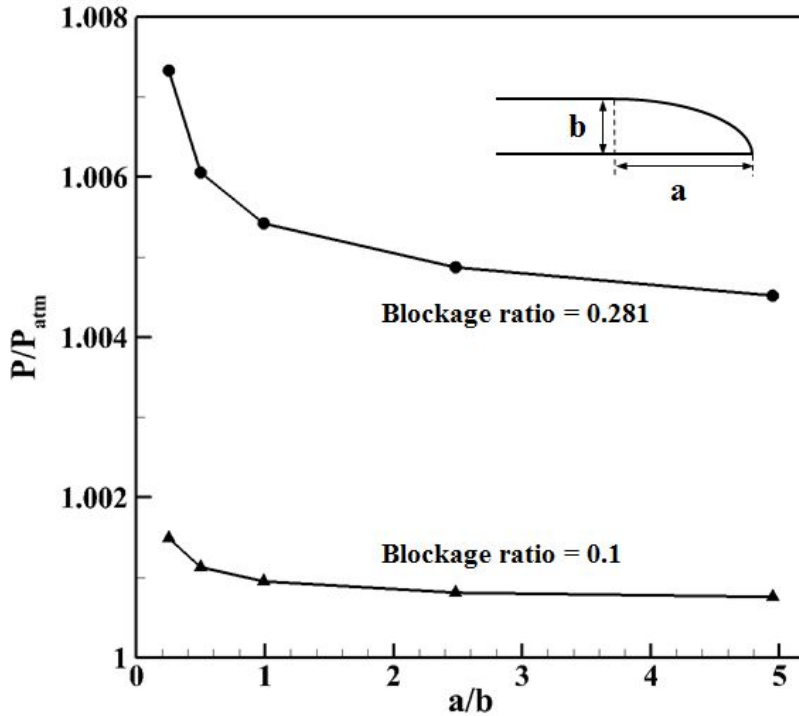


Fig. 42 Strength of compression wave in accordance with nose shape and blockage ratio

4.1.2.3 Effect of tunnel cross-sectional area

The increase of the tunnel cross-sectional area has a considerable effect to decrease the pressure. The pressure measured at the Station 1 and 2 decreases considerably: the maximum negative pressure (from $-291 Pa$ to $-51 Pa$) and the maximum positive pressure (from $+477 Pa$ to $+87 Pa$) (Fig. 43). The energy generated by the train run is diffused

by the increase of the tunnel cross-sectional area into the tunnel space. Therefore, the energy propagating forward is reduced. The safety criteria of the platform screen door is satisfied.

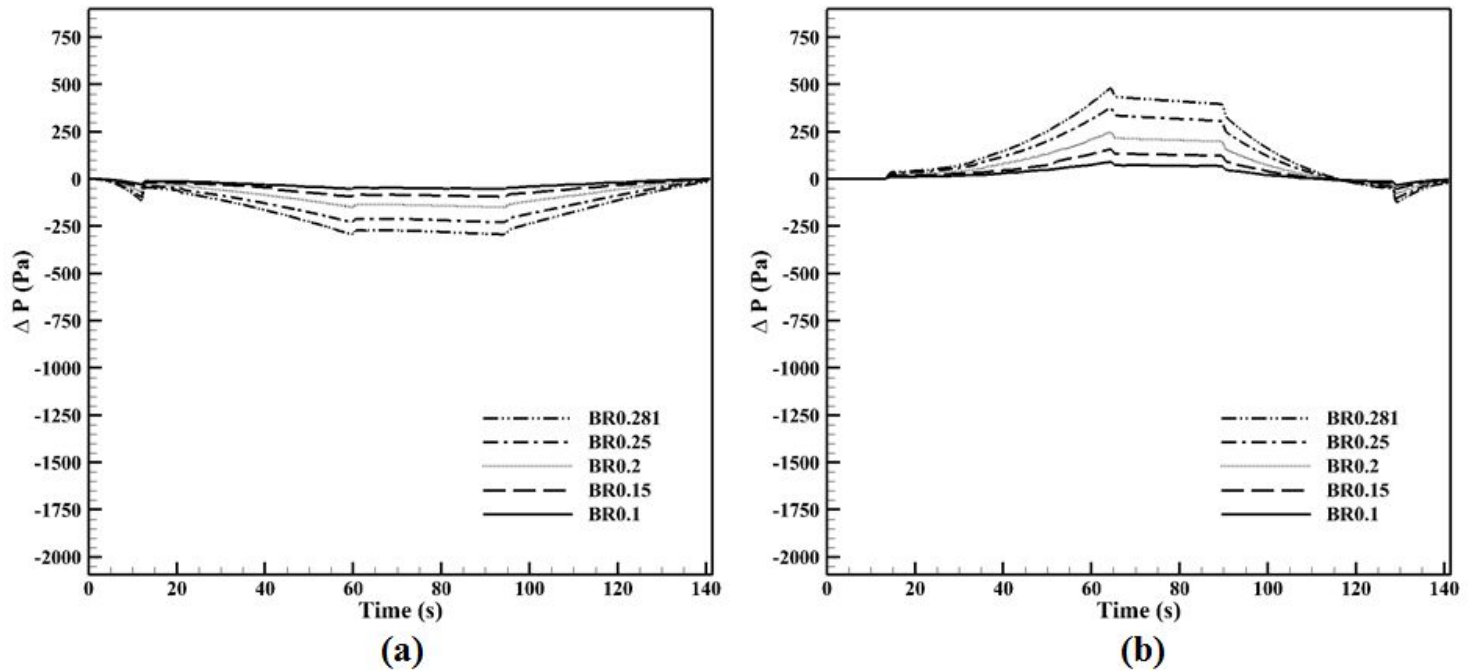


Fig. 43 Comparison of wind load on the platform screen door according to the blockage ratio at Station 1 and 2:
 (a) Wind load at the Station 1, (b) Wind load at the Station 2

The increase of the tunnel cross-sectional area is also effective in the case that the train is passing by the station. The maximum negative pressure considerably decreases from $-1,962 \text{ Pa}$ to -476 Pa (Fig. 44). Because more space that the air flows is secured by the increase of the tunnel cross-sectional area though the train speed is the same as 200 km/h . Thus, the flow speed decreases and the pressure increases. The fatigue load and maximum wind pressure are satisfied.

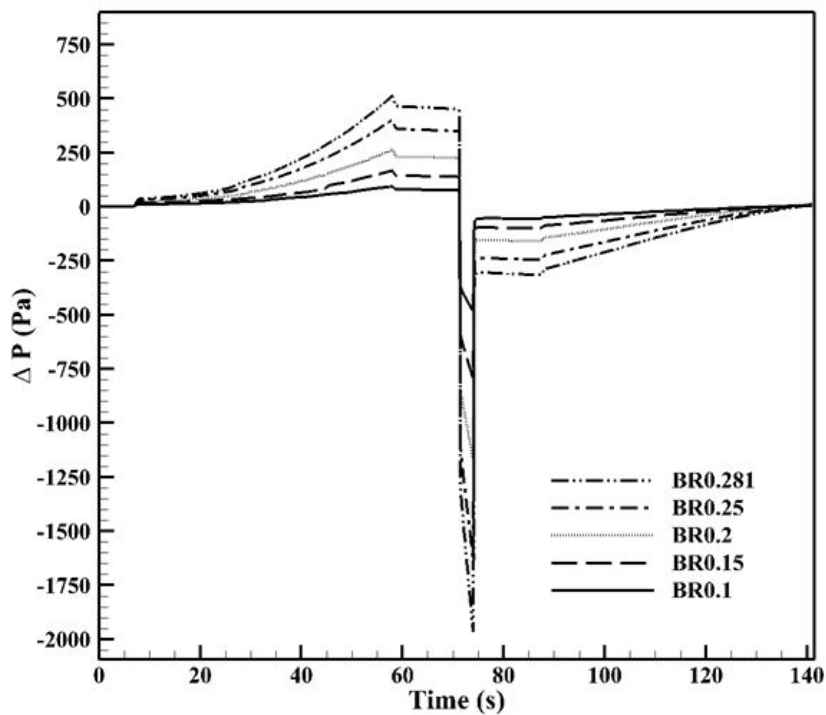


Fig. 44 Comparison of wind load on the platform screen door according to the blockage ratio at Middle

4.1.2.4 Effect of train interference

A simulation using two trains is performed to identify the interaction of the pressure wave induced by the trains. One train starts to run from Station 1 and the other train starts to run from Station 2. Pressure is measured at five points: Station 1, 2 and 3, Middle between Station 1 and 2 and Middle between Station 2 and 3.

The maximum negative pressure (-912 Pa) at Station 1 is about 2 times lower than the result (-457 Pa) of the single train run as the expansion wave propagated from the tail of two trains is overlapped each other at Station 1 (Fig. 45). A similar phenomenon is happened at Station 3. The compression wave generated by the head of two trains is overlapped each other at Station 3. The maximum positive pressure ($+1,414 \text{ Pa}$) at Station 3 is about 2 times higher than the result ($+746 \text{ Pa}$) of the single train run. However, a different phenomenon is happened at Station 2. The maximum positive pressure is lower than the result of the single train run. The compression wave generated by the following train is interfered with the expansion wave generated by the lead train. Thus, the waves are offset and the amplitude is reduced.

Two results measured at the middle of stations has a similar trend but the magnitude is different (Fig. 46). Before the train arrives at the measurement point, the pressure increases. The magnitude of the pressure at two points is different. The compression wave generated by two trains is overlapped at the middle between Station 2 and 3. But the compression wave by the following train and the expansion wave by the lead train are offset at the middle between Station 1 and 2. After the train is passing by, the pressure drops. The pressure between Station 1 and 2 is lower than that between Station 2 and 3. The expansion wave (negative pressure) by two trains is overlapped at the

middle between Station 1 and 2. But The expansion wave by the lead train and the compression wave by the following train are offset at the middle between Station 2 and 3.

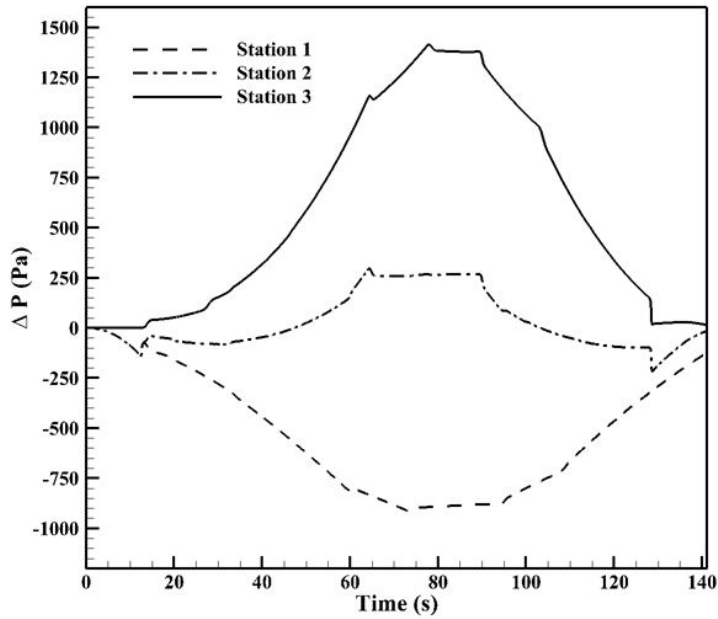


Fig. 45 Comparison of the pressure histories measured at Station 1, 2 and 3 to identify the train interference

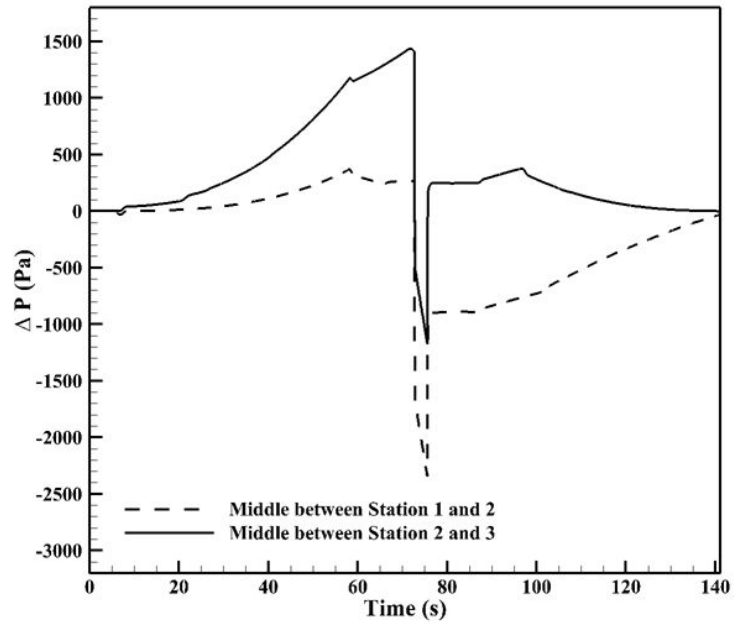


Fig. 46 Comparison of the pressure histories measured at the middle of the stations to identify the train interference

4.1.2.5 Effect of shaft

The pressure wave propagating in tunnels is reduced by the existence of the shaft (Fig. 47). The pressure which is measured at Station 2 during acceleration is lower than the pressure in tunnels without the shaft. If the compression wave induced by the train meets the shaft, some of the wave is transmitted to the shaft and the last of the wave is transmitted through the tunnel. However, the pressure rapidly increases at the constant velocity section. The pressure is more than double than the initial pressure of constant velocity section as the train is passing by the shaft. The increased pressure is transmitted to Station 2 though the magnitude is reduced. The pressure exceeds the fatigue load.

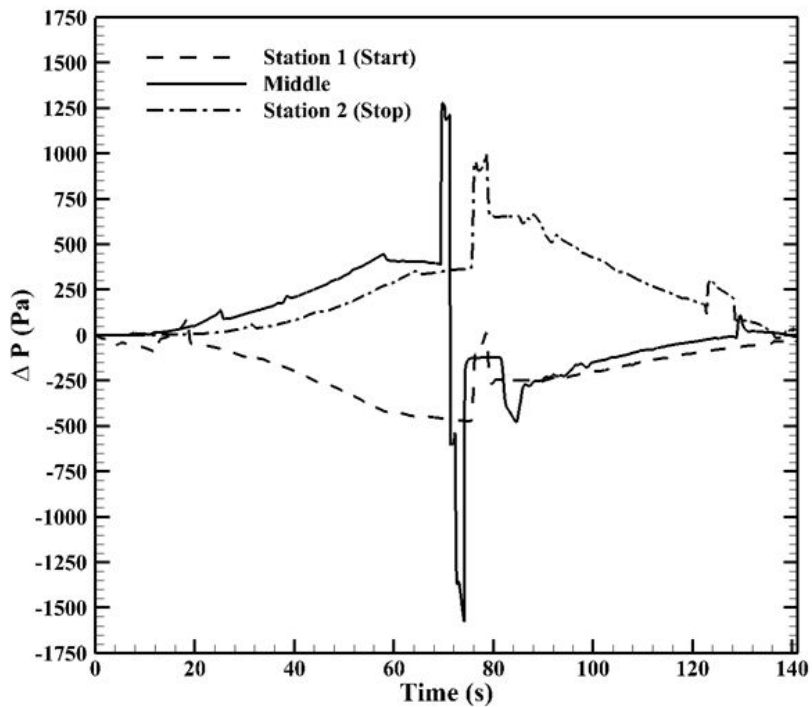


Fig. 47 Pressure history measured in the tunnel with shafts

4.1.3 Pressure change inside train

Computation simulations were performed to identify the effects of design parameters in regard to pressure change inside train based on Seoul Subway Line 8. The effects of aerodynamic parameters are evaluated using five parameters like the wind pressure case: train speed, nose shape, tunnel cross-sectional area, train interference and shaft.

The external pressure of the train is needed to estimate the internal pressure. Two points are selected to measure the external pressure (Fig. 48). When the train runs in tunnels, the pressure outside the train decreases linearly along a longitudinal direction. The beginning (A) and end (B) point of the linear section are selected as the measuring points.

Internal pressure is estimated from the external pressure using a simple equation. τ is used to specify the sealing quality of a train. It describes the time in which a difference between the internal and external pressure has decreased from 100 % to 37 % of the initial pressure difference. If a train is not sealed like Seoul subway, τ value is zero. τ value of high-speed train in South Korea is 18 s. The pressure change inside the train is evaluated on the safety criteria of the railway train (Table 10).

$$\frac{dP_{internal}}{dt} = \frac{1}{\tau} (P_{external} - P_{internal})$$

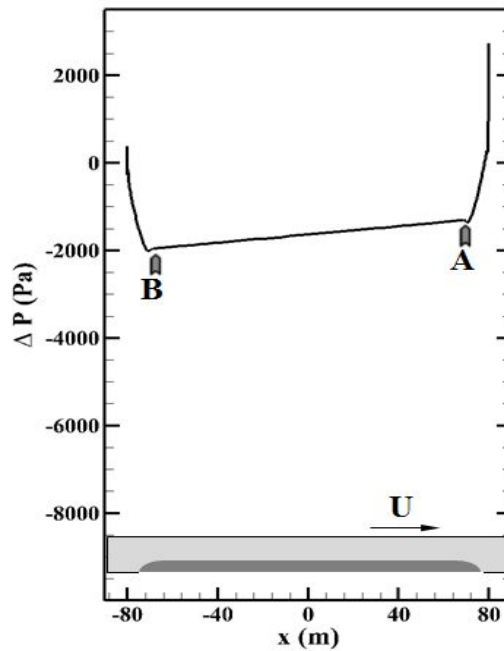


Fig. 48 Two measurement points (*A* and *B*) to analyse the pressure change inside the train

Table 10 The safety criteria of the railway train related to the pressure change inside the train [51]

Pressure change criteria in the cabin	
while travelling at the maximum speed	
Pressure change per unit time	: $\Delta P/\Delta t \leq 500 \text{ Pa/s}$
Pressure change during 3 seconds	: $\Delta P \leq 800 \text{ Pa}$
Pressure change during 10 seconds	: $\Delta P \leq 1000 \text{ Pa}$
Pressure change during 60 seconds	: $\Delta P \leq 2000 \text{ Pa}$

4.1.3.1 Effect of speed increase

External pressure varies depending on a train schedule. External pressure gradually decreases during acceleration, almost constantly retains during constant velocity and gradually decreases during deceleration (Fig. 49). External pressure of the front and rear point is different. External pressure of the rear point is lower than that of the front point. The pressure difference becomes larger as the train speed increases. The maximum negative pressure ($-1,959 Pa$) of 200 km/h is about 4 times lower than that ($-524 Pa$) of 100 km/h.

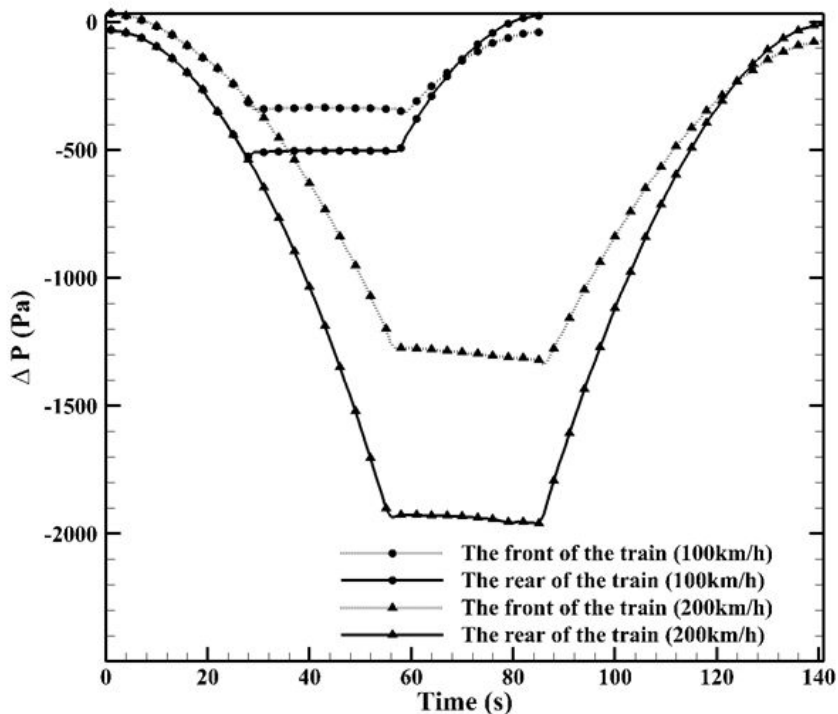


Fig. 49 External pressure history according to the train speed

Pressure change inside the train is evaluated using pressure of the rear of the train because the low pressure of the rear of the train has a great effect on pressure change inside the train than the relatively high pressure of the front of the train. Pressure inside the train is the same as the external pressure because it is assumed that the train is not sealed ($\tau=0$). Internal pressure is used to evaluate whether or not the pressure change inside the train satisfies the criteria specified in the rules for safety criteria of the railroad car.

When the train runs in tunnels, the flow between the walls of the train and tunnel is induced in opposite direction of the train. By the way, because the flow is accelerated by the increase of the train speed, the pressure between the train and tunnel is lower. Thus, the lower pressure affects the pressure change inside the train. The results of 100 km/h and 200 km/h satisfy the criteria although the maximum pressure change increases as the train speed increases (Fig. 50, 51 and 52). However, the maximum pressure change for 60 s is just below the limit of the criterion (Fig. 53).

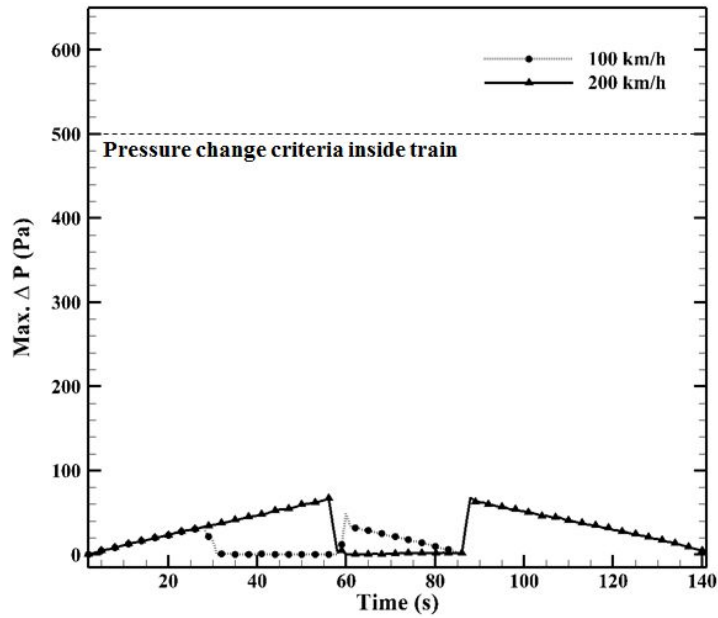


Fig. 50 Comparison of pressure change per second according to the train speed

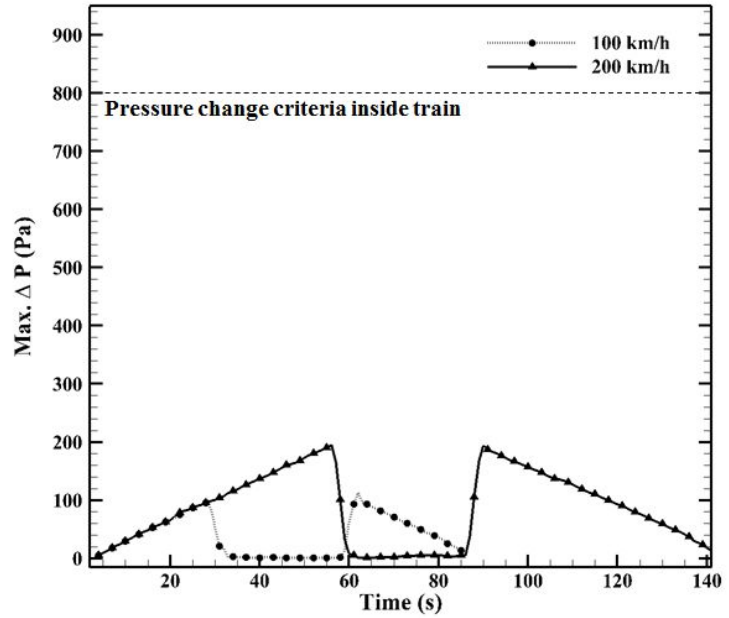


Fig. 51 Comparison of pressure change for 3 seconds according to the train speed

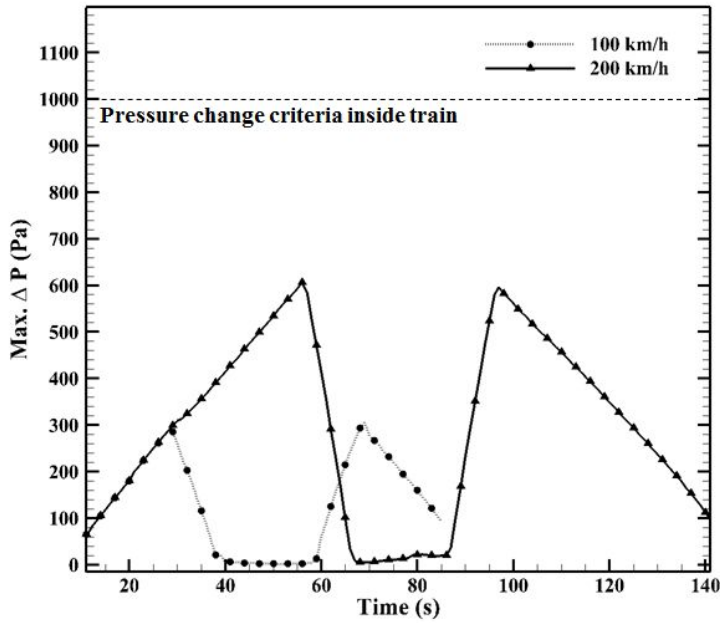


Fig. 52 Comparison of pressure change for 10 seconds according to the train speed

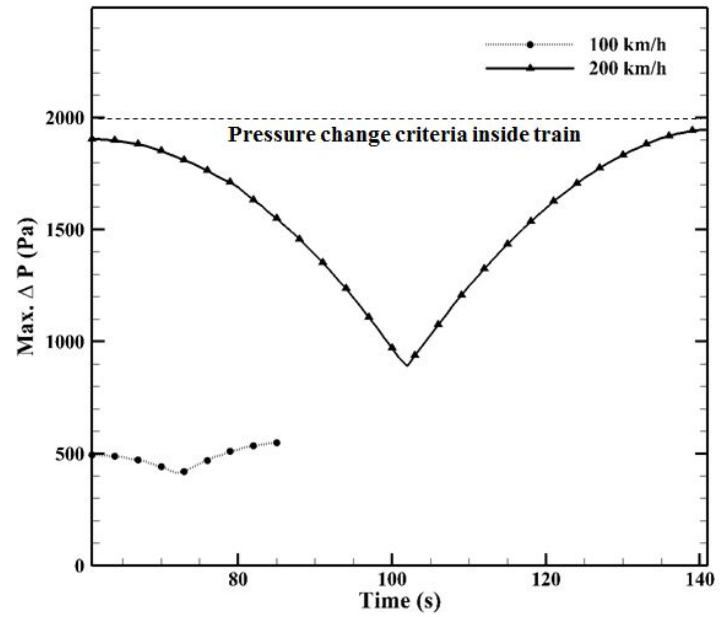


Fig. 53 Comparison of pressure change for 60 seconds according to the train speed

4.1.3.2 Effect of nose shape

External pressure according to the nose shape is almost the same as each other (Fig. 54). This result can be anticipated by the previous results. When the nose shape changed to identify the effect of the nose shape in regard to aerodynamic drag, the flow characteristic near the head and tail is only changed and the flow characteristic of the body part except the head and tail is almost the same in cases. As external pressure is measured at the train body, they are similar values.

Pressure change according to the nose shape is also similar values. They satisfy the pressure change criteria inside the train (Fig. 55, 56, 57 and 58).

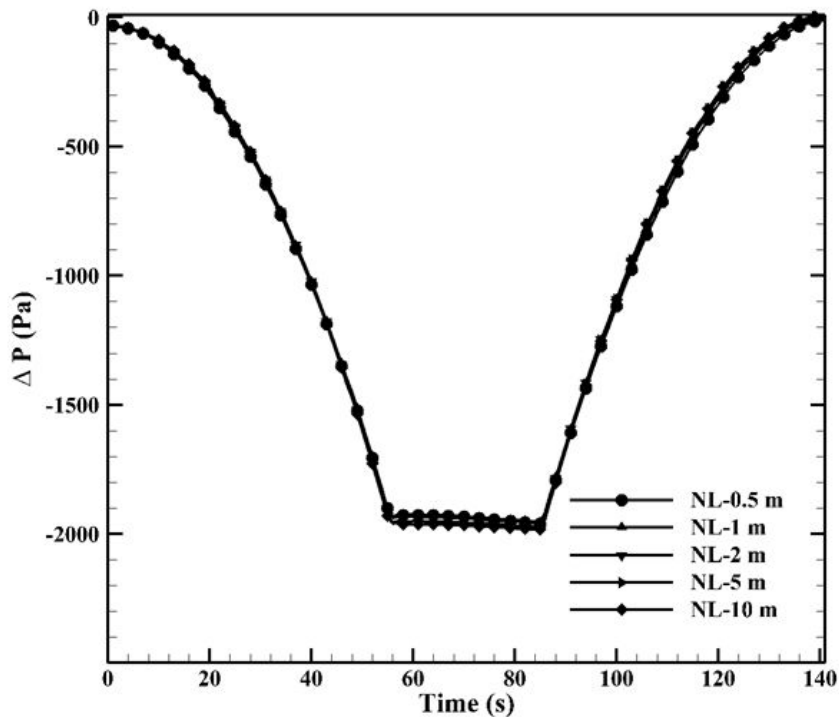


Fig. 54 External pressure history according to the nose length

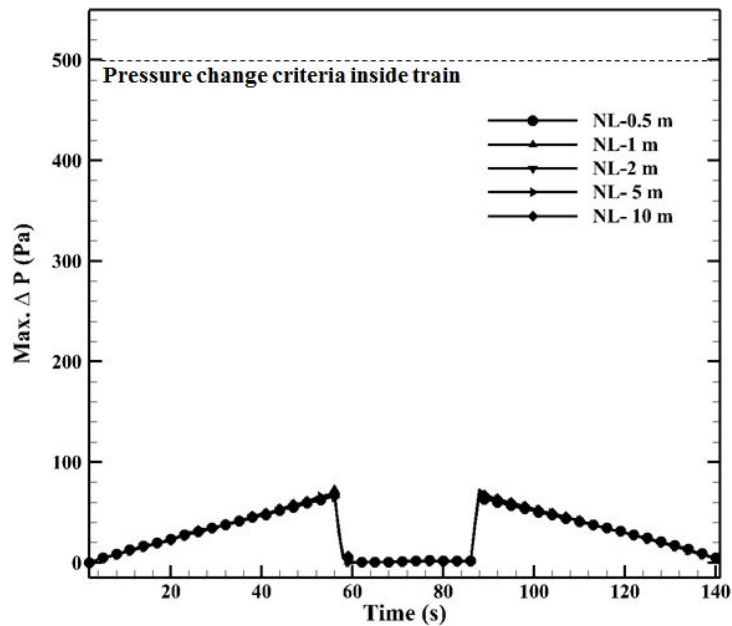


Fig. 55 Comparison of pressure change per second according to the nose length

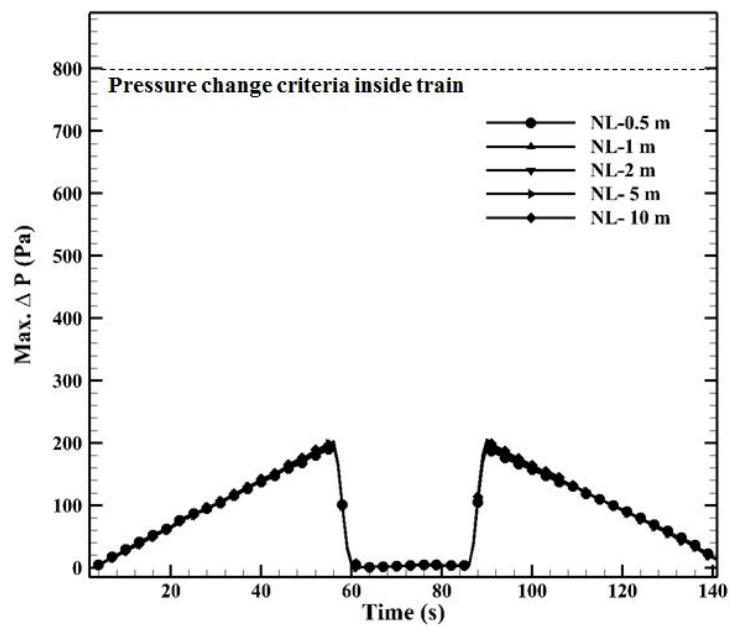


Fig. 56 Comparison of pressure change for 3 seconds according to the nose length

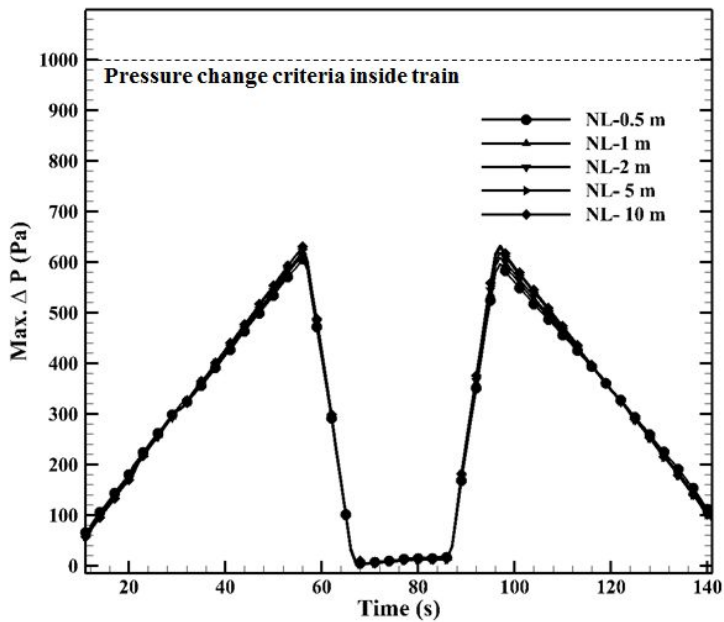


Fig. 57 Comparison of pressure change for 10 seconds according to the nose length

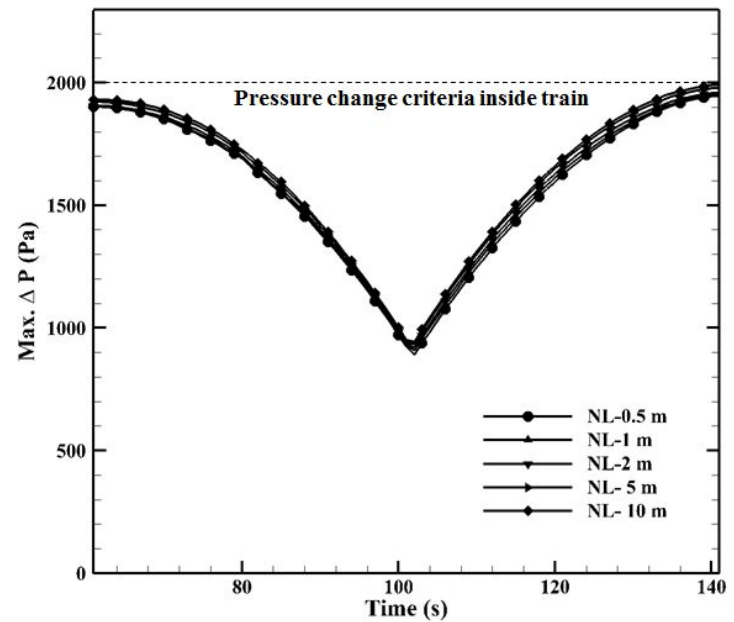


Fig. 58 Comparison of pressure change for 60 seconds according to the nose length

4.1.3.3 Effect of tunnel cross-sectional area

The maximum value of the external pressure drop is reduced from $-1,983 \text{ Pa}$ to -504 Pa by the increase of the tunnel cross-sectional area (Fig. 59). The acceleration of the air flowing backward along the train surface slowed down due to the increase of the tunnel cross-sectional area. Consequently, the pressure is risen by slowdown of the flow acceleration.

Pressure change inside the train is considerably reduced and satisfies the pressure change criteria inside the train (Fig. 60, 61 and 62). Pressure change for 60 s also easily satisfies the criteria (Fig. 63). It is a natural result as the external pressure drop decreases.

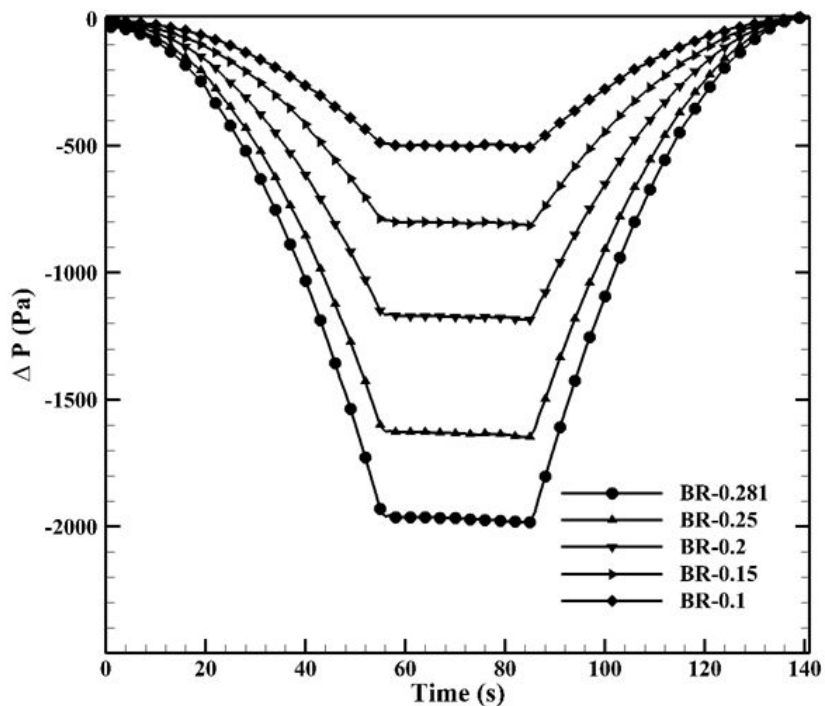


Fig. 59 External pressure history according to the blockage ratio

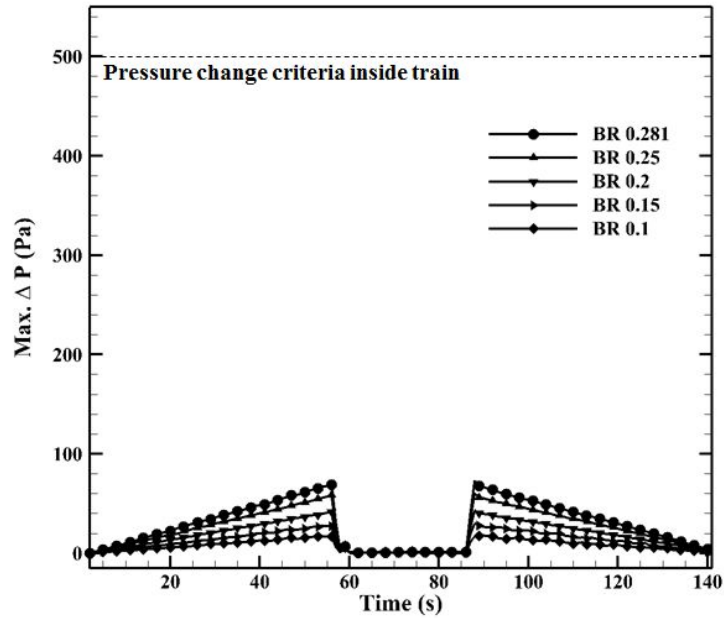


Fig. 60 Comparison of pressure change per second according to the blockage ratio

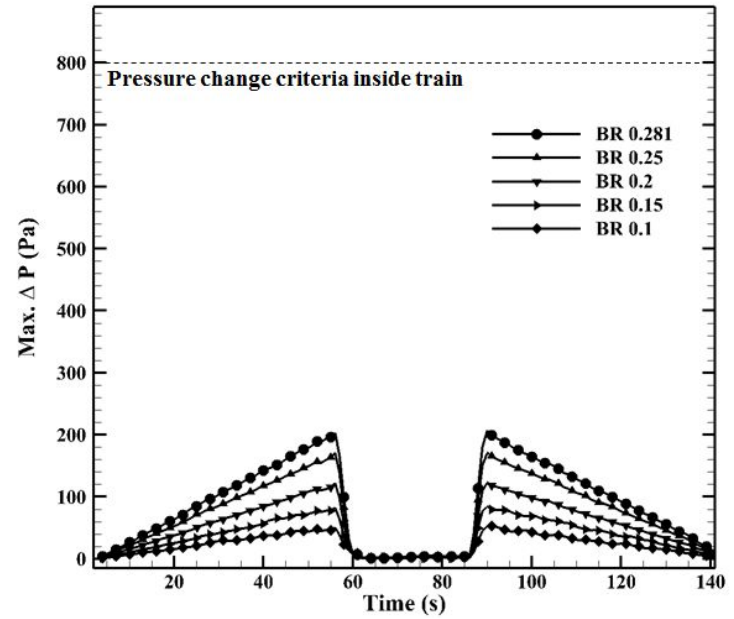


Fig. 61 Comparison of pressure change for 3 seconds according to the blockage ratio

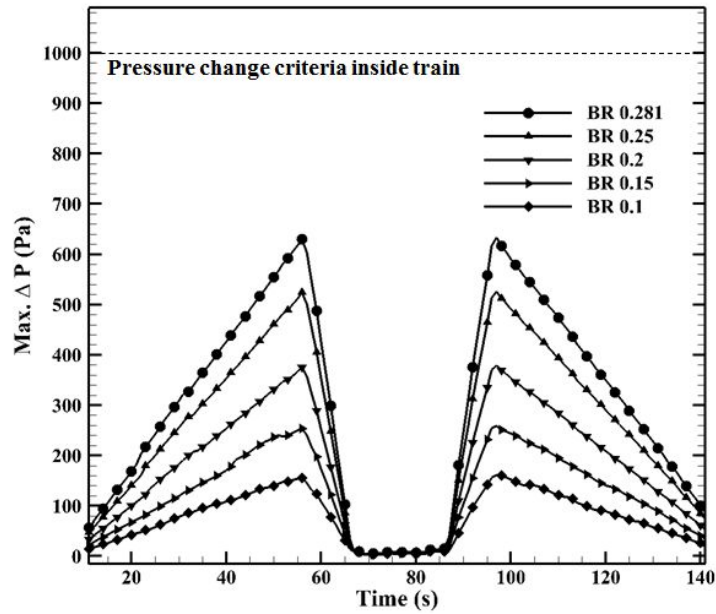


Fig. 62 Comparison of pressure change for 10 seconds according to the blockage ratio

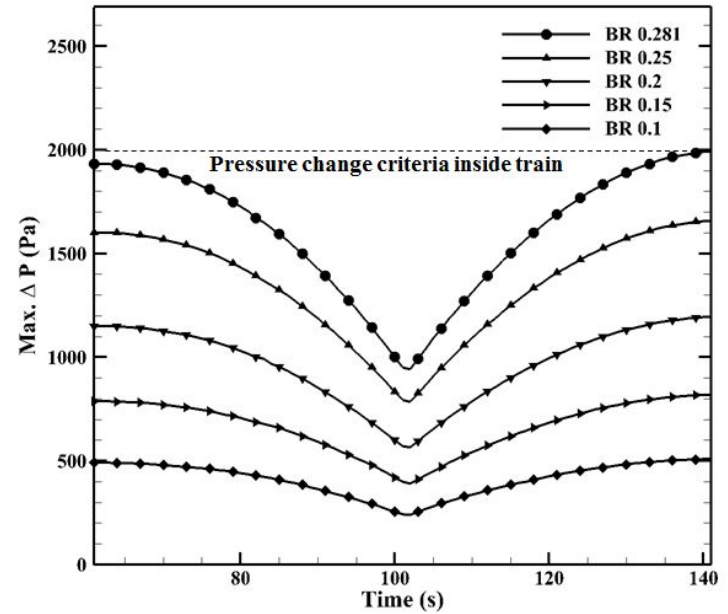


Fig. 63 Comparison of pressure change for 60 seconds according to the blockage ratio

4.1.3.4 Effect of train interference

External pressure by the train interference is different with that by the single train. External pressure of two trains in this case is located at upper and lower of the sing train result. The maximum negative pressure of two trains is respectively $-1,457 Pa$ (lead train) and $-2,334 Pa$ (trailing train) (Fig. 64).

The external pressure gap of two trains is caused by interference of the pressure wave induced by the trains. When the train runs in tunnels, the compression and expansion wave propagates forward and backward through the tunnels. If two trains runs in tunnels, they are influenced by different pressure waves. The lead train is influenced by the compression wave generated by the trailing train. On the contrary, the trailing train is influenced by the expansion wave generated by the lead train. The compression wave from the trailing train has a effect to offset the negative pressure around the surface of the lead train; the external pressure of the lead train is higher than the single train. On the other hand, the expansion wave from the lead train has a effect to overlap the negative pressure around the surface of the trailing train; the external pressure of the trailing train is lower than the single train.

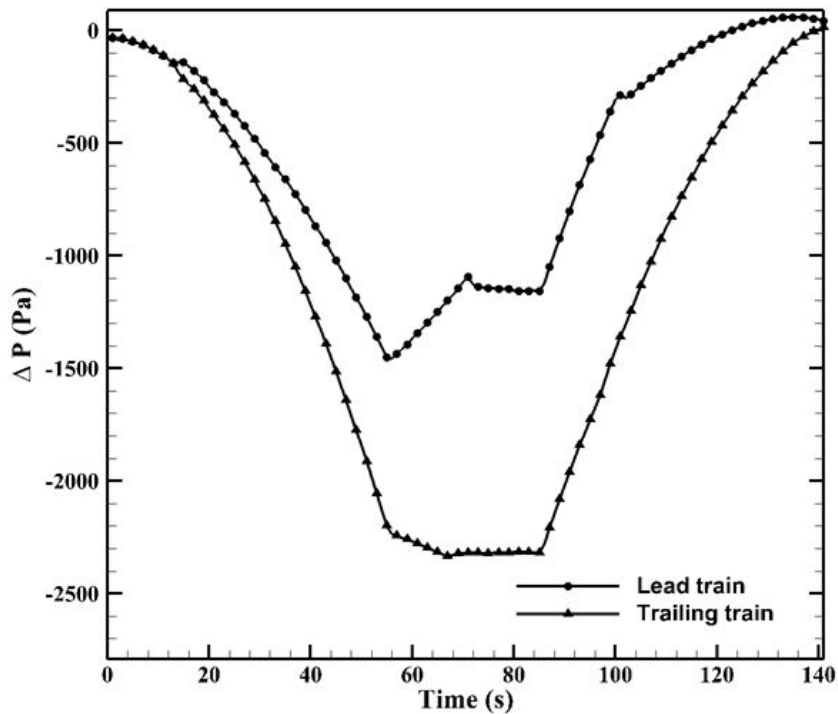


Fig. 64 External pressure history of the lead and trailing train

Pressure change inside two trains for 1 s, 3 s and 10 s satisfies the pressure change criteria inside the train (Fig. 65, 66 and 67). Although the value of pressure change is different a little, the shape of pressure change is similar with each other. The value and shape of pressure change is also similar with the single train. However, pressure change for 60 s is different to 1 s, 3 s and 10 s. Pressure change of the trailing train exceeds the criteria (Fig. 68). The maximum value of pressure change is 2,322 Pa which is about 300 Pa higher value than the criteria, 2,000 Pa. Pressure change of the lead train becomes lower than the single train. The maximum value of pressure change is 1,426 Pa which is about 600 Pa lower than the criteria.

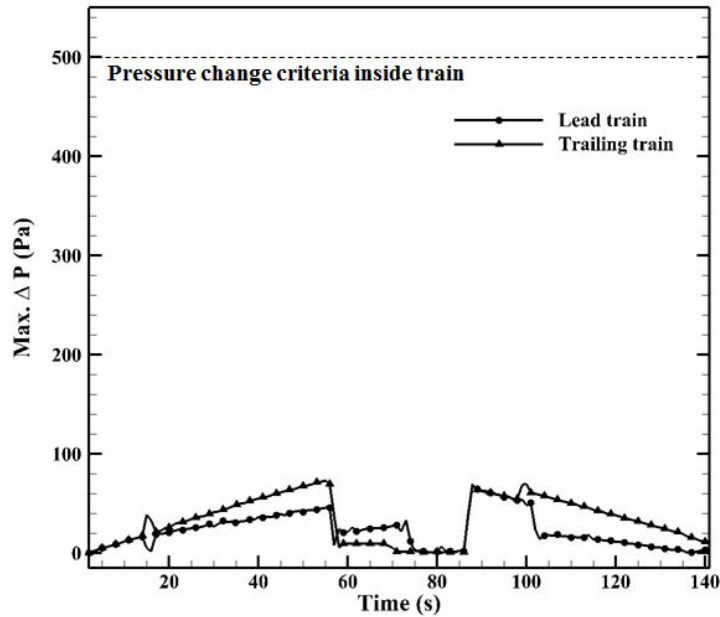


Fig. 65 Comparison of pressure change per second between the lead and trailing train

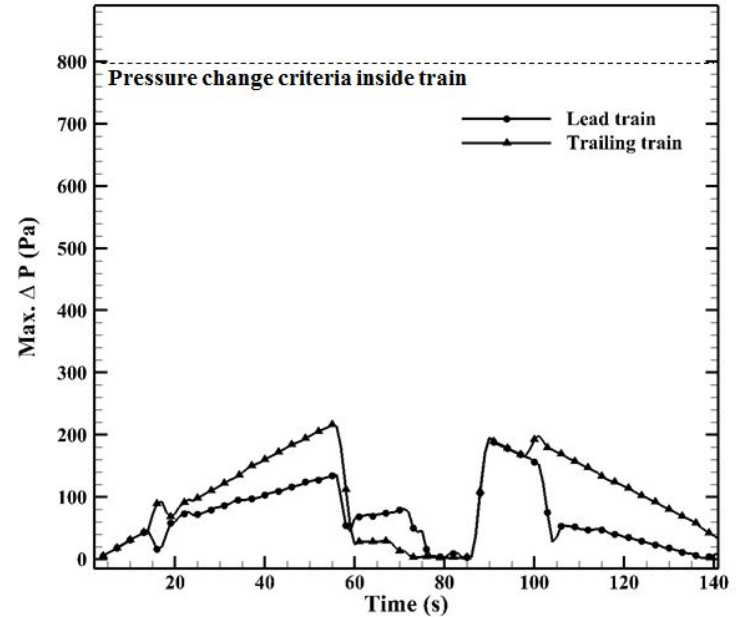


Fig. 66 Comparison of pressure change for 3 seconds between the lead and trailing train

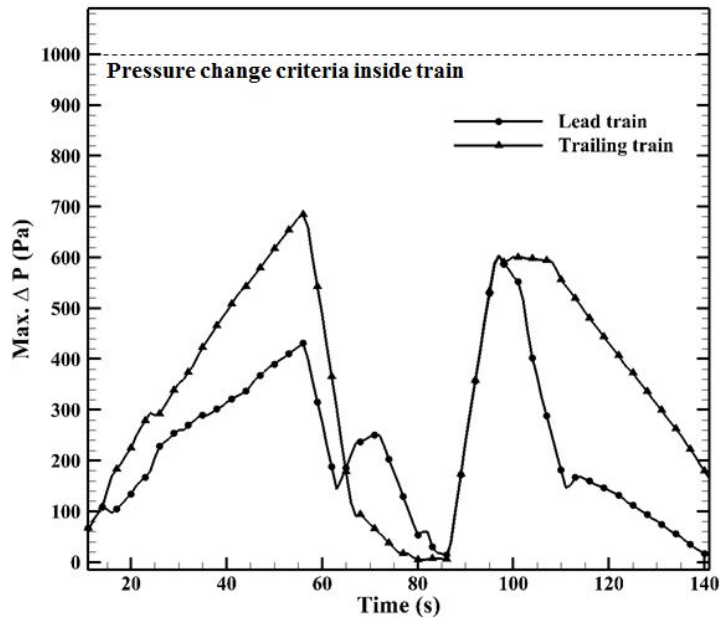


Fig. 67 Comparison of pressure change for 10 seconds between the lead and trailing train

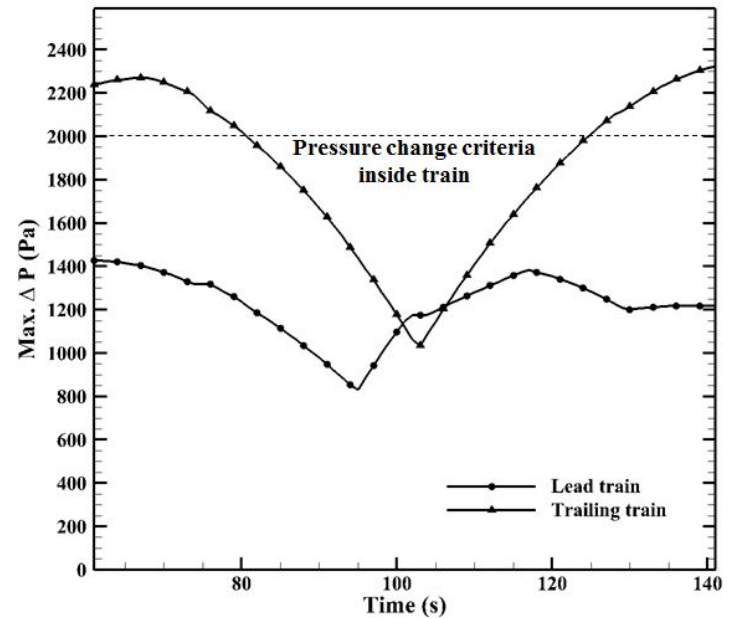


Fig. 68 Comparison of pressure change for 60 seconds between the lead and trailing train

4.1.3.5 Effect of shaft

External pressure of the front and rear of the train has a similar trend with the single train; external pressure of the front is higher than that of the rear (Fig. 69). However, the value of external pressure is different each other. The rear external pressure of this case is similar with the rear external pressure of the single train in constant speed section. But the front external pressure of this case is lower than that of the single train in constant speed section because a part of the compression wave propagating in front of the train is transmitted into the shaft.

The different characteristic of the tunnel with shaft is that the pressure jump is occurred as the train is passing by the shaft. When the train is passing by the shaft, the surface pressure of the train is lower than the atmosphere pressure at the end of the shaft. Thus, the air whose pressure is higher than the surface pressure of the train is flown into the tunnels. This phenomenon is maintained while the train is passing by the shaft. After the train is passing by the shaft, the surface pressure is higher than the surface pressure at the starting point of the constant speed section. The reason is that the air in the atmosphere is still flown into the tunnels because of the low pressure of the train rear.

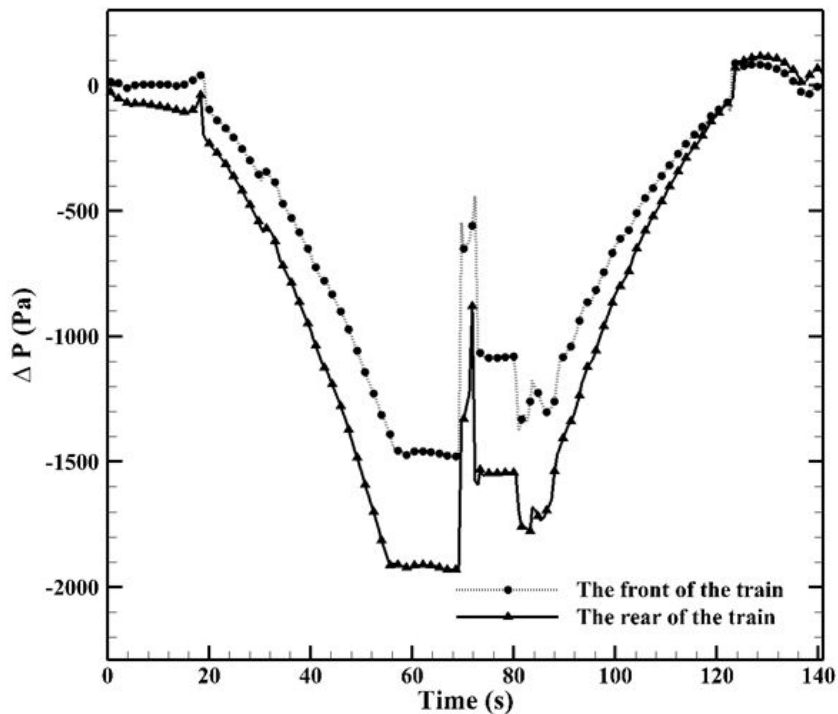


Fig. 69 External pressure history of the train in the tunnel with shaft

Pressure change for 1 s, 3 s, 10 s and 60 s exceeds the pressure change criteria inside the train (Fig. 70, 71, 72 and 73). The standard excess of pressure change at the front and rear of the train for 1 s, 3 s and 10 s happens as the train is passing by the shaft because external pressure suddenly rises at that moment. However, the standard excess of pressure change for 60 s just happens at the rear of the train. The front of the train satisfies the criteria. And the excess point is later in the train run unlike 1 s, 3 s and 10 s. The reason is the pressure rise as the train is passing by last shaft near the destination.

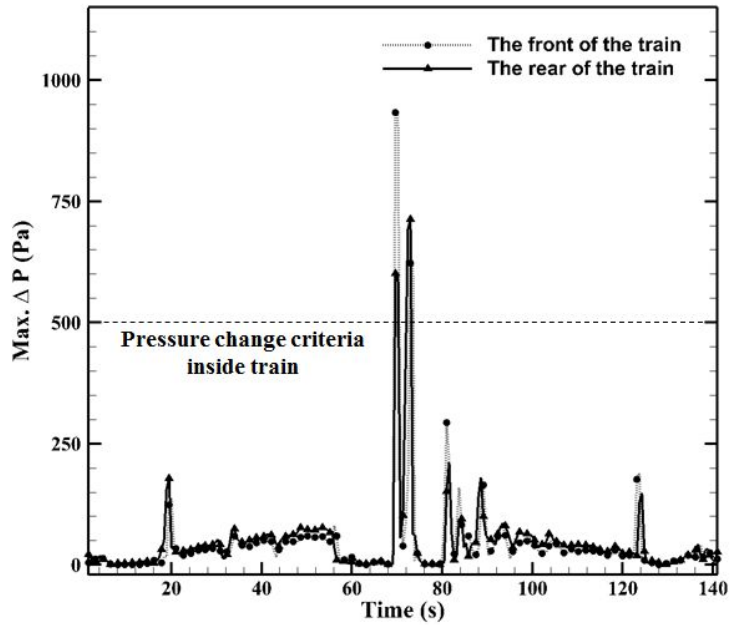


Fig. 70 Pressure change per second of the train in the tunnel with shaft

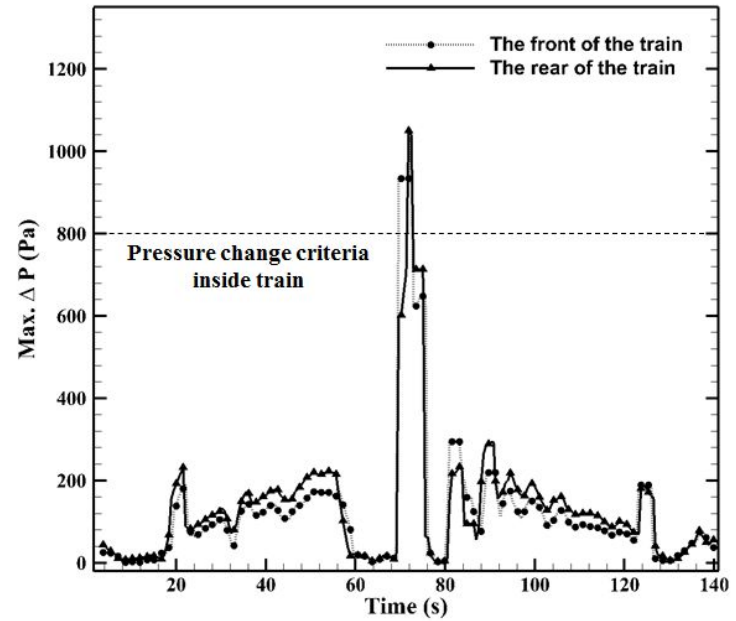


Fig. 71 Pressure change for 3 seconds of the train in the tunnel with shaft

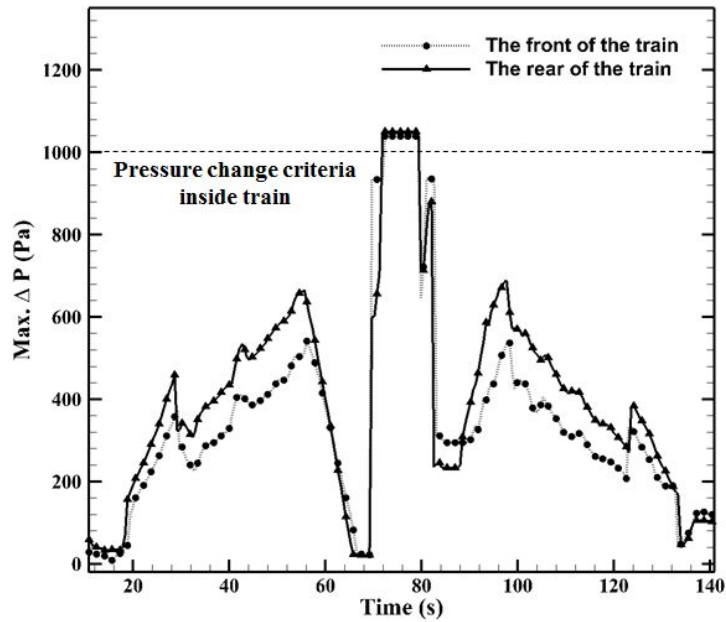


Fig. 72 Pressure change for 10 seconds of the train in the tunnel with shaft

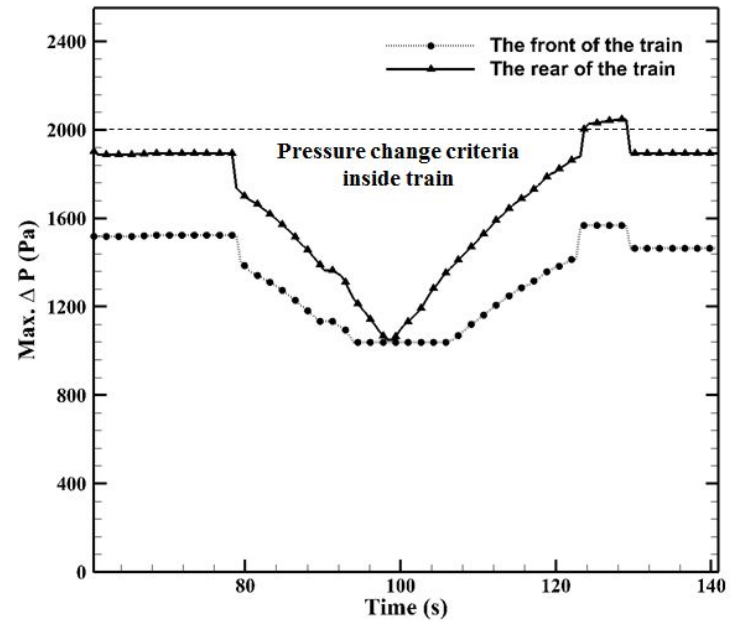


Fig. 73 Pressure change for 60 seconds of the train in the tunnel with shaft

4.2. Conceptual design of GTX considering aerodynamic drag and evaluation

4.2.1 Conceptual design

Conceptual design and evaluation are performed in this chapter based on the previous parametric study. A nose shape and blockage ratio was a important parameters which are related to the aerodynamic drag, pressure wave and pressure change inside the train. A shaft also played a important role in regard to the pressure wave and pressure change inside the train. Design parameters (train nose shape, tunnel cross-sectional area, tunnel length and shafts) are chosen by referring to the previous results and aerodynamic parameters are evaluated by the design criteria.

Nose shape was a key parameter to reduce the aerodynamic drag. A streamlined shape is proper to reduce the aerodynamic drag at high-speed train. Therefore, the train data of KTX-Sancheon which is operating in South Korea is chosen for the conceptual design [12]. Nose shape is 5.56 m long and streamlined shape. KTX-Sancheon consists of 10 cars, 200 m long (Table 11). The cross-sectional area is smaller than the cross-sectional area of Seoul Subway Line 8 which was used for the parametric study.

Table 11 Configuration data of KTX-Sancheon

Train data of KTX-Sancheon	
Nose length	5.56 m
Train length (10 cars)	200 m
Cross-sectional area	9.634 m ²

Tunnel cross-sectional area is selected by the numerical simulation. The simulation is performed by varying the blockage ratio from 0.3 to 0.1. The trend of aerodynamic drag in regards to the tunnel cross-sectional area is obtained by the simulation. Now, the maximum service speed of KTX-Sancheon is 300 km/h. It means that the thrust of KTX-Sancheon overcomes the aerodynamic drag at 300 km/h in an open field. Thus, two simulations (200 km/h and 300 km/h) are performed to predict the aerodynamic drag of KTX-Sancheon in an open field.

The aerodynamic drag of the conceptual train travelling at 200 km/h in tunnels is compared with the aerodynamic drag of the KTX-Sancheon travelling at 200 and 300 km/h in an open field to select the tunnel cross-sectional area (Fig. 74). The tunnel cross-sectional area should satisfy the condition, which is that the aerodynamic drag in tunnels is smaller than that in an open air. The tunnel cross-sectional area should be over 150 m² to run in tunnels with the thrust travelling at 200 km/h in an open air. However, the magnitude of the area is so large that it needs a lot of money to construct. Thus, it is not a practical size. The aerodynamic drag at 300 km/h in an open air is between the blockage ratios which are 0.25 and 0.2. Therefore, the tunnel cross-sectional area, 48.17 m² (the blockage ratio is 0.2) is selected for the conceptual design. This area is larger than the area (45.62 m²) used in the parametric study. The area is not increased a lot compared with the area of Seoul Subway because the train cross-sectional area of KTX-Sancheon is smaller than that of Seoul Subway.

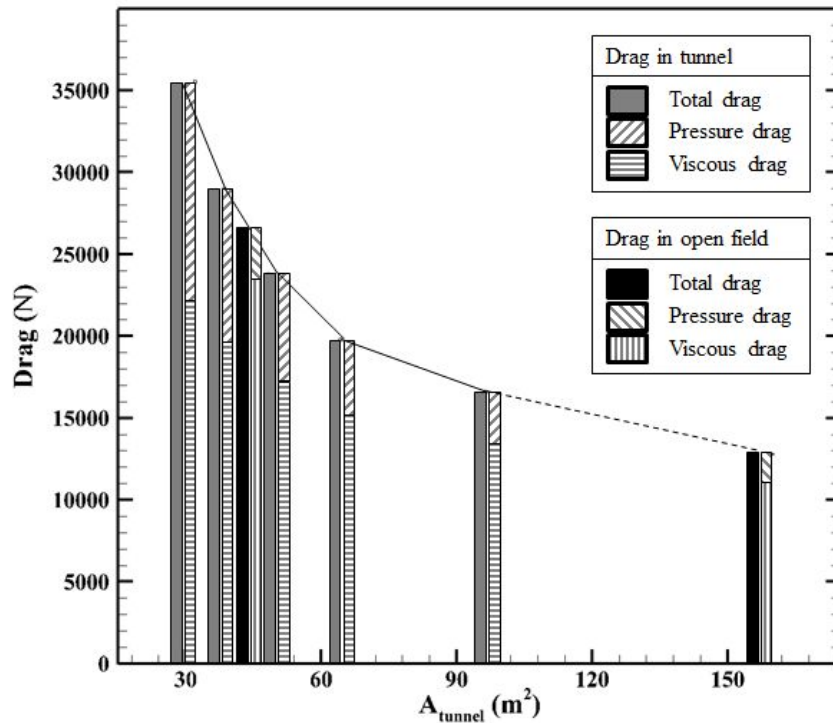


Fig. 74 Selection of tunnel cross-sectional area based on the drag; comparison of the drags between in tunnel and in open field

There was a considerable increase of the aerodynamic drag in the tunnel although the train speed in the tunnel is the same as the speed in an open field. Thus, the drag comparison according to the speed between the tunnel and open field was performed to analyze the increasing trend of the aerodynamic drag. The speed range is from 100 km/h to 200 km/h. The simulation in the tunnel whose blockage ratio is 0.2 was performed.

The aerodynamic drag increases in accordance with the speed increase (Fig. 75). As expected, the drag in the tunnel increase more

rapidly than that in an open field. The drag coefficients are compared to analyze the flow field around the train. The drag coefficient is calculated as

$$C_D = \frac{D}{\frac{1}{2} \rho_{\infty} V_{train}^2 A_{train}}$$

where D is the aerodynamic drag, A_{train} is the cross-sectional area of the train and V_{train} represents the maximum cruise speed of the train (100 km/h, 125 km/h, 150 km/h, 175 km/h and 200 km/h). The drag coefficients according to the train speed are similar with each other. The difference of the drag coefficient between the tunnel and an open field is almost the same as 2 times according to the train speed. It means that the flow field within the speed range from 100 km/h to 200 km/h is also similar with each other.

The tunnel length and the number of shaft are the same as the parametric study: tunnel length is 5 km and the number of shaft is 3. Because train interference affected the pressure wave and pressure change inside the train, the single train and two trains are compared with each other.

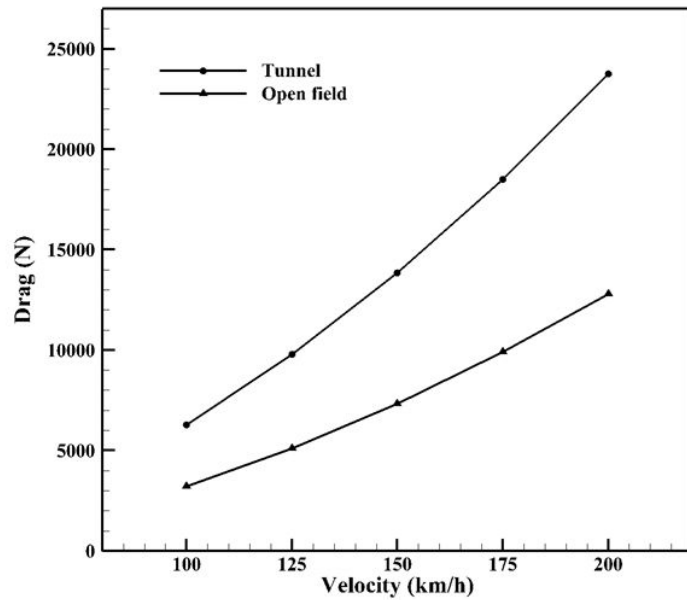


Fig. 75 Comparison of the drag in the tunnel and an open field in accordance with the train speed from 100 km/h to 200 km/h

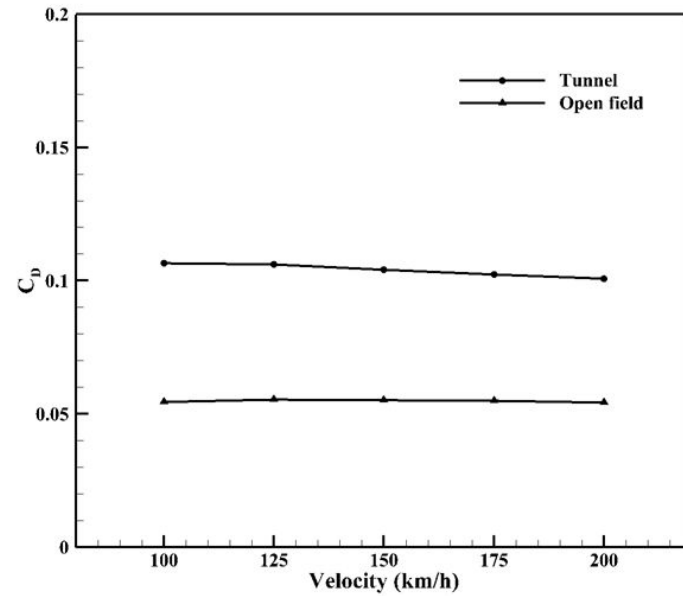


Fig. 76 Comparison of the drag coefficient in the tunnel and an open field in accordance with the train speed from 100 km/h to 200 km/h

4.2.2 Evaluation of wind pressure on platform screen door

4.2.2.1 Single train

The pressure wave in single train is similar with the result of the shaft effect in the parametric study. Pressure measured at Station 1, Station 2 and Middle gradually changes except the period which the train is passing by the shaft located at the center (Fig. 77). The air pressure of the train surface is lower than atmospheric pressure at the end of the shaft. Thus, pressure suddenly rises because of the air inflow from the atmosphere. And the maximum negative pressure ($-1,025 Pa$) at Middle is measured by low pressure of the train surface.

There is no point exceeding the fatigue load and maximum wind pressure at Station 1 and 2. The reason is that the nose shape is a streamlined shape and the blockage ratio is small. However, the pressure exceeding the fatigue load is measured at Middle. The positive peak value ($+743 Pa$) is related with the air inflow from the atmosphere and the negative peak value ($-1,025 Pa$) is related with the train surface pressure.

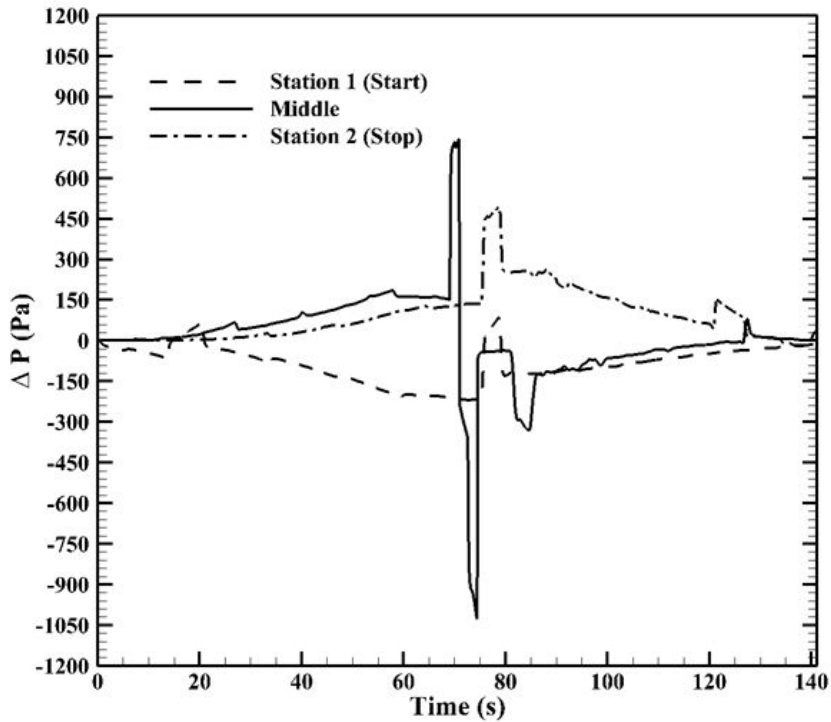


Fig. 77 Wind load measured at Station 1, 2 and Middle from the conceptual design

4.2.2.2 Two trains

Pressure is measured at three stations and the center between stations. The negative pressure is overlapped at Station 1 and the positive pressure is overlapped at Station 3 (Fig. 78). The negative and positive pressure are offset at Station 2. The overlap of positive pressure at Station 3 is caused by the compression wave generated from the train head. The overlap of negative pressure at Station 1 is caused by the expansion wave generated from the train tail. The offset of the negative and positive pressure at Station 2 is caused by

interfering between the expansion wave from the lead car and the compression wave from the trailing car.

A sudden pressure rise is happened at some points. The points are the time that the pressure generated by passing by shafts is propagated to the stations. The maximum peak value (+571 Pa) is measured at Station 3. The value exceeds the fatigue load.

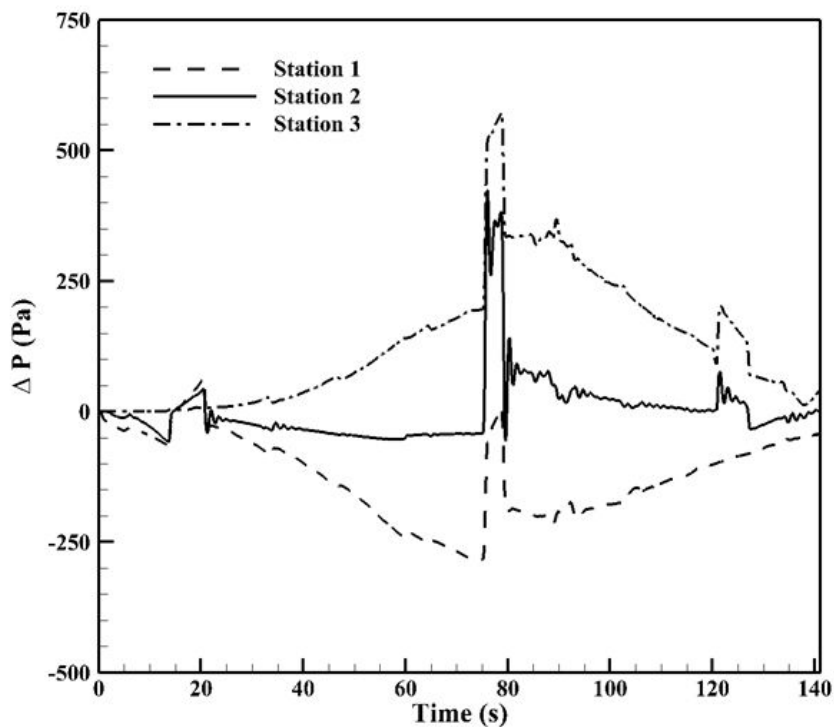


Fig. 78 Wind load measured at Station 1, 2 and 3 from the conceptual design to identify the train interference

The pressure trends measured at the center between the stations are similar with each other but the magnitude at the center of Station 2 and 3 is a little higher than the magnitude at the center of Station 1

and 2 (Fig. 79). This difference is caused by the interference of pressure wave generated by two trains. There are two peak points: the maximum positive and negative pressure. The maximum positive pressure is generated by passing by the shaft because the relatively high pressure from the atmosphere is flown into the tunnel. The maximum negative pressure is generated when the train is passing by the measuring point because the surface pressure of the train travelling in tunnels becomes lower than the atmosphere. The maximum positive pressure of both points are +633 Pa and +880 Pa. The maximum negative pressure of both points are -1,094 Pa and -900 Pa. The maximum values exceed the fatigue load. There is not a big difference between the results by two trains and single train. The reason is that the pressure generated by the streamlined shape nose is not strong. Furthermore, the pressure is decreased when the pressure wave is passing by the shaft.

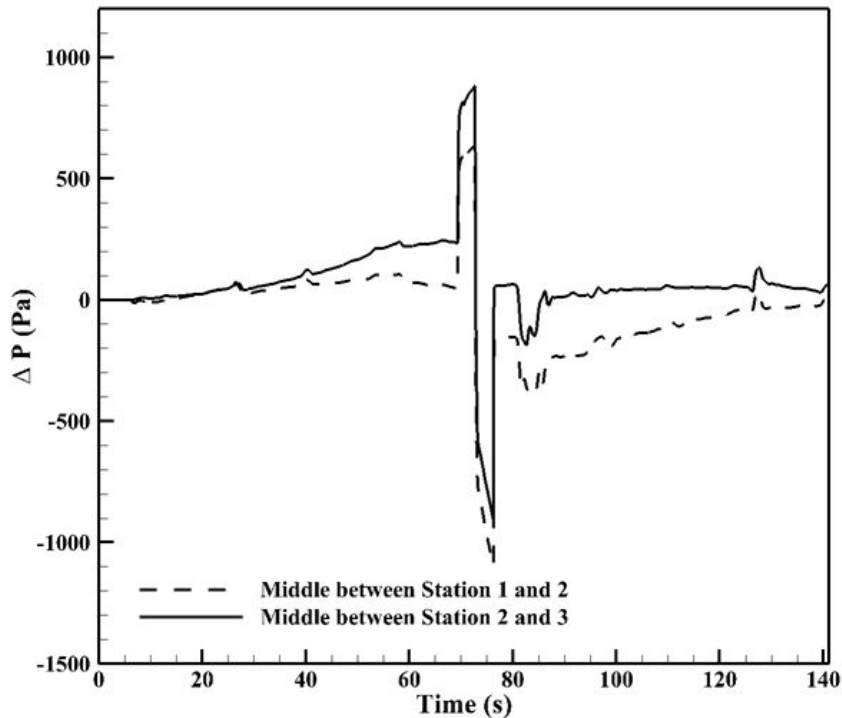


Fig. 79 Wind load measured at the middle between the stations from the conceptual design to identify the train interference

4.2.3 Evaluation of Pressure change inside train

4.2.3.1 Single train

External pressure in single train is similar with the result of the shaft effect in the parametric study (Fig. 80). The pressure at the rear of the train is lower than the pressure at the front of the train because the air flowing backward near the train surface is accelerated. The pressure suddenly rises by the air inflow from the atmosphere.

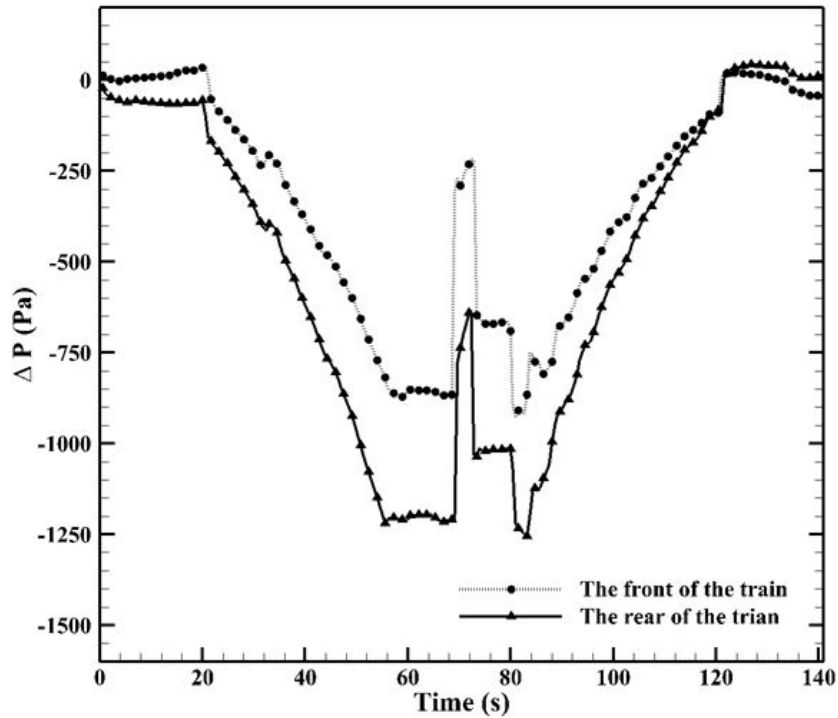


Fig. 80 External pressure history measured from the conceptual design

Pressure change for 1 s exceeds the pressure change criteria inside the train (Fig. 81). It is caused as the train is passing by the shaft. At that time, the air whose pressure is higher than the tunnel is flown into the tunnel from the atmosphere because the pressure of the train surface is lower than the atmosphere at the end of the shaft.

Pressure change for 3 s, 10 s and 60 s does not exceed the pressure change criteria inside the train (Fig. 82, 83 and 84). The reason is that the air between the train and tunnel is accelerated less because of the small blockage ratio; the train surface pressure does not sufficiently decrease.

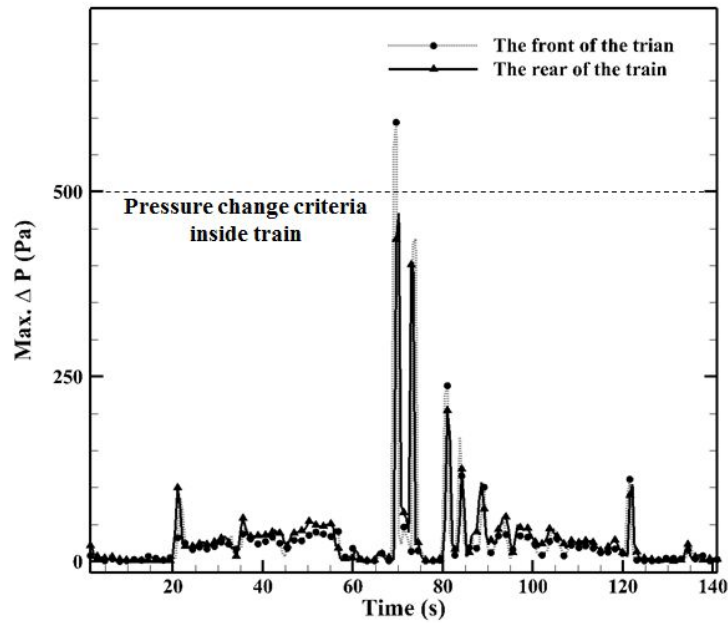


Fig. 81 Pressure change per second from the conceptual design

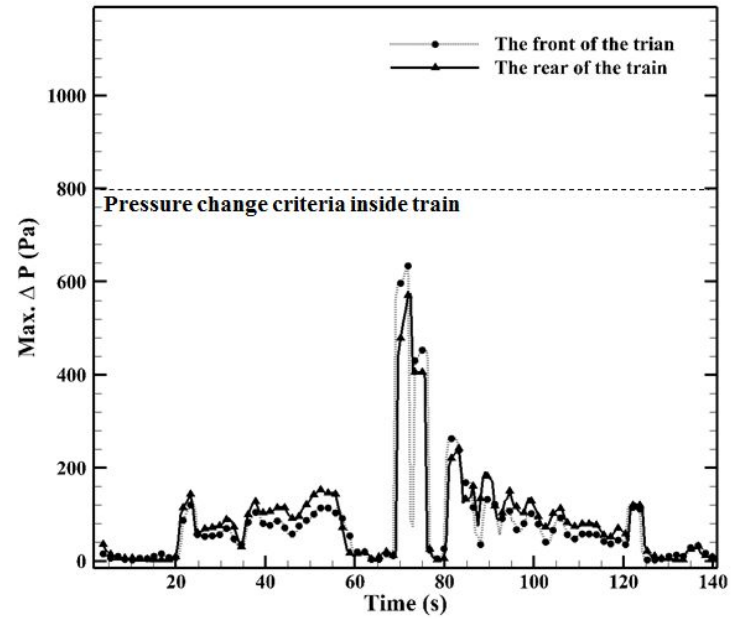


Fig. 82 Pressure change for 3 seconds from the conceptual design

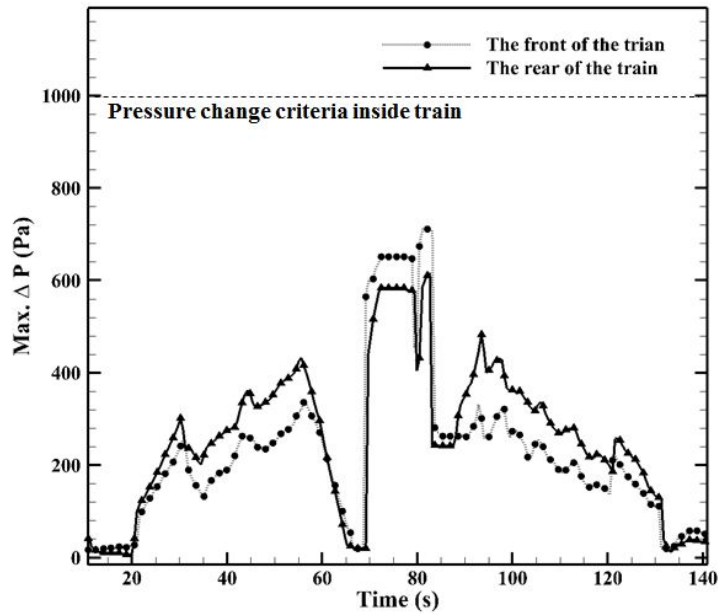


Fig. 83 Pressure change for 10 seconds from the conceptual design

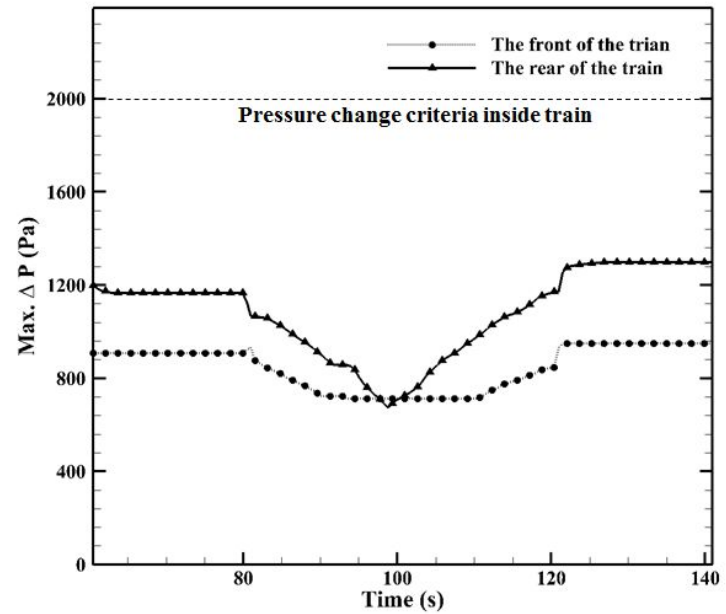


Fig. 84 Pressure change for 60 seconds from the conceptual design

4.2.3.2 Two trains

External pressure history of the lead and trailing train is similar with the pressure history of single train (Fig. 85). Pressure decreases during the acceleration and pressure recovers during the deceleration. Pressure suddenly rises when the train is passing by the shaft. Pressure at the rear is lower than pressure at the front.

Although the trend of pressure history is similar with each other, there is a little difference of the value among them. The jumped pressure passing by the shaft in single train is $-220 Pa$ at the front. The jumped pressure passing by the shaft in two trains is respectively $-109 Pa$ at the front of lead train and $-334 Pa$ at the front of trailing train. The pressure of single train is between the pressure of lead train and the pressure of trailing train. Because the lead train is affected by the compression wave generated by the trailing train and the trailing train is affected by the expansion wave generated by the lead train. However, the effect of the pressure interference is slight as the pressure wave generated by the streamlined nose shape is not strong.

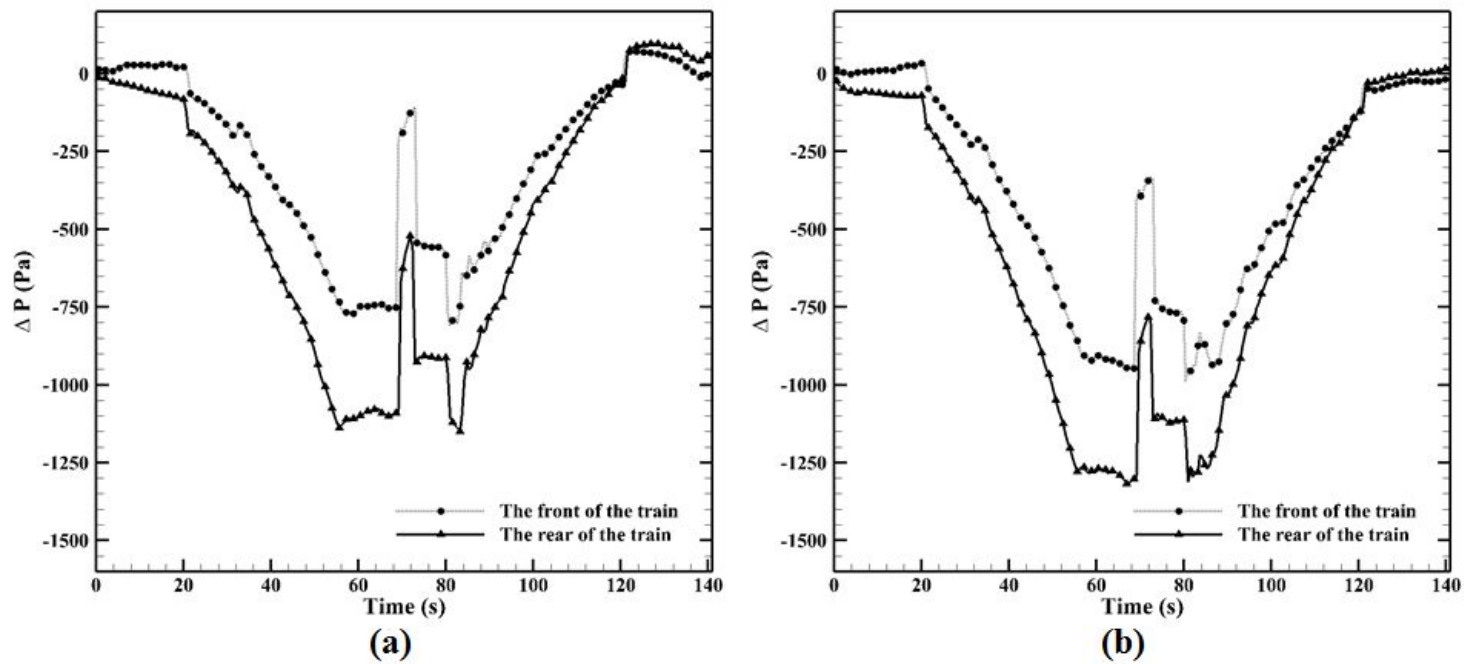


Fig. 85 Comparison of external pressure from the conceptual design to identify the train interference:

(a) Lead train, (b) Trailing train

Pressure change inside the train for 1 s, 3 s, 10 s and 60 s has similar trends with the results of single train. Pressure change for 1 s also exceeds the pressure change criteria inside the train but pressure change for 3 s, 10 s and 60 s does not exceed the criteria like in the single train case (Fig. 86, 87, 88 and 89).

There is a little difference in pressure change between the lead and trailing train. Pressure interference between two trains is slight because the tunnel has shafts as well as a streamlined nose shape. Pressure wave made by a streamlined nose shape is not strong and shafts has a role to reduce the pressure wave.

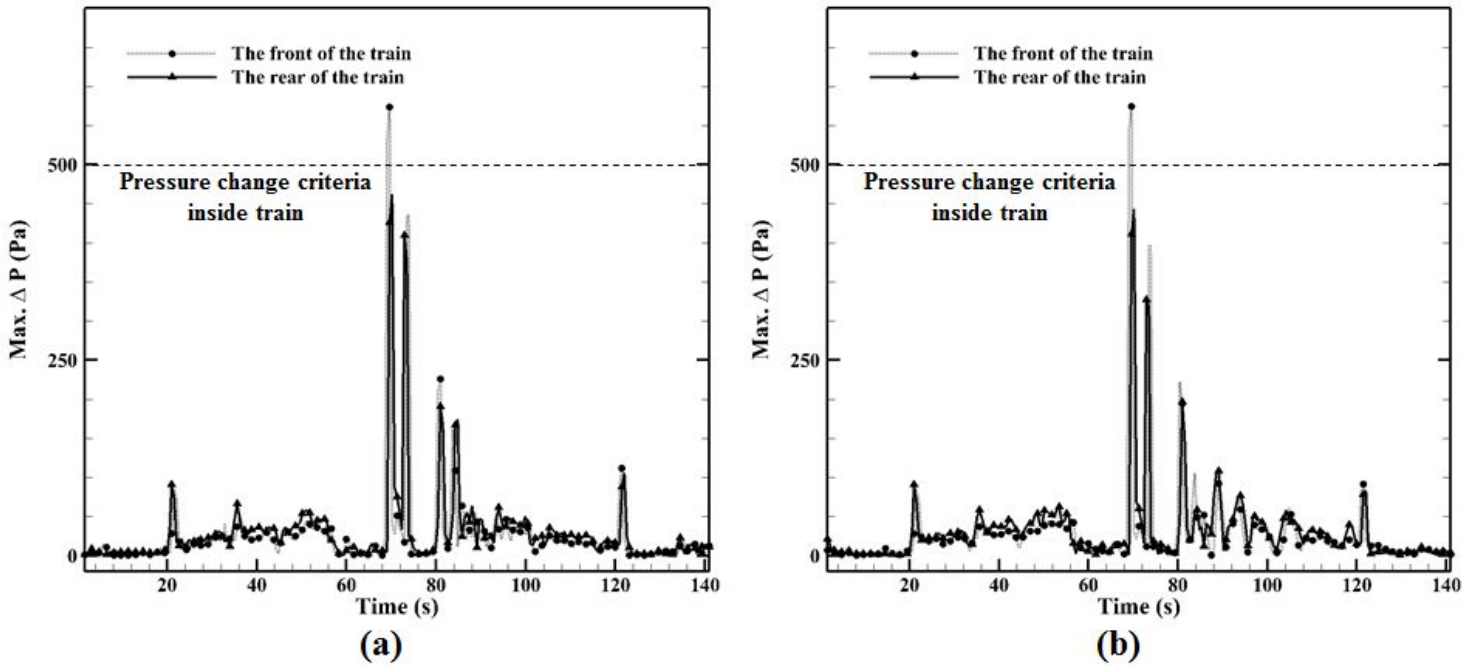


Fig. 86 Comparison of pressure change per second from the conceptual design to identify the train interference:
 (a) Lead train, (b) Trailing train

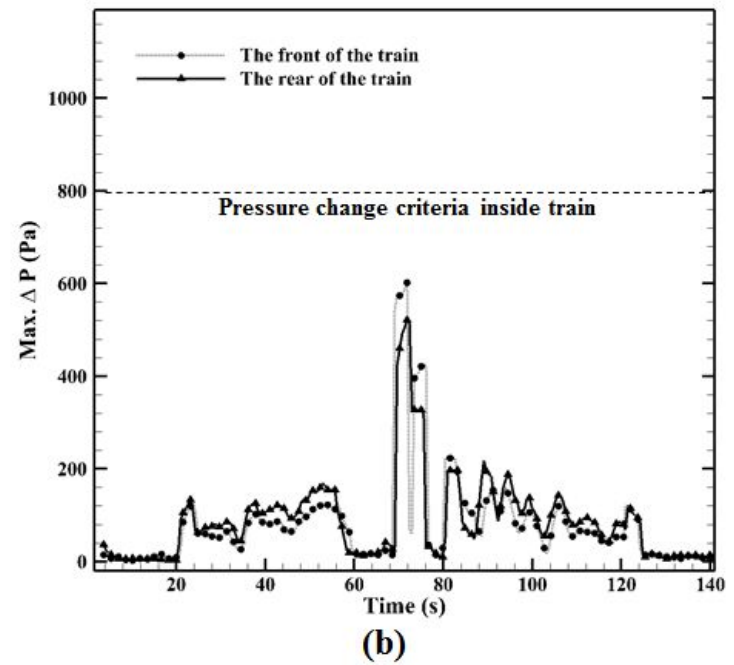
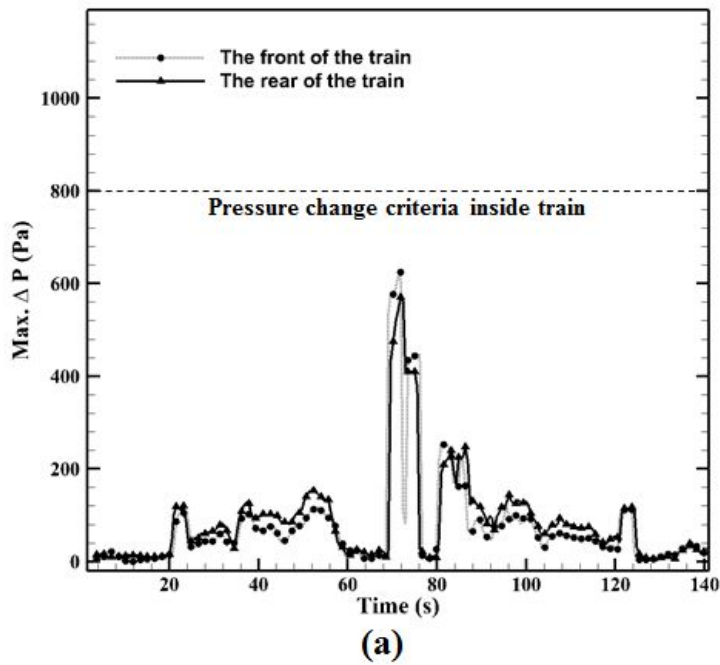


Fig. 87 Comparison of pressure change for 3 seconds from the conceptual design to identify the train interference: (a) Lead train, (b) Trailing train

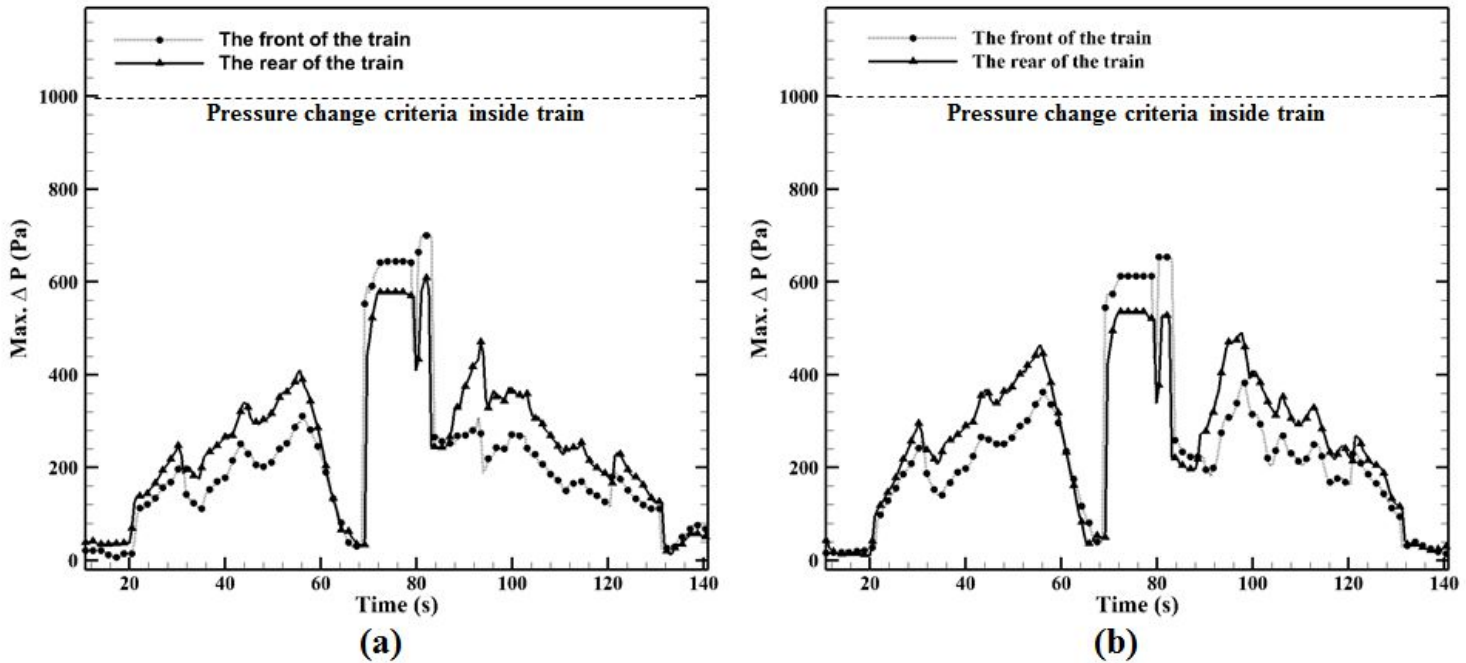


Fig. 88 Comparison of pressure change for 10 seconds from the conceptual design to identify the train interference: (a) Lead train, (b) Trailing train

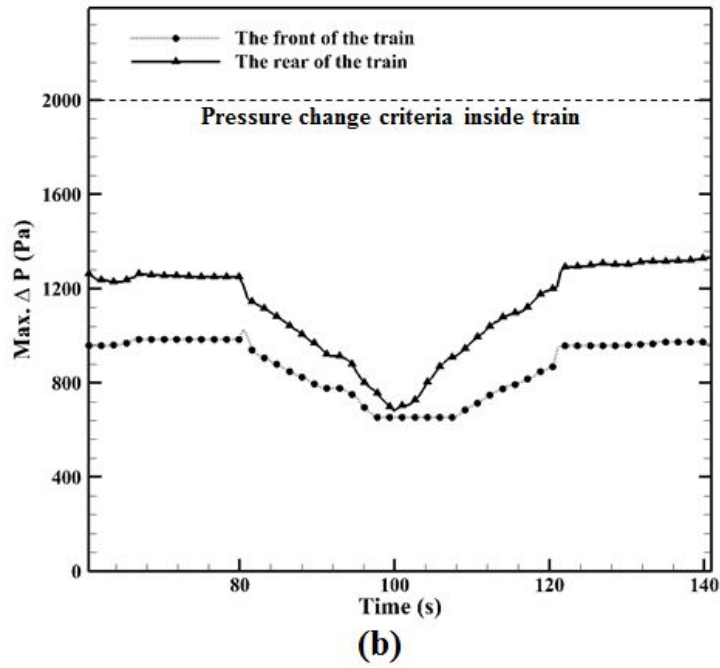
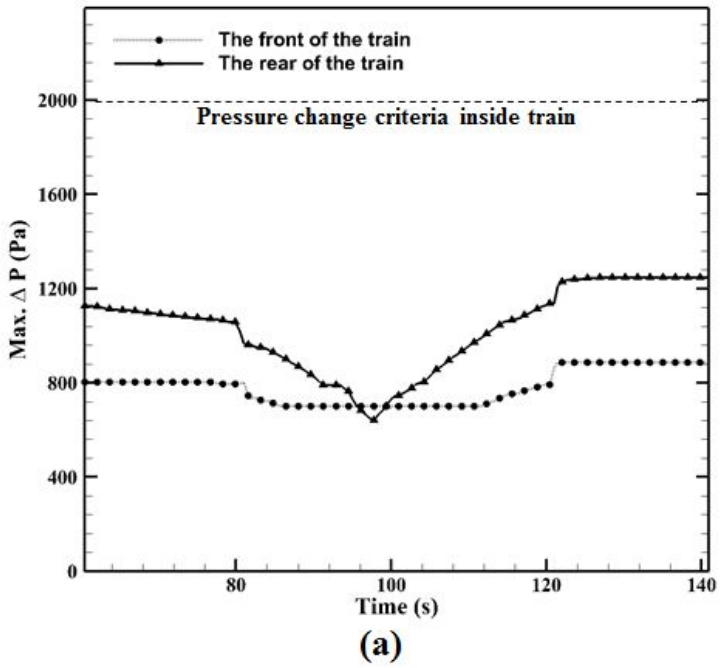


Fig. 89 Comparison of pressure change for 60 seconds from the conceptual design to identify the train interference: (a) Lead train, (b) Trailing train

5. Conclusions

Various tests with the aerodynamic parameters and design parameters related to a new transport system, GTX, were performed based on Seoul Subway. The physical phenomena of the high-speed train travelling in tunnels were analyzed from the tests. The results are reflected in the conceptual design and the design is evaluated by the design criteria of Seoul Subway.

If the speed of Seoul Subway increases by the required speed (200 km/h) of GTX, the more thrust than the KTX-Sancheon can be required to operate GTX. Pressure change by the speed increase can cause the passenger discomfort. Therefore, the design of GTX should be carried out carefully.

It is a fair fact that the current nose shape of subway should be changed to the streamlined shape. The pressure drag of blunt shape is significantly big than the pressure drag of streamlined shape. However, even if the train nose is longer, pressure drag dose not proportionally decrease. The effect of drag decrease is reduced at a certain length. The nose length more than 5 m has a low effect to reduce the pressure drag acting on the train. The nose shape of KTX-Sancheon seems appropriate for GTX.

The tunnel cross-sectional of Seoul Subway is small for the high-speed subway, GTX. Thus, it should be widened if the train having the same cross-sectional area of Seoul Subway is used for GTX. However, if a train having a little small cross-sectional area like KTX-Sancheon is used, the increase of the tunnel cross-sectional area can be reduced. Appropriate blockage ratio for GTX is expected to be between 0.2 and 0.15 because the tunnel cross-sectional areas in regards to 0.3 and 0.1 are too small and too big respectively. The small tunnel

cross-sectional area is difficult to achieve the desired speed and the big tunnel cross-sectional area costs too much to construct the tunnel.

Pressure acting on platform screen door increases when the train speed increases. However, pressure acting on platform screen door is not a problem, as the train runs according to the normal schedule which has a gradual acceleration and deceleration. It is expected that a problem happens when the express train is passing by the platform screen door at high speed. A shaft near the stations and a surface pressure of train cause a rapid pressure change. The rapid pressure change affects on the platform screen door because there is the big difference of the pressure between the train surface and atmosphere linked with the shaft. At that time, the pressure acting on platform screen door might exceed the design criteria. Therefore, tighter criteria is needed for the high-speed subway like GTX.

The speed increase causes a pressure drop around the outside of the train and it affects the internal pressure change. The internal pressure change can satisfy the criteria in a certain condition; the blockage ratio is below 0.2 and the train gradually accelerates and decelerates. But there is a condition that the pressure change might not satisfy the criteria. The condition is the constant speed section that the train is passing by the shaft at the maximum speed. At that time, the train experiences the rapid pressure change because the pressure of the train surface is rapidly increased by the inflow of the atmospheric pressure from the shaft. Thus, a sealed train is needed to prevent the internal pressure change from the rapid external pressure change for passenger safety and comfort.

This research is performed on the condition that one train is travelling in tunnels. However, the research about trains crossing in the tunnel should be also performed because the tunnel of GTX is a

double track tunnel and the interaction between trains crossing in the tunnel is one of the important problems. The train system having tunnels like GTX has one-dimensional phenomena (tunnel section) as well as three-dimensional phenomena (around the train and shafts). Therefore, a hybrid method in which one-dimensional method and three-dimensional method are mixed is needed for detailed analysis.

References

- [1] Anderson, J. D., 2001, "Fundamentals of aerodynamics", Third ed. McGRAW-HILL, New York.
- [2] Baron, A., Mossi, M. and Sibilla, S., 2001, "The alleviation of the aerodynamic drag and wave effects of high-speed trains in very long tunnels", *Journal of Wind Engineering and Industrial Aerodynamics*, 89, 365-401.
- [3] Bellenoue, M. and Kageyama, T., 2002, "Reduced scale simulation of the compression wave generated by the entry of a high-speed train into a tunnel", *TRANSAERO*, 206-216.
- [4] Bourquin, V., Mossi, M., Gregoire, R. and Rety, J. M., 1997, "The importance of aerodynamics on the design of high-speed transportation systems in tunnels: an illustration with the TGV and the Swissmetro", *World Congress on Railway Research E*, Florence, 507-713
- [5] Ehrendorfer, K., Reiterer, M. and Sockel, H., 2002, "Numerical investigation of the micro pressure wave", *TRANSAERO*, 321-341
- [6] Huang, Y. D., Gong, X. L. and Peng, Y. J., 2011, "Effects of the ventilation duct arrangement and duct geometry on ventilation performance in a subway tunnel", *Tunnelling and Underground Space Technology*, 26, 725-733.
- [7] Juraeva, M., Lee, J. H. and Song, D. J., 2011, "A computational analysis of the train-wind to identify the best position for the air-curtain installation", *Journal of Wind Engineering and Industrial Aerodynamics*, 99, 554-559.
- [8] Kim, B. H., Lee, K. and Kim, J. H., 2001, "Status of Gyeongbu high speed railway tunnels", *Journal of Korean Tunnelling and Underground Space Association*, 26-31

- [9] Kim, J. Y. and Kim, K. Y., 2007, "Experimental and numerical analyses of train-induced unsteady tunnel flow in subway", *Tunnelling and Underground Space Technology*, 22, 166-172.
- [10] Kim, J. Y. and Kim, K. Y., 2009, "Effects of vent shaft location on the ventilation performance in a subway tunnel", *Journal of Wind Engineering and Industrial Aerodynamics*, 97, 174-179.
- [11] Kim, T. K., Kim, K. H. and Kwon, H. B., 2011, "Aerodynamic characteristics of a tube train", *Journal of Wind Engineering and Industrial Aerodynamics*, 99, 1187-1196.
- [12] Kwon, H. B., Nam, S. W. and Kwak, J. H., 2009, "Assessment of the pressure transient inside the passenger cabin of high-speed train using computational fluid dynamic", 2009 Conference of the Korean Society for Railway, 12, 65-71.
- [13] Maeda, T., Matsumura, T., Iida, M., Nakatani, K. and Uchida, K., 1993, "Effect of shape of train nose on compression wave generated by train entering tunnel", In *Proceedings of the International Conference on Speedup Technology for Railway and Maglev vehicles*, Yokohama, Japan, 2, 315-319 (Japan Society for Mechanical Engineers, Tokyo).
- [14] Mossi, M. and Sibilla, S., 2002, "Swissmetro : aerodynamic drag and wave effects in tunnels under partial vacuum", *Lausanne, Switzerland*, 1-12.
- [15] Nam, S. W., 2010, "Review on Aerodynamical Parameters considered to determine the Cross-sectional Area of Railway Tunnel", 2010 Conference of the Korean Society for Railway, 10, 723-728.
- [16] Pope, S. B., 2000, "Turbulent Flows", Cornell University, New York.
- [17] Roh, J. S., Ryou, H. S. and Park, W. H., 2009, "CFD simulation

- and assessment of life safety in a subway train fire”, *Tunnelling and Underground Space Technology*, 24, 447-453.
- [18] Schulte-Werning, B., Gregoire, R., Malfatti, A. and Matschke, G., 2002, ”TRANSAERO A European Initiative on Transient Aerodynamics for Railway System Optimization”, Springer.
- [19] Taille, J. Y., Brulard, J., Rety, J. M. and Fauvel, P., 1995, ”Les recherches techniques pour l' etude de faisabilite du tunnel de base de la liaison transalpine Lyon-Turin”, *Revue Generale des Chemins de Fer* 197, 17-27
- [20] Uystepuyst, D., William-Louis, M., Creuse, E., Nicaise, S. and Monnoyer, F., 2011, ”Efficient 3D numerical prediction of the pressure wave generated by high-speed trains entering tunnels”, *Computers & Fluids*, 165-177.
- [21] Vardy, A. E., 1996a, ”Aerodynamic drag on trains in tunnels .1. Synthesis and definitions”, *Proceedings of the Institution of Mechanical Engineers Part F-Journal of Rail and Rapid Transit*, 201, 29-38.
- [22] Vardy, A. E., 1996b, ”Aerodynamic drag on trains in tunnels .2. Prediction and validation”, *Proceedings of the Institution of Mechanical Engineers Part F-Journal of Rail and Rapid Transit*, 201, 39-49.
- [23] Kwon, H. B., 2001, ”A Study on the unsteady compressible flow field induced by a high-speed train passing through a tunnel”, Seoul National University, Seoul national university (Thesis), South Korea
- [24] Retrieved 17.July.2013. URL: <http://thermotun.com/airshaft>
- [25] Takanobu, O. and Kozo, F., ”Effect of Train Shape on a Compression Wave Generated by a Train Moving into a Tunnel”, 30-36

- [26] Yoon, T. S., Lee, S., Hwang, J. H. and Lee, D. H., 2001, "Prediction and validation on the sonic boom by a high-speed train entering a tunnel", *Journal of Sound and Vibration*, 247(2), 195-211
- [27] Kwun Hing, W., 2008, "Aerodynamic Aspects of High-speed Railway Underground Station with Adjoining Tunnels", Hong Kong University(Thesis), Hong Kong
- [28] Kwon, H. B., Kim, T. Y., Lee, D. H. and Kim, M. S., 2003, "Numerical simulation of unsteady compressible flows induced by a high-speed train passing through a tunnel", *Proceedings of the Institution of Mechanical Engineers, Part F: Journal of Rail and Rapid Transit*, 217, 111-124
- [29] Rochard, B. P. and Schmid, F., 2000, "A review of methods to measure and calculate train resistances", *Proceedings of the Institution of Mechanical Engineers, Part F: Journal of Rail and Rapid Transit*, 214, 185-199
- [30] Palmero, N. M. and Vardy, A., 2013, "Tunnel gradients and aural health criterion for train passengers", *Proceedings of the Institution of Mechanical Engineers, Part F: Journal of Rail and Rapid Transit*, 0, 1-12
- [31] Kwon, H. B. and Hong, J. S., 2013, "Aerodynamic Drag Reduction on High-performance EMU Train by Streamlined Shape Modification", *Journal of The Korean Society for Railway*, 16(3), 169-174
- [32] Kwon, H. B., Yun, S. H. and Nam, S. W., 2012, "Numerical simulation of pressure change inside cabin of a train passing through a tunnel", *Journal of computational fluids engineering*, 17(1), 23-28
- [33] Yun, S. H., Kwak, M. H., Lee, D. H., Kwon, H. B. and Ko, T.

- H., 2009, "Experimental Study of the internal/external pressure variation of TTX travelling through a tunnel", The Korean Society for Railway, 12(2), 309-314
- [34] Riccoa, P., Baron, A. and Molteni, P., 2007, "Nature of pressure waves induced by a high-speed train travelling through a tunnel", Journal of Wind Engineering and Industrial Aerodynamics, 95, 781-808
- [35] Huang, Y., Hong, T. H. and Kim, C. N., 2012, "A numerical simulation of train-induced unsteady airflow in a tunnel of Seoul subway", Journal of Mechanical Science and Technology, 26(3), 785-792
- [36] Kim, D. W., Kim, J. M., Joo, S. J. and Park, J. H., 2009, "Characteristics of wind pressure on the platform screen door and ceiling due to train wind", The Wind Engineering Institute of Korea, 13(1), 11-18
- [37] Kim, Y. S., Kim, D. H., Kim, Y. H., Shin, K. B. and Lee, E. K., 2008, "Unsteady wind pressure analysis on PSD considering subway station configurations", The Korean Society for Railway, 11(1), 13-18
- [38] Jang, Y. J., Ryu, J. M. and Kim, Y. K., 2013, "Analysis of smoke distribution in the subway-station platform with and without the main tunnel ventilation", The conference of the korean society for railway, 124-129
- [39] Kim, N. Y., Lee, H. and Ban, J. J., 2009, "Verification of distance between ventilation shafts in the GTX(Great Train Express) project", The society of Air-Conditioning and Refrigerating Engineers of Korea, 124-129
- [40] Oh, H. J., Shin, D. Y., Lee, S. G., Kim, D. H. and Kim, C. J., 2012, "Numerical study with vent shaft position in underground

- station”, *Journal of Computational Fluids Engineering*, 17(1), 36-43
- [41] Retrieved 17.July.2013. URL:
http://www.seoul.go.kr/info/organ/office/subwaydevco/data/1231851_14094.html
- [42] Retrieved 19.July.2013. URL: <http://www.gtx.go.kr/index.do>
- [43] Retrieved 4.October.2013. URL:
http://en.wikipedia.org/wiki/Eurostar#Channel_Tunnel
- [44] Retrieved 5.October.2013. URL: <http://www.hstrain.re.kr/>
- [45] Retrieved 9.October.2013. URL: <http://en.wikipedia.org/wiki/TGV>
- [46] Retrieved 10.October.2013. URL:
<http://www.railway-technology.com/projects/ice-high-speed-rail/>
- [47] Retrieved 13.October.2013. URL:
http://en.wikipedia.org/wiki/Seikan_tunnel
- [48] Retrieved 14.October.2013. URL:
http://en.wikipedia.org/wiki/High_speed_train
- [49] Ku, Y. C., Rho, J. H., Yun, S. H., Kwak, M. H., Kim, K. H., Kwon, H. B. and Lee, D. H., 2010, ”Optimal cross-sectional area distribution of a high-speed train nose to minimize the tunnel micro-pressure wave”, *Journal of Structural and Multidisciplinary Optimization*, 42(6), 965-976
- [50] ANSYS 13.0 Manual
- [51] Retrieved 28.May.2014. URL: <http://www.molit.go.kr>
- [52] Kim, H. D., Kim, T. H. and Seo, T. W., 1998, ”Effect of train nose shape on the high-speed railway tunnel entry compression wave”, *The conference of the korean society for railway*, 596-603
- [53] Hwang, J. H., Yoon, T. S., Lee, D. H. and Lee, S. G.. 2011, ”Numerical study of unsteady flowfield around high speed trains passing by each other”, *JSME International Journal, Series B*, Vol.44, 451-464

- [54] Yoon, T. S. and Lee, S. G., 2001, "Prediction and validation on the sonic boom by a high speed train entering a tunnel", Journal of Sound and Vibration, Vol.247, No.2, 195-211
- [55] Yoon, T. S. and Lee, S. G., 2001, "Efficient prediction methods for the micro-pressure wave from a high-speed train entering a tunnel using the Kirchhoff formulation", Journal of Acoustical Society of America, Vol. 110, No. 5, 2379-2389

국문초록

대심도 터널에서 운행되는 고속열차의 공력특성 및 철도차량 안전기준을 적용한 분석

최중근

기계항공공학부 항공전공

서울대학교

국내에서 새로운 대중 교통수단이 건설될 계획에 있다. 대심도 급행철도 (Great Train eXpress) 는 현재의 지하철과 같이 지하에 건설될 것이다. 그러나 최대 주행속도가 현재의 지하철보다 약 2 배 빠른 200 km/h 이다. 열차의 속력이 터널에서 증가할 때, 공기역학과 관련된 문제들이 주요관심사들 중에 하나가 된다. 공력 문제들을 예로 들면 공력 저항, 스크린도어에 작용하는 풍압과 승객을 위한 이명감 등을 들 수 있다.

그러므로 본 논문에서는 지하철 터널에서의 공력현상 분석과 GTX의 개념설계를 수행하였다. 우선, 현재 지하철 속도 (100 km/h)에서 GTX의 속도 (200 km/h) 로 열차속도의 증가에 따른 공력효과를 평가하였다. 그리고 공력 변수들의 (공력저항, 풍압과 차량 내부압력 변화) 경향성을 설계 변수들을 (차량 전두부 형상, 터널 단면적과 환기구) 변화시켜 가며 분석하였다. 그 후에, 경향성 분석을 통한 GTX의 개념설계를 수행하였다. GTX의 개념설계는 고속열차와 지하철의 설계 기준에 의해 평가되었다.

터널에서 열차의 공력특성을 분석하기 위해 전산유체역학을 (Computational Fluid Dynamics) 사용하였으며 축대칭 방법으로 해석을 수행하였다.

해석 결과의 분석을 통해 GTX의 설계가 현재 지하철과는 다르

게 진행되어야 한다는 것을 알게 되었다. 전두부 형상은 공력저항을 줄이기 위하여 현재 지하철의 무딘 형상이 아닌 KTX-산천과 같은 유선형 형상으로 설계되어야 하며, 터널 단면적은 현재의 지하철보다 넓어져야 한다. 스크린 도어의 경우 설계기준의 강화가 필요하며, GTX 차량은 승객의 편의를 위해 기밀이 유지되지 않는 현재 지하철 차량과는 다르게 기밀이 유지되는 차량으로 설계되어야 할 것으로 판단된다.

주요어 : 대심도 급행철도, 공력저항, 열차 전두부 형상, 터널 단면적, 풍압, 이명감

학 번 : 2007 - 30821